THERMOMECHANICAL STUDY OF COLD ROLLING

by

B . R . VINAY KUMAR

DEPARTMENT OF MECHANICAL ENGINEERING

INDIAN INSTITUTE OF TECHNOLOGY, KANPUR

JUNE, 1988

THERMOMECHANICAL STUDY OF COLD ROLLING

A Thesis Submitted
In Partial Fulfilment of the Requirements
for the Degree of
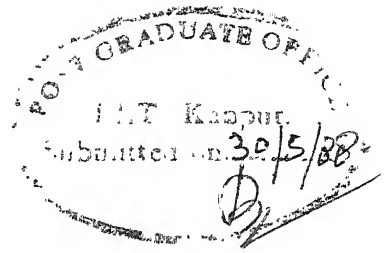
MASTER OF TECHNOLOGY

by

B . R . VINAY KUMAR

to the

DEPARTMENT OF MECHANICAL ENGINEERING

INDIAN INSTITUTE OF TECHNOLOGY, KANPUR

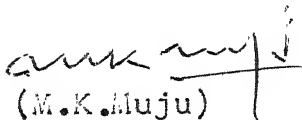**JUNE, 1988**

CERTIFICATE

This is to certify that the present work on "Thermomechanical Study of Cold Rolling " by B.R.Vinay Kumar has been carried out under our supervision and has not been submitted elsewhere for the award of a degree.

(M.K.Muju)
Professor
Mechanical Engg. Dept.
I.I.T. Kanpur.

(P.M. Dixit)
Assistant Professor
Mechanical Engg. Dept.
I.I.T. Kanpur.

ACKNOWLEDGEMENTS

CONTENTS

LIST OF FIGURES

$\underline{A}$ Assembled global matrix

$\underline{\underline{A}}_1$ Unknown part of RHS containing u^b, v^b and T^b

$\underline{B}$ Assembled right hand side

$\underline{\underline{B}}$ Non-dimensionalised strain matrix

c Specific heat (J/kg-$^\circ$C)

e Internal energy (J/kg)

h_o Initial half thickness of the sheet metal (m)

h_1 Final half thickness of the sheet metal (m)

$\underline{K}^e$ Elemental area matrix

K Thermal conductivity (W/m-$^\circ$C)

l_b Length of the boundary element

$\underline{N}$ Shape function vector for temperature

$\underline{N}_p$ Shape function vector for pressure

$\underline{N}V$ Shape function matrix for velocities

p Hydrostatic component of stress tensor (N/m^2)

$\underline{p}^e$ Elemental nodal pressure vector

q Heat flux (W/m^2)

q_n Normal heat flux (W/m^2)

R Reduction ratio

r Radius of the roll (m)

T Temperature ($^\circ$K)

$\underline{T}^e$ Elemental nodal temperature vector

t_n Normal traction on the boundary (N/m^2)

t_s Tangential traction on the boundary (N/m^2)

t_x x-direction traction on the boundary (N/m^2)

t_y y-direction traction on the boundary (N/m^2)

ABSTRACT

In the present thesis an attempt was made to predict the pressure, velocity and temperature distribution in a strip during cold rolling. The continuity, momentum and energy equations were used for formulating the problem theoretically. The friction on the roll-work interface was assumed to be of both sticking and slipping type. The mechanical and thermal properties of the work were assumed to be temperature dependent. The heat was assumed to dissipate by convection on free sides and by conduction on roll-work interface. The set of non-linear equations resulting from the above formulation were then solved iteratively using FEM procedure based on Galerkin's approach until convergence. The validity of the theoretical model is confirmed by comparing the temperatures experimentally. The velocity profiles also turn out on expected lines.

CHAPTER I

INTRODUCTION

Numerical and computer aided analysis of forming processes have recently started to make an important contribution in industries. From the physical point of view, the analysis of forming processes poses a range of complex problems in continuum mechanics and heat transfer. Solution of the problems involve usage of sophisticated numerical techniques. The finite element method emerges as the preferred approach and its flexibility leads to the development of powerful programme packages capable of treating wide range of problems.

The forming of many industrial products can be accomplished by many different process all of which involve large, permanent deformation. Rolling is one of the most important industrial process in this respect. Rolling may be done as hot or cold rolling. Rolling operations done above the recrystallization temperature of the material are said to be hot rolling process and cold rolling process if done below recrystallization temperature.

So far the traditional approach to predict the flow, roll pressures, forces and torques is to establish an average temperature in the roll gap and use it in the determination of an average flow strength. Since this

method of analysis does not take into account the heat
generated due to either plastic deformation or friction
at the interface, the dependence of yield strength and
other thermally sensitive properties of the material
cannot be satisfactorily incorporated in the analysis.
The thermal gradients in the material are dependent on
the roll-material used, reduction ratio, angular velocity
of rolls etc.

Previous Work

The importance of temperature calculation have
been long recognised. Until recently, the majority of
the work has been to decouple the problem of heat transfer
from the metal deformation problem. The approach has been
to determine the flow fields in the problem either experi-
mentally or by calculations and then by using these fields
for the calculation of heat generation.

From earlier works [1] on metal-forming analysis,
two different approaches have emerged: the 'flow' approach
and the 'solid approach'. In the flow approach, the metal
is considered to behave as a non-Newtonian fluid and the
finite element equations are solved accordingly. This
method, no doubt being very effective does not take many
subtleties of the elastic-plastic constitutive equations
into account and is not in a position to predict residual

stresses. In the solid approach, the material is considered to behave as a classical elastic-plastic solid and the finite element equations are solved with methods used in small-strain plasticity problems.

In 1978, Altan, Shah and Laholi did a computer aided simulation [2] of strip rolling process by combining analysis of rolling mechanics and by developing a finite-difference method for predicting time-dependent temperatures in the strip and the work rolls. In 1981, Zien Kicwiez, Onate and Heinrich carried out a coupled thermomechanical analysis [3] for flow of metals using flow formulation. Present thesis has used the idea of flow formulation from this paper. Other notable work in this area has been carried out by Cornfield and Johnson [4] , in hot rolling, Johnson and Kudo [5] using upper-bound solution technique. On the experimental side, Bishop, Rice, Jeswiet, Altan, Karagiozis, Lenard and others have carried out various experiments in determining the temperature distribution and finding out roll-interface temperatures. Jesewiet and Rice [6] had embedded thermo-couples into the work rolls and evaluated the temperature distribution on the interface. Karagiozu and Lenard [7] also used embedded thermocouple technique but they embedded it in the workpiece to evaluate the temperature distributions.

Scope of Present Work:

In the present work, the main thrust has been to
evaluate the velocity or flow distribution and the
temperature distribution in cold rolling process. Previ-
ously most of the researchers who have worked in the numer-
ical thermomechanical analysis of cold rolling had used
the technique of decoupling the mechanics and heat transfer
problems. Zienkiewicz et al., for the first time applied
the technique of coupling thermal and mechanical problems
using flow formulation. Of the several assumptions they
assumed a 'sticking' condition on the roll-interface.
This implied that the velocity of the work material on
the interface was same as the roll-surface speed. The
present thesis differs from Zienkiewicz's work in that
slipping is assumed to occur at the interface and Coulombic
frictional forces with some upper limit as the sticking
friction condition. Further more, the frictional constant
is assumed to be constant over the interface due to lack
of exact data.

The neutral zone was assumed to be a point. The
mode of heat transfer on the free surface is assumed to
be through free or natural convection. The experiments
which were carried out in the present work were aimed at
measuring the interface temperature.

CHAPTER II

MATHEMATICAL MODELLING OF ROLLING PROCESS

In this chapter the model for the rolling process is
developed. The process is modelled as a steady-state two
dimensional problem. The interaction with the roll and
the surroundings is represented by appropriate boundary
conditions. The constitutive equations for mechanical
and thermal behaviour of the strip are stated. Non-
dimensionalisation of the governing equations and the weak
formulation is presented at the end of this chapter.

2.1 Mechanics of Rolling Process

Many experimental and theoretical investigations
have shown that the velocities, strains, stresses associated
with motion of a rolled strip are not uniformly distributed
across the sections.

The material being rolled undergoes varied velocity
and strain distribution (see fig. 2.1). The velocity across
the section of the strip in the unstrained zone is distri-
buted uniformly, whilst in the contact zone of deformation,
the outer layers of the metal touching the rolls tend to
move faster than the inner layers. The outer layers of
the metal in contact with the roll have less velocity than

the roll near the entry. But the velocity of the outer layers (denoted by v_s) increases as it reaches the exit and finally becomes more than the speed of the roll (denoted by v_r) near the exit. The zone of transition where v_s becomes equal to v_r is called the neutral zone. Even though experimental evidence shows that this transition occurs over a zone, many researchers have considered this zone as a point in their analysis for lack of exact data and the difficulty in modelling it as a zone. The zone in which v_s is less than v_r is called backward slip region and the frictional force on the metal is in the direction of rolling. The zone in which v_s is greater than v_r is called the zone of forward slip region and the frictional force acting on the strip tries to retard the motion.

Many researchers have come with an analytical expression for determining the neutral point. Notable among them and given below are:

(1) Avitzur's formula [8] :

$$n = \frac{1}{2}\sqrt{\frac{h_o}{R}}\{\tan^{-1}\sqrt{\frac{h_1}{h_o}} - 1 - \frac{1}{m}\sqrt{\frac{h_o}{R}}[\ln\frac{h_1}{h_o} + \frac{1}{4}$$

$$\sqrt{\frac{h_o}{R}}\sqrt{\frac{h_1}{h_o}} - 1 + \frac{\sigma_{xb} - \sigma_{xf}}{\frac{2}{3}y}]\} \qquad (2.1)$$

(2) Chaturvedi's formula [9] :

$$\alpha_n = \frac{\alpha}{2}(1 - \frac{\alpha}{2\Psi}) \qquad (2.2)$$

(3) Modified Sim's Formula:

$$\alpha_n = \tan\left[\frac{\pi}{8}\left(\frac{h_0}{R}\right)^{1/2}\ln(1-r) + \frac{1}{2}\tan^{-1}\left(\frac{r}{1-r}\right)^{1/2}\right]\left(\frac{h_0}{R}\right)^{1/2}$$

(2.3)

where,

r = reduction ratio = $\dfrac{h_1 - h_0}{h_0}$

h_1 = initial thickness of strip

h_0 = final thickness of strip

α_n = neutral angle

Ψ = friction angle

α = angle of contact

R = radius of the roll

m = friction factor

σ_{xb} = back tension

σ_{xf} = front pull.

Avitzur's formula was chosen to calculate entry and exit velocities of the strip. The choice was based because this particular formula was most general in form and

2.2 Governing Equations

The thermomechanical behaviour of a material is governed by the following three equations:

(1) Conservation of mass or the continuity equation:

$$\overset{\bullet}{\rho} + \rho \operatorname{div} \underline{V} = 0, \qquad\qquad (2.4)$$

(2) The balance of momentum or equation of motion:

$$\rho \overset{\bullet}{\underline{V}} = \nabla \cdot \underline{\underline{\sigma}} - \underline{0} \quad \text{(for zero body forces)} \qquad (2.5)$$

(3) Conservation of energy or the first law of thermodynamics:

$$\rho \overset{\bullet}{e} + \nabla \cdot \underline{q} - \underline{\underline{\sigma}} \cdot \underline{V} - 0 \qquad\qquad (2.6)$$

Besides the above equations, we also need the constitutive equations. The strip behaviour is modelled by the following constitutive equations:

(1) Stress-strain rate relation:

In a flow process, the deformation is normally represented by the strain-rate tensor (neglecting elastic strain)

$$\overset{\bullet}{\underline{\underline{\varepsilon}}} = \frac{1}{2} (\nabla \underline{V} + \nabla \underline{V}^{T})$$

Let $\underline{\underline{S}}$ and $\overset{\bullet}{\underline{\underline{\varepsilon}}}{}'$ be the deviatoric parts of the stress and strain rate tensor:

$$\underline{\underline{\sigma}} = - p \underline{\underline{1}} + \underline{\underline{S}} \ , \quad p = \frac{1}{3} \operatorname{tr} \underline{\underline{\sigma}}$$

$$\overset{\bullet}{\underline{\underline{\varepsilon}}} = (\frac{1}{3} \operatorname{tr} \overset{\bullet}{\underline{\underline{\varepsilon}}}) \underline{\underline{1}} + \overset{\bullet}{\underline{\underline{\varepsilon}}}{}'$$

Then they are related by

$$\underline{\underline{S}} = 2\mu \, \underline{\underline{\dot{\varepsilon}}}'$$

(2.7)

where the viscosity μ is given by

$$\mu = \frac{1}{6} \frac{\sigma_Y}{\sqrt{\underline{\underline{\dot{\varepsilon}}} \cdot \underline{\underline{\dot{\varepsilon}}} - \frac{1}{3}(tr\,\underline{\underline{\dot{\varepsilon}}})^2}}$$

for a rigid plastic material which yields according to Von-Mises criterion.

(2) The density-temperature relation:

In a plastic material, volume changes only when there is a change in temperature T. Therefore   depends only on T.

$$\rho = \rho_0 \, \exp\left[- \int_{T_0}^{T} 3\alpha(s) \, ds \right]$$

(2.8)

where α = coefficient of linear expansion of the metal

ρ_0 = density at room temperature

T_0 = room temperature.

(3)   Heat flux-temperature gradient relation:

$$q = -K \nabla T \qquad (2.9)$$

where,

K = thermal conductivity.

(4)   Specific internal energy-temperature relation:

$$e = \int_0^T c(s)\, ds \qquad (2.10)$$

where,

c = specific heat.

Here the material properties σ_y, μ, α and c are considered to be temperature dependent.

Substituting the constitutive equations [2.7-2.10] into the governing equations [2.4-2.6] we get the following equations:

$$\nabla \cdot \underline{V} - 3\alpha\left(\frac{\partial T}{\partial t} + \underline{V} \cdot \nabla T\right) = 0 \qquad (2.11)$$

$$\rho\left(\frac{\partial \underline{V}}{\partial t} + \underline{V} \cdot \nabla \underline{V}\right) - \nabla \cdot \underline{\underline{\sigma}} = \underline{0} \qquad (2.12)$$

and

$$\rho\, c\left[\frac{\partial T}{\partial t} + \underline{V} \cdot \nabla T\right] - \nabla \cdot (K \nabla T) + p\, \mathrm{tr}\, \underline{\dot{\varepsilon}} - 2\mu$$

$$\left[\, \underline{\dot{\varepsilon}} \cdot \underline{\dot{\varepsilon}} - \frac{1}{3}\, (\mathrm{tr}\, \underline{\dot{\varepsilon}})^2 \,\right] \tag{2.12}$$

2.3 Equations for Steady State Two Dimensional Problem

The strip is assumed to be very broad in relation to
the length of the arc of contact and the thickness of the
strip. Consequently the effect of spread may be neglected
and the problem can be considered as two-dimensional flat
rolling.

Rectangular cartesian coordinate system as depicted
in fig. 2.2 is considered, with the X-axis along the length
of the strip being rolled and Y-axis along the thickness of
the strip.

For a 2-D problem the velocity vector has only two
components and hence

$$\underline{V} = u\, i + v\, j$$

while the stress and strain-rate tensor have the following
form:

$$\underline{\underline{\sigma}} = \begin{bmatrix} \sigma_{xx} & \sigma_{xy} \\ \\ \sigma_{xy} & \sigma_{yy} \end{bmatrix} \quad ; \quad \underline{\underline{\dot{\varepsilon}}} = \begin{bmatrix} \dfrac{\partial u}{\partial x} & \dfrac{1}{2}\left(\dfrac{\partial u}{\partial y} + \dfrac{\partial v}{\partial x}\right) \\ \\ \dfrac{1}{2}\left(\dfrac{\partial u}{\partial y} + \dfrac{\partial v}{\partial x}\right) & \dfrac{\partial v}{\partial y} \end{bmatrix}$$

The governing equations [2.11 - 2.13] are then reduced to:

$$\dot{\varepsilon}_{xx} + \dot{\varepsilon}_{yy} - 3\alpha \left(u\, \frac{\partial T}{\partial x} + v\, \frac{\partial T}{\partial y} \right) = 0 \qquad (2.14)$$

$$\left(u\, \frac{\partial u}{\partial x} + v\, \frac{\partial u}{\partial y} \right) - \left(\frac{\partial \sigma_{xx}}{\partial x} + \frac{\partial \sigma_{xy}}{\partial y} \right) = 0 \qquad (2.15a)$$

$$\left(u\, \frac{\partial v}{\partial x} + v\, \frac{\partial v}{\partial y} \right) - \left(\frac{\partial \sigma_{xy}}{\partial x} + \frac{\partial \sigma_{yy}}{\partial y} \right) = 0 \qquad (2.15b)$$

and

$$c\left(\frac{\partial T}{\partial x} u + \frac{\partial T}{\partial y} v \right) - \left[\frac{\partial}{\partial x} \left(K\, \frac{\partial T}{\partial x} \right) + \frac{\partial}{\partial y} \left(K\, \frac{\partial T}{\partial y} \right) \right] + p \left(\dot{\varepsilon}_{xx} + \dot{\varepsilon}_{yy} \right)$$

$$-2\mu \left[\dot{\varepsilon}_{xx}^2 + \dot{\varepsilon}_{yy}^2 + 2\, \dot{\varepsilon}_{xy}^2 - \frac{1}{3} \left(\dot{\varepsilon}_{xx} + \dot{\varepsilon}_{yy} \right)^2 \right] = 0$$

$$(2.16)$$

2.4   Penalty Formulation

On observing equation [2.14] it is observed that it devoid of pressure terms.   Because of this the finite element formulation of this equation results in a matrix with zero diagonal terms.   If the number of zeroes in the diagonal are significantly large, the coefficient matrix becomes singular. To overcome this difficulty, we modify the equation [2.14] as follows:

$$\dot{\varepsilon}_{xx} + \dot{\varepsilon}_{yy} - 3\alpha \left(u \frac{\partial T}{\partial x} + v \frac{\partial T}{\partial y} \right) + \frac{p}{\lambda} = 0 \qquad (2.17)$$

where λ is a large number. In the limit $\lambda \to \infty$
equation [2.17] reduces to eq. [2.14].

2.5 Boundary Conditions

The boundary conditions specified on any part of
the boundary can be classified as

(1)   essential boundary conditions i.e., specification
        of temperature T and velocity $\underline{V}$.

(2)   natural boundary conditions i.e., specifications
        of stress vector $\underline{t} = \underline{\sigma} \cdot \hat{n}$ and normal heat
        flux $q_n = \underline{q} \cdot \hat{n}$.

(3)   mixed type are components of $\underline{V}$ and the remaining of
        $\underline{t}$ are specified. Sometimes the relation between
        the components of $\underline{V}$ and $\underline{t}$ are specified.

2.5.1 Entry and Exit Boundaries

This is the region shown by sides 1 and 5 in the
fig. 2.3. These boundaries are assumed to be far away
from the zone of deformation. Thus the temperature on
these sides can be assumed to be at room temperature.
Furthermore the y-velocity component (v) of velocity
vector $\underline{V}$) is zero on both the boundaries. The X-velocity
components (u) are calculated from the roll surface speed

and Avitzurs formula [2.1].

The u-velocity components are found as follows:
First the neutral angle α_n is calculated. Then the
following continuity equation is used in obtaining
u-velocity component at exit.

$$u_o = \frac{v_r \; Cos \; n}{h_o} \; [h_o + 2R(1 - Cos\,\alpha_n)] \qquad (2.19)$$

Then the velocity at the entry is:

$$u_1 = \frac{u_o h_o}{h_1}$$

In actual practice it would be more appropriate if
the u-velocity components at both entry and exit are found
experimentally.

Thus to summarise, the boundary conditions are:

$$T = T_{oo} \quad \text{on both side 1 and side 5}$$

$$\begin{aligned} u &= u_o \\ v &= 0 \end{aligned} \quad \text{on side 5}$$

and
$$\begin{aligned} u &= u_1 \\ v &= 0 \end{aligned} \quad \text{on side 1 .}$$

2.5.2   Convective Boundary Sides

The sides on which convective boundary conditions are to be applied are the sides 2 and 4 as shown in fig. 2.3. The losses due to radiation are considered negligible.

The heat that is being convected away to atmosphere by free convection is given by

$$q = h \left(T - T_{\infty}\right) \tag{2.1}$$

where h = heat transfer coefficient given by the formula [10]

$$h = 1.32 \left(\frac{\Delta T}{w}\right)^{0.25} \tag{2.2}$$

where,

ΔT =   temperature difference between the free surface and room temperature.

w =   width of the plate.

Since the strip velocity is along the free surface the following conditions are considered:

$$v = 0 \text{ and } t_x = 0$$

Then the boundary conditions can be summarised as follows:

$$v = 0$$
$$t_x = 0$$
$$\text{and} \quad q = h(T - T_{\infty})$$

2.5.3 Roll-Contact Boundary

This interface is shown by the side 3. On this surface, due to the frictional work, heat is generated. A part of this heat is conducted into the rolls. The rest goes into the strip. The expression for the heat conducted into the rolls is:

$$q_r = K_r \frac{(T - T_\infty)}{2R}$$

where,

K_r = roll conductivity and

R = roll radius .

Assuming that the diametrically opposite end of the roll to the interface is at room temperature.

The heat generated by friction is:

$$q = t_s v_s ;$$

where,

t_s = frictional force and

v_s = tangential velocity of strip.

Therefore the heat flowing into the metal is :

$$q_n = -q + q_r$$

$$= -t_s v_s + K_r \frac{(T - T_\infty)}{2R} \qquad (2.21)$$

The mechanical boundary conditions for velocity and tractions are bit complex in the roll contact zone. The normal velocity component along the radius v_n is zero

$$v_n = 0 .$$

Mixed type of friction model is considered which incorporates both slipping and sticking friction. The relation between tangential force t_s and the normal force t_n is given as

$$t_s = \mu t_n \quad \text{if} \quad t_s < \frac{Y}{3} \quad \text{(slipping friction)} \qquad (2.22a)$$

and

$$t_s = \frac{\sigma_Y}{3} \quad \text{if } t_s \geq \frac{Y}{3} \quad \text{(sticking friction)} \qquad (2.22b)$$

μ is considered to be constant along the arc length. In the sticking friction zone the layer of the metal in contact with the metal moves with same speed as the roll and the frictional force acting is equal to the yield shear stress. This type of formulations leads to unknown terms in t_x and t_y in the expression for q_n on the interface. The elimination of these unknown terms is dealt with in detail in the next chapter.

2.5.4 Axis of Symmetry

The y-velocity component v is zero along the axis of symmetry, i.e., side 6. Furthermore, t_x is zero along the side. The heat transfer across this boundary is also

on this side can be summarised as:

$$v = 0$$
$$t_x = 0$$
$$\text{and} \quad q_n = 0$$

2.6 Non-dimensionalisation

Non-dimensionalisation is usually done to avoid ill conditioning and numerical difficulties. In this section all the physical quantities are non-dimensionalised using some characteristic dimensional quantities related to the process parameter like roll velocity v_r, final thickness of the sheet h_o, ambient temperature T_∞ etc. Thus

$$\bar{x} = \frac{x}{h_o} \; ; \; \bar{y} = \frac{y}{h_o} \; ; \; \bar{u} = \frac{u}{w_r} ; \; \bar{v} = \frac{v}{w_r} \; ; \; T = \frac{T}{T_\infty}$$

(2.23a)

The mechanical and thermal properties are nondimensionalised with respect to their room temperature values:

$$\bar{\rho} = \frac{\rho}{\rho_o} \; ; \; \bar{\mu} = \frac{\mu}{\mu_o} \; ; \; \bar{\alpha} = \frac{\alpha}{\alpha_o} \; ; \; \bar{c} = \frac{c}{c_o} \; ; \; \bar{K} = \frac{K}{K_o}$$

(2.23b)

where

$$\mu_o = \frac{(\sigma_y)_o}{(\frac{\omega_r}{h_o})}$$

and $(\sigma_y)_o$, ρ_o, α_o, c_o and K_o are the room temperature values. The pressure and the stress tensor are nondimensionalised by the relation:

$$\bar{p} = \frac{p}{\dfrac{\mu_o \omega r}{h_o}} \quad ; \quad \bar{\sigma}_{ij} = \frac{\sigma_{ij}}{\dfrac{\mu_o \omega r}{h_o}} \qquad (2.23c)$$

Substituting equations [2.23a, 2.23b, 2.23c] into equations [2.15a, 2.15b, 2.16, 2.17] we get:

$$(\bar{\dot{\varepsilon}}_{xx} + \bar{\dot{\varepsilon}}_{yy}) - 3\alpha_o T_{oo} [\bar{\alpha}(\bar{u}\frac{\partial \bar{T}}{\partial \bar{x}} + \bar{v}\frac{\partial \bar{T}}{\partial \bar{y}})] + \frac{\mu_o}{\lambda}\bar{p} = 0 \qquad (2.24)$$

$$\frac{\rho_o(\omega r)h_o}{\mu_o}[\bar{\rho}(\bar{u}\frac{\partial \bar{u}}{\partial \bar{x}} + \bar{v}\frac{\partial \bar{u}}{\partial \bar{y}})] - (\frac{\partial \bar{\sigma}_{xx}}{\partial \bar{x}} + \frac{\partial \bar{\sigma}_{xy}}{\partial \bar{y}}) = 0 \qquad (2.25a)$$

$$\frac{\rho_o(\omega r)h_o}{\mu_o}[\bar{\rho}(\bar{u}\frac{\partial \bar{u}}{\partial \bar{x}} + \bar{v}\frac{\partial \bar{u}}{\partial \bar{y}})] - (\frac{\partial \bar{\sigma}_{xy}}{\partial \bar{x}} + \frac{\partial \bar{\sigma}_{yy}}{\partial \bar{y}}) = 0 \qquad (2.25b)$$

$$\frac{\rho_o c_o T_{oo} h_o}{\mu_o \omega r}\bar{\rho}\bar{c}(\bar{u}\frac{\partial \bar{T}}{\partial \bar{x}} + \bar{v}\frac{\partial \bar{T}}{\partial \bar{y}}) - \frac{K_o T_{oo}}{\mu_o(\omega r)^2}$$

$$[\frac{\partial}{\partial \bar{x}}(\bar{K}\frac{\partial \bar{T}}{\partial \bar{x}}) + \frac{\partial}{\partial \bar{y}}(\bar{K}\frac{\partial \bar{T}}{\partial \bar{y}}) + \bar{p}(\bar{\dot{\varepsilon}}_{xx} + \bar{\dot{\varepsilon}}_{yy})]$$

$$-2\bar{\mu}[\bar{\dot{\varepsilon}}_{xx}^2 + \bar{\dot{\varepsilon}}_{yy}^2 + 2\bar{\dot{\varepsilon}}_{xy}^2 - \frac{1}{3}(\bar{\dot{\varepsilon}}_{xx} + \bar{\dot{\varepsilon}}_{yy})^2] = 0 \qquad (2.26)$$

The nondimensional normal heat flux and the stress vector are:

$$\bar{q}_n = \frac{q_n}{\left(\dfrac{K_o \, T_\infty}{h_o}\right)} \quad ; \quad \bar{t} = \frac{t}{\left(\dfrac{\mu_o \, \omega \, r}{h_o}\right)}$$

$$(2.27)$$

2.7 Galerkin Formulation

The governing equations in the model are non-linear and variational formulation does not exist here. Galerkin's weighted residual method is adopted in the present case. The weak form of the problem is derived in this section. The Finite Element Formulation of this follows in the next chapter.

Let $\bar{u}$, $\bar{v}$, $\bar{p}$ and $\bar{T}$ be the functions which satisfy the equations [2.24 - 2.26] and all the boundary conditions exactly. Then they will constitute a weak solution of the problem if the following integrals are zero:

$$\int_D \left[\dot{\bar{\varepsilon}}_{xx} + \dot{\bar{\varepsilon}}_{yy} - 3 \alpha_o \, T_\infty \{ \bar{\alpha} \, (\bar{u} \, \frac{\partial \bar{T}}{\partial \bar{x}} + \bar{v} \, \frac{\partial \bar{T}}{\partial \bar{y}}) \} \right.$$

$$\left. + \frac{\mu_o}{\lambda} \, \bar{p} \right] W_p \quad dA \; = \; 0$$

$$\int_D \frac{\rho_o(\omega r)h_o}{\mu_o} \{ \bar{\rho} (\bar{u}\frac{\partial \bar{u}}{\partial \bar{x}} + \bar{v}\frac{\partial \bar{u}}{\partial \bar{y}}) W_u + \bar{\rho}(\bar{u}\frac{\partial \bar{v}}{\partial \bar{x}} + \bar{v}\frac{\partial \bar{v}}{\partial \bar{y}})W_v \}$$

$$- (\frac{\partial \bar{\sigma}_{xx}}{\partial \bar{y}} + \frac{\partial \bar{\sigma}_{xy}}{\partial \bar{y}})W_u - (\frac{\partial \bar{\sigma}_{xy}}{\partial \bar{x}} + \frac{\partial \bar{\sigma}_{yy}}{\partial \bar{y}})W_v] dA$$

and

$$\int_D [\frac{\rho_o c_o T_{oo} H_o}{\mu_o \omega r} \bar{\rho} \bar{c} (\bar{u}\frac{\partial \bar{T}}{\partial \bar{x}} + \bar{v}\frac{\partial \bar{T}}{\partial \bar{y}}) \frac{K_o T_{oo}}{\bar{\mu}_o (\omega r)^2} \{\frac{\partial}{\partial \bar{x}}(\bar{K}\frac{\partial \bar{T}}{\partial \bar{x}}) + \frac{\partial}{\partial \bar{y}}$$

$$(\bar{K}\frac{\partial \bar{T}}{\partial \bar{y}}) \} + \bar{p}(\dot{\bar{\varepsilon}}_{xx} + \dot{\bar{\varepsilon}}_{yy}) - 2\bar{\mu}\{ \dot{\bar{\varepsilon}}_{xx}^{-2} + \dot{\bar{\varepsilon}}_{yy}^{-2} + 2\dot{\bar{\varepsilon}}_{xy}^{-2} - \frac{1}{3}$$

$$(\dot{\bar{\varepsilon}}_{xx} + \dot{\bar{\varepsilon}}_{yy})^2 \}] W_T \quad dA = 0$$

where W_p, W_u, W_v and W_T are the weight functions which satisfy the homogeneous versions of the boundary conditions.

Integrating by parts certain terms and using the relations

$$\bar{\bar{\sigma}} = -\bar{p}\underline{1} + 2\bar{\mu}\mu_o \dot{\bar{\varepsilon}} ; \bar{\underline{\varepsilon}} = \bar{\bar{\sigma}}\cdot\hat{n} \quad \text{and} \quad \bar{q}_n = \bar{K}\nabla \bar{T}\cdot\hat{n}$$

and the boundary conditions on the weight, we get the following weak form of the problem,

$$\int_D I_1 \, d\bar{A} = 0 \tag{2.28}$$

$$\int_D I_2 \, d\bar{A} = \int_C I_4 \, d\bar{A} + \int_C I_5 \, d\bar{A} \tag{2.29}$$

$$\int_D I_3 \, d\bar{A} = \int_{C_C} I_6 \, d\bar{A} \qquad (2.30)$$

where

$$I_1 = [\, (\dot{\bar{\varepsilon}}_{xx} + \dot{\bar{\varepsilon}}_{yy}) - 3\alpha_0 \, T_\infty \{ \bar{\alpha} \, (\bar{u} \frac{\partial \bar{T}}{\partial \bar{x}} + \bar{v} \frac{\partial \bar{T}}{\partial \bar{y}}) \} + \frac{\mu_0}{\lambda} \bar{p} \,] \, W_p$$

$$(2.31)$$

$$I_2 = \frac{\rho_0 (\omega r) h_0}{\mu_0} [\, \bar{p} \, (\bar{u} \frac{\partial \bar{u}}{\partial \bar{x}} + \bar{v} \frac{\partial \bar{u}}{\partial \bar{y}}) W_u + \bar{p} \, (\bar{u} \frac{\partial \bar{v}}{\partial \bar{x}} + \bar{v} \frac{\partial \bar{v}}{\partial \bar{y}}) W_v$$

$$- \bar{p} [\, \dot{\varepsilon}_{xx}(W) + \dot{\varepsilon}_{yy}(W)] + [\, \bar{\dot{\varepsilon}}_{xx} \, \dot{\varepsilon}_{xx}(W) + \bar{\dot{\varepsilon}}_{yy} \, \dot{\varepsilon}_{yy}(W)$$

$$+ 2 \bar{\dot{\varepsilon}}_{xy} \, \dot{\varepsilon}_{xy}(W) \,] \qquad (2.32)$$

$$I_3 = [\frac{\rho_0 c_0 T_\infty h_0}{\mu_0 \omega r} \, \bar{\rho} \, \bar{c} \, (\bar{u} \frac{\partial \bar{T}}{\partial \bar{x}} + \bar{v} \frac{\partial \bar{T}}{\partial \bar{y}}) + \frac{K_0 T_\infty}{\mu_0 (\omega r)^2} \, \bar{K}$$

$$(\frac{\partial \bar{T}}{\partial \bar{x}} \frac{\partial W_T}{\partial \bar{x}} + \frac{\partial \bar{T}}{\partial \bar{y}} \frac{\partial W_T}{\partial \bar{y}}) + \bar{p} \, (\dot{\bar{\varepsilon}}_{xx} + \dot{\bar{\varepsilon}}_{yy}) + 2 \bar{\mu}$$

$$(\dot{\bar{\varepsilon}}_{xx}^2 + \dot{\bar{\varepsilon}}_{yy}^2 + 2 \dot{\bar{\varepsilon}}_{xy}^2 - \frac{1}{3} (\dot{\bar{\varepsilon}}_{xx} + \dot{\bar{\varepsilon}}_{yy})^2)] \, W_T$$

$$(2.33)$$

$$I_4 = \bar{t}_x \, W_u \qquad (2.34)$$

$$I_5 = \bar{t}_y \, W_v \qquad (2.35)$$

$$I_6 = -q_n \, W_T \, . \qquad (2.36)$$
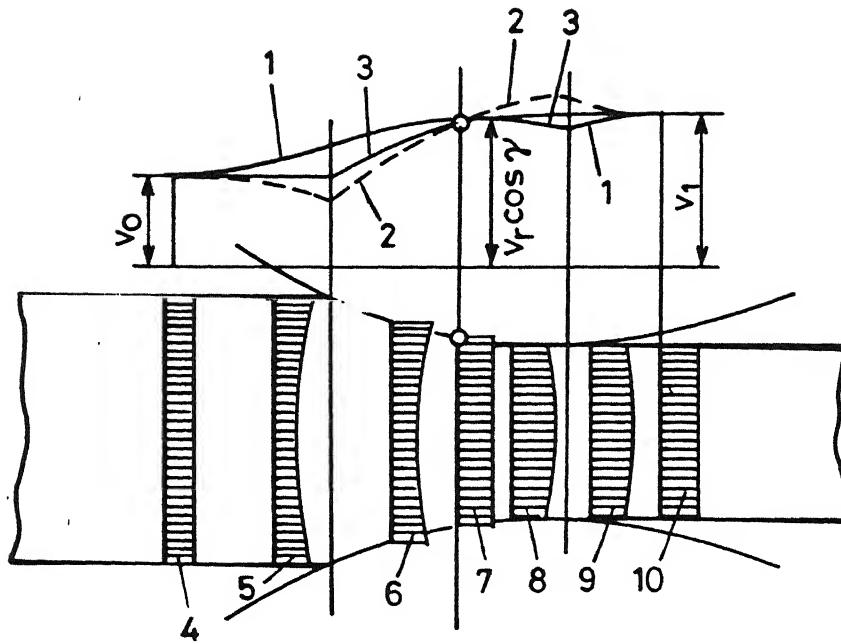
1- the velocity of the outer portions of the strip cross section ;
2- the velocity of the middle portons of the strip cross section ;
3- the mean velocity of the strip cross section; 4- velocit dia-
gram for the unstrained zone ; 5- velocity diagram for the defor-
mation zone at the entery, away from the contact zone ; 6- velocity
diagram for the zone of backward slip ; 7- velocity diagram for
the natural zone ; 8- velocity diagram for the zone of forward slip;
9- velocity diagram for the deformation zone at the exit, away
from the contact zone ; 10- velocity diagram for the unstrained
zone at the exit.

Fig. 2.1 Distribution of velocities in rolling.
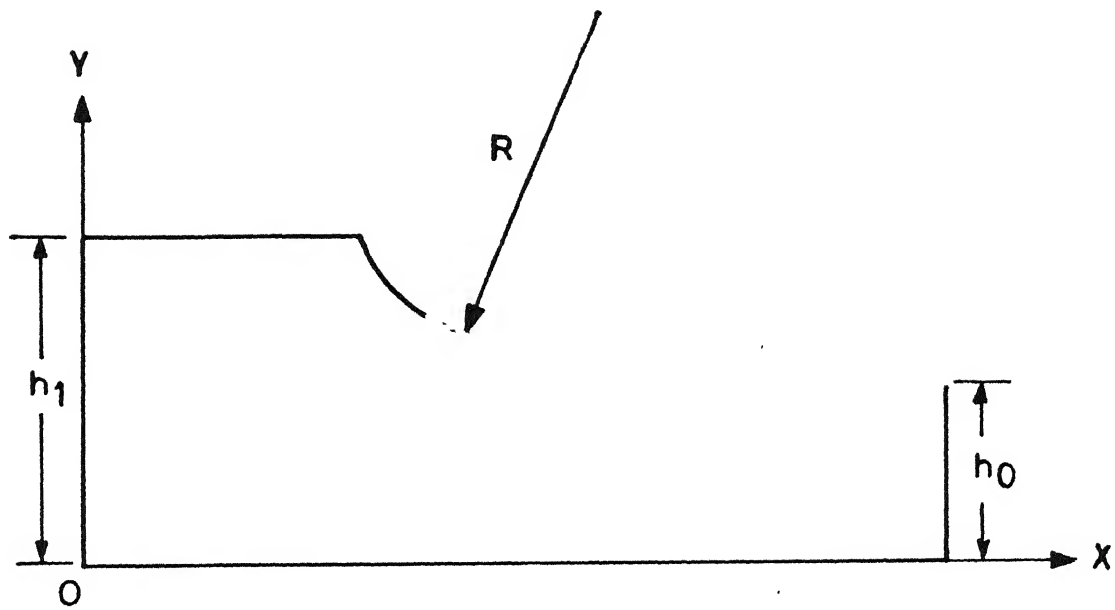
Fig. 2.2 Rectangular Cartesion coordinates for the domain
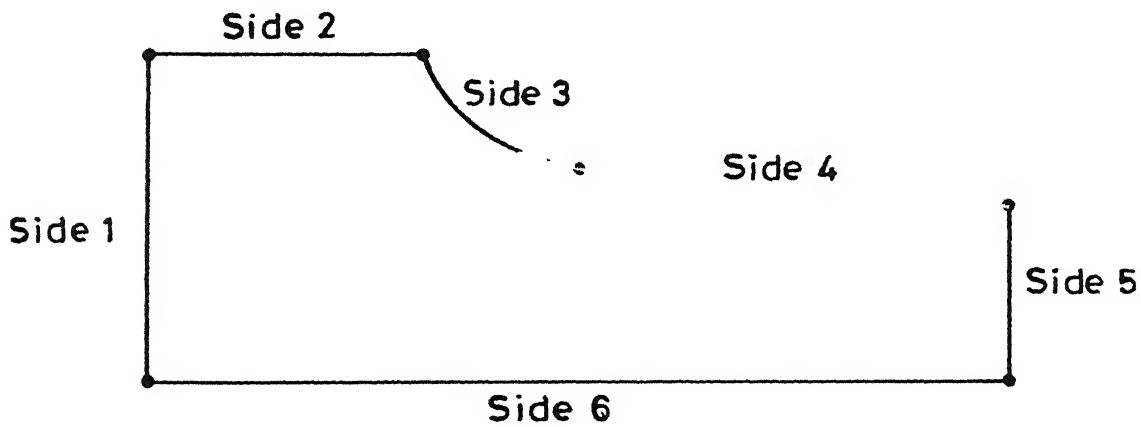
Side 1 - Entry   Side 4 - Convective boundary
Side 2 - Convective boundary   Side 5 - Exit
Side 3 - Roll-work interface   Side 6 - Axis of symmetry.

Fig. 2.3 Boundary codes for the domain.

CHAPTER III

FINITE ELEMENT MODELLING AND IMPLEMENTATION

In this chapter, the method of discretisation, shape functions and the elemental area expressions are discussed. The method adopted in applying the essential and the natural boundary conditions especially the conditions on the roll-work interface are discussed.

3.1 Discretisation and Shape Functions

We use the convergence of the variational FEM in selecting the shape functions or the convergence criteria for the Galerkin FEM are not well established. The order of the highest derivative of $\bar{p}$, $\bar{u}$, $\bar{v}$ and $\bar{T}$ is respectively zero, one, and one. For the completeness criteria, $\bar{p}$, $\bar{u}$, $\bar{v}$, $\bar{T}$ and the first derivative of $\bar{u}$, $\bar{v}$ and $\bar{T}$ should tend to non-zero values as the element size goes to zero. The compatability criteria places no restriction on $\bar{p}$ but demands that $\bar{u}$, $\bar{v}$ and $\bar{T}$ be continuous across the interelement boundaries. To satisfy the above conditions, a zeroth degree polynomial for $\bar{p}$ and linear polynomial for $\bar{u}$, $\bar{v}$ and $\bar{T}$ suffice. However, zeroth degree polynomial is not feasible in FEM. Therefore we use a linear polynomial for $\bar{p}$. To avoid certain numerical difficulties, the polynomials for $\bar{u}$, $\bar{v}$ and $\bar{T}$ should be one degree higher than that for $\bar{p}$. Therefore we choose quadratic polynomials

for $\bar{u}$, $\bar{v}$ and $\bar{T}$. For this we need 6-noded traingle as shown in fig. (3.1).

The approximations for $\bar{u}$, $\bar{v}$, $\bar{p}$, $\bar{T}$ are as follows:

$$
\begin{matrix} \bar{u} \\ \\ \bar{v} \end{matrix} = \begin{bmatrix} N_1 & 0 & N_2 & 0 & N_3 & 0 & \cdots N_6 & 0 \\ \\ 0 & N_1 & 0 & N_2 & 0 & N_3 \cdots 0 & N_6 \end{bmatrix} \begin{bmatrix} u_1 \\ v_1 \\ u_2 \\ v_2 \\ u_3 \\ v_3 \\ \vdots \\ u_6 \\ v_6 \end{bmatrix}_e
$$

i.e.,

$$\underline{\bar{V}} = \underline{\underline{N}}V \; \underline{V}^e \tag{3.2}$$

$$
\bar{p} = \begin{bmatrix} N_1^p & N_2^p & N_3^p \end{bmatrix} \begin{bmatrix} \bar{p}_1 \\ p_2 \\ p_3 \end{bmatrix}_e
$$

i.e., $\bar{p} = \underline{N}_p^T \; \underline{\bar{p}}^e$ (3.3)

and

$$\bar{T} = [N_1 \quad N_2 \quad N_3 \quad N_4 \quad N_5 \quad N_6] \begin{bmatrix} T_1 \\ T_2 \\ T_3 \\ T_4 \\ T_5 \\ T_6 \end{bmatrix}_e$$

i.e.,

$$\bar{T} = \underline{N}^T \underline{T}^e \tag{3.4}$$

Similarly the expressions for the weight functions $W_u, W_v,$ W_T and W_p are approximated as:

$$\underline{W}_V = \begin{matrix} W_u \\ W_v \end{matrix} = \underline{\underline{NV}} \; \underline{W}_V^e \tag{3.5}$$

$$W_p = \underline{N}_p^T \; \underline{W}_p^e \tag{3.6}$$

and

$$W_T = \underline{N}^T \; \underline{W}_T^e \tag{3.7}$$

The vectors $\underline{V}^e$, $\underline{T}^e$, $\underline{p}^e$ and $\underline{W}_V^e$, $\underline{W}_T^e$, $\underline{W}_p^e$ contain the nodal values of velocities, pressures, temperatures and the corresponding weights.

The expressions for the shape functions for velocity and temperature are given by:

$$N_1 = \xi_1(2\xi_1 - 1) \qquad\qquad 3.8(-$$

$$N_2 = \xi_2(2\xi_2 - 1) \qquad\qquad 3.8(\text{l}$$

$$N_3 = (1 - \xi_1 - \xi_2)(1 - 2\xi_1 - 2\xi_2) \qquad\qquad 3.8(c$$

$$N_4 = 4\xi_1\xi_2 \qquad\qquad 3.8(c$$

$$N_5 = 4\xi_2(1 - \xi_1 - \xi_2) \qquad\qquad 3.8(c$$

$$N_6 = 4\xi_1(1 - \xi_1 - \xi_2) \qquad\qquad 3.8($$

The pressure shape functions being:

$$N_1^p = \xi_1 \qquad\qquad 3.9($$

$$N_2^p = \xi_2 \qquad\qquad 3.9(\text{l}$$

$$N_3^p = 1 - \xi_1 - \xi_2 \qquad\qquad 3.9(c$$

where ξ_1 and ξ_2 are the local coordinates and are related the global coordinates $\bar{x}$ and $\bar{y}$ by the following expressions:

$$\xi_1 = a_1 + a_2\bar{x} + a_3\bar{y}$$

$$\xi_2 = b_1 + b_2\bar{x} + b_3\bar{y}$$

where

$$a_1 = (\bar{x}_2\bar{y}_3 - \bar{x}_3\bar{y}_2)/2\Omega_e /2\Omega_e, \quad b_1 = (\bar{x}_3\bar{y}_1 - \bar{x}_1\bar{y}_3)/2\Omega_e$$

$$a_2 = (\bar{y}_2 - \bar{y}_3)/2\Omega_e, \quad b_2 = (\bar{y}_3 - \bar{y}_1)/2\Omega_e$$

$$a_3 = (\bar{x}_3 - \bar{x}_2)/2\Omega_e, \quad b_3 = (\bar{x}_1 - \bar{x}_3)/2\Omega_e$$

and

$$\Omega_e = \text{area of the element} = \frac{1}{2}\{\bar{x}_1(\bar{y}_2-\bar{y}_3)+\bar{x}_3(\bar{y}_3-\bar{y}_1)\}$$

$$+ \bar{x}_3(\bar{y}_1 - \bar{y}_2)\}.$$

3.2 Elemental Area Expressions

The elemental area expressions are the contributions of the element to the left-side matrix. Before deriving the elemental area equations, the following vectors are defin for achieving compactness in the equations.

Temperature gradient vector:

$$\nabla \bar{T} = \begin{bmatrix} \dfrac{\partial \bar{T}}{\partial \bar{x}} \\[2ex] \dfrac{\partial \bar{T}}{\partial \bar{y}} \end{bmatrix} \tag{3.10}$$

Strain-rate vector:

$$\dot{\bar{\varepsilon}} = \begin{bmatrix} \dot{\bar{\varepsilon}}_{xx} \\[1.5ex] \dot{\bar{\varepsilon}}_{yy} \\[1.5ex] \sqrt{2}\ \dot{\bar{\varepsilon}}_{xy} \end{bmatrix} = \begin{bmatrix} \dfrac{\partial \bar{u}}{\partial \bar{x}} \\[1.5ex] \dfrac{\partial \bar{v}}{\partial \bar{y}} \\[1.5ex] \dfrac{1}{\sqrt{2}}\left(\dfrac{\partial \bar{u}}{\partial \bar{y}} + \dfrac{\partial \bar{v}}{\partial \bar{x}}\right) \end{bmatrix} \tag{3.11}$$

and

$$\dot{\underline{\varepsilon}}(W) = \begin{bmatrix} \dot{\overline{e}}_{xx}(W) \\ \\ \dot{\overline{\varepsilon}}_{yy}(W) \\ \\ \sqrt{2}\ \dot{\overline{\varepsilon}}_{xy}(W) \end{bmatrix} = \begin{bmatrix} \dfrac{\partial W_u}{\partial \overline{x}} \\ \\ \dfrac{\partial W_v}{\partial \overline{y}} \\ \\ \sqrt{\dfrac{1}{2}}\ (\dfrac{\partial W_u}{\partial \overline{y}} + \dfrac{\partial W_v}{\partial \overline{x}}) \end{bmatrix} \qquad (3.11b)$$

Then

$$\nabla \cdot \overline{V} = \dot{\overline{\varepsilon}}_{xx} + \dot{\overline{\varepsilon}}_{yy} + \underline{m}^T\ \dot{\overline{\varepsilon}}$$

and

$$\dot{\overline{\varepsilon}}_{xx}(W) + \dot{\overline{\varepsilon}}_{yy}(W) = \underline{m}^T\ \dot{\overline{\varepsilon}}\ (W)$$

where

$$m = \begin{bmatrix} 1 \\ 1 \\ 0 \end{bmatrix}$$

Also the following matrices are defined:

$$\underline{\underline{C}} = \begin{bmatrix} \dfrac{\partial N_1}{\partial \overline{x}} & 0 & \dfrac{\partial N_2}{\partial \overline{x}} & 0 & \dfrac{\partial N_6}{\partial \overline{x}} & 0 \\ \\ 0 & \dfrac{\partial N_1}{\partial \overline{x}} & \dfrac{\partial N_2}{\partial \overline{x}} & \cdots & 0 & \dfrac{\partial N_6}{\partial \overline{x}} \end{bmatrix} \qquad (3.12a)$$

$$\underline{\underline{D}} = \begin{vmatrix} \dfrac{\partial N_1}{\partial \bar{y}} & 0 & \dfrac{\partial N_2}{\partial \bar{y}} & 0 & \cdots & \dfrac{\partial N_6}{\partial \bar{y}} & 0 \\[4mm] 0 & \dfrac{\partial N_1}{\partial \bar{y}} & 0 & \dfrac{\partial N_2}{\partial \bar{y}} & \cdots & 0 & \dfrac{\partial N_6}{\partial \bar{y}} \end{vmatrix}$$

$$\qquad\qquad\qquad\qquad (3.12b)$$

$$\underline{a} = \begin{bmatrix} 1 \\ 0 \end{bmatrix} \qquad \text{and} \qquad \underline{b} = \begin{bmatrix} 0 \\ 1 \end{bmatrix} \qquad (3.13)$$

Substituting equations [3.2 – 3.6] into equations [3.10 – 3.11] we get,

$$\nabla \bar{\underline{T}} = \underline{\underline{H}} \ \underline{T}^e$$

$$\bar{\dot{\underline{\varepsilon}}} = \underline{\underline{B}} \ \underline{V}^e$$

and

$$\bar{\dot{\underline{\varepsilon}}} (W) = \underline{\underline{B}} \ \underline{W}_v^e$$

$$\underline{\underline{H}} = \begin{bmatrix} \dfrac{\partial N_1}{\partial \bar{x}} & \dfrac{\partial N_2}{\partial \bar{x}} & \dfrac{\partial N_3}{\partial \bar{x}} & \cdots & \dfrac{\partial N_6}{\partial \bar{x}} \\[4mm] \dfrac{\partial N_1}{\partial \bar{x}} & \dfrac{\partial N_2}{\partial \bar{x}} & \dfrac{\partial N_3}{\partial \bar{x}} & \cdots & \dfrac{\partial N_6}{\partial \bar{x}} \end{bmatrix} \qquad (3.14)$$

and

$$
B = \begin{bmatrix}
\dfrac{\partial N_1}{\partial \bar{x}} & 0 & \dfrac{\partial N_2}{\partial \bar{x}} & 0 & \cdots & \dfrac{\partial N_6}{\partial \bar{x}} & 0 \\[2ex]
0 & \dfrac{\partial N_1}{\partial \bar{y}} & 0 & \dfrac{\partial N_2}{\partial \bar{y}} & \cdots & 0 & \dfrac{\partial N_6}{\partial \bar{y}} \\[2ex]
\dfrac{1}{\sqrt{2}}\dfrac{N_1}{\bar{y}} & \dfrac{1}{\sqrt{2}}\dfrac{\partial N_1}{\partial \bar{y}} & \dfrac{1}{\sqrt{2}}\dfrac{\partial N_2}{\partial y} & \sqrt{\dfrac{1}{2}} \cdot \dfrac{\partial N_1}{\partial \bar{x}} & \cdots & \sqrt{\dfrac{1}{2}}\dfrac{\partial N_6}{\partial \bar{y}} & \sqrt{\dfrac{1}{2}}\dfrac{\partial N_6}{\partial \bar{x}}
\end{bmatrix}
$$

$$(3.15)$$

on observing the equations [2.31 – 2.33] from Chapter II it
is noted that there are some non-linear terms. These
non-linear terms can be made linear by calculating the
terms using the previous iteration values. For example
the non-linear term in equation [2.31] is linearised as
follows:

$\bar{\alpha}$ is calculated from the temperature $\bar{T}$ calculated
from previous iteration and $\underline{\bar{V}}$ is approximated as $\underline{\bar{V}}_n$
where

$$
\underline{\bar{V}}^n = \begin{bmatrix} \bar{u}_n \\[1ex] \bar{v}_n \end{bmatrix} = \underline{\underline{N}}_V \; \underline{\bar{V}}^e_n
\qquad (3.16)
$$

similarly for $\bar{T}^n$.

The other non-linear terms are also treated along
similar lines in the equations [2.32 – 2.33].

Substituting equations [3.12 – 3.16] into equations
[2.31 – 2.33] and integrating over elemental area Ω^e,
the following area equations result:

$$
B = \begin{bmatrix}
\dfrac{\partial N_1}{\partial \bar{x}} & 0 & \dfrac{\partial N_2}{\partial \bar{x}} & 0 & \cdots & \dfrac{\partial N_6}{\partial \bar{x}} & 0 \\[2ex]
0 & \dfrac{\partial N_1}{\partial \bar{y}} & 0 & \dfrac{\partial N_2}{\partial \bar{y}} & \cdots & 0 & \dfrac{\partial N_6}{\partial \bar{y}} \\[2ex]
\dfrac{1}{\sqrt{2}}\dfrac{N_1}{\bar{y}}\dfrac{\partial N_1}{\sqrt{2}\partial \bar{y}} & \dfrac{1\partial N_2}{\sqrt{2}\partial y} & \sqrt{\dfrac{1}{2}}\cdot\dfrac{\partial N_1}{\partial \bar{x}} & & \cdots & \dfrac{1}{\sqrt{2}}\dfrac{\partial N_6}{\partial \bar{y}} & \dfrac{1}{\sqrt{2}}\dfrac{\partial N_6}{\partial \bar{x}}
\end{bmatrix}
$$

$$(3.15)$$

on observing the equations [2.31 – 2.33] from Chapter II it
is noted that there are some non-linear terms. These
non-linear terms can be made linear by calculating the
terms using the previous iteration values. For example
the non-linear term in equation [2.31] is linearised as
follows:

$\bar{\alpha}$ is calculated from the temperature $\bar{T}$ calculated
from previous iteration and $\underline{\bar{V}}$ is approximated as $\underline{\bar{V}}_n$
where

$$
\underline{V}^{-n} = \begin{bmatrix} \bar{u}_n \\ \bar{v}_n \end{bmatrix} = \underline{\underline{NV}}\ \underline{\bar{V}}^e_n \tag{3.16}
$$

similarly for $\bar{T}^n$.

The other non-linear terms are also treated along
similar lines in the equations [2.32 – 2.33].

Substituting equations [3.12 – 3.16] into equations
[2.31 – 2.33] and integrating over elemental area Ω^e,
the following area equations result:

$$\int_{\Omega_e} I_1 \; d\bar{x} \; d\bar{y}$$

$$\int_{\Omega_e} I_2 \; d\bar{x} \; d\bar{y} \qquad = \qquad \underline{W}^{eT} \; \underline{\underline{k}}^e \; \underline{\Delta}^e \qquad\qquad (3.17)$$

$$\int_{\Omega_e} I_3 \; d\bar{x} \; d\bar{y}$$

where $\quad \underline{W}^e \; = \; \begin{bmatrix} W_P^e \\ W_V^e \\ W_T^e \end{bmatrix}$ and $\quad \underline{\Delta}^e \; = \; \begin{bmatrix} \bar{P}_e \\ \bar{V}_e \\ \bar{T}_e \end{bmatrix}$

The elemental matrix $\underline{\underline{k}}^e$ is given by

$$\underline{\underline{k}}^e \quad = \quad \begin{bmatrix} \underline{\underline{k}}_{11}^e & \underline{\underline{k}}_{12}^e & \underline{\underline{k}}_{13}^e \\[1em] \underline{\underline{k}}_{21}^e & \underline{\underline{k}}_{22}^e & \underline{\underline{k}}_{23}^e \\[1em] \underline{\underline{k}}_{31}^e & \underline{\underline{k}}_{32}^e & \underline{\underline{k}}_{33}^e \end{bmatrix}$$

where

$$\underline{\underline{k}}_{11}^e \quad = \quad \frac{\mu_o}{\lambda} \int_{\Omega_e} [\, \underline{N}_P \;\; \underline{N}_P^T \,] \; d\bar{A} \qquad\qquad (3.18)$$

$$\underline{\underline{k}}_{12}^e \quad = \quad \int_{\Omega_e} [\, \underline{N}_P \; \underline{m}^T \;\; \underline{\underline{B}} \,] \; d\bar{A} \qquad\qquad (3.19)$$

$$\underline{\underline{k}}_{13}^e \quad = \quad -3\alpha_o \; T_{oo} \; \int_{\Omega_e} \bar{\alpha}_n [\, \underline{N}_P \; \underline{V}_n^{eT} \;\; \underline{\underline{NV}}^T \;\; \underline{\underline{H}} \,] \; d\bar{A} \qquad\qquad (3.20)$$

$$\underset{=21}{k^e} = - \underset{\Omega_e}{\int} [\underline{\underline{B}}^T \; \underline{m} \; \underline{N}_p^T] \; d\bar{A} \qquad (3.21)$$

$$\underset{=22}{k^e} = \frac{\rho_o (\omega r) h_o}{\mu_o} \; \underset{\Omega_e}{\int} \; \bar{\rho}_n [\underline{\underline{NV}}^T \; \underline{\underline{C}} \; \underline{V}_n^{eT} \; \underline{a}^T \underline{\underline{NV}}^T + \underline{\underline{NV}}^T \underline{\underline{D}} \underline{V}_n^{eT} \underline{\underline{b}}^T \; \underline{\underline{N}}] \; d\bar{A}$$

$$+ \underset{\Omega_e}{\int} \; 2\bar{\mu} [\underline{\underline{B}}^T \; \underline{\underline{B}} - \frac{1}{3} \; \underline{\underline{B}}^T \; \underline{m} \; \underline{m}^T \; \underline{\underline{B}}] \; d\bar{A} \qquad (3.22)$$

$$\underset{=23}{k^e} = 0 \qquad (3.23)$$

$$\underset{=31}{k^e} = \underset{\Omega_e}{\int} [\underline{N}_T \; \underline{m}^T \; \underline{\underline{B}} \; \underline{V}_n^e \; \underline{N}_p^T] \; d\bar{A} \qquad (3.24)$$

$$\underset{=32}{k^e} = \underset{\Omega_e}{\int} \; 2 \; \bar{\mu}_n \{ \underline{N}_T [-\underline{V}_n^{eT} \; \underline{\underline{B}}^T \; \underline{\underline{B}} + \frac{1}{3} \; \underline{m}^T \; \underline{\underline{B}} \; \underline{V}_n^e \; \underline{m}^T \; \underline{\underline{B}}] \}d\bar{A} \qquad (3.25)$$

$$\underset{=33}{k^e} = \frac{\rho_o \, c_o \, T_\infty \, h_o}{\mu_o \, \omega r} \underset{\Omega_e}{\int} \; \bar{\rho}_n \; \bar{c}_n [\underline{N}_T \; \underline{V}_n^{eT} \; \underline{\underline{NV}}^T \; \underline{\underline{H}}] \; d\bar{A}$$

$$+ \frac{K_o \, T_\infty}{\mu_o (\omega r)^2} \underset{\Omega_e}{\int} \; \bar{K}_n \; [\underline{\underline{H}}^T \; \underline{\underline{H}}] \; d\bar{A} \qquad (3.26)$$

To convert the above equations from the global coordinates to local coordinates $\bar{x}$ and $\bar{y}$ are changed into ξ_1 and ξ_2:

$$\underset{\Omega_e}{\int} (\dots) \; d\bar{x} \; d\bar{y} = \int_0^1 \int_0^{1-\xi_2} (\dots) J \; d\xi_1 \; d\xi_2 \qquad (3.27)$$

where J = determinant of the Jacobian matrix $\begin{vmatrix} \dfrac{\partial \bar{x}}{\partial \xi_1} & \dfrac{\partial \bar{x}}{\partial \xi_2} \\[3mm] \dfrac{\partial \bar{y}}{\partial \xi_1} & \dfrac{\partial \bar{y}}{\partial \xi_2} \end{vmatrix}$

The above expressions are then evaluated by 7-point Gauss integration scheme for triangle.

$$\int_0^1 \int_0^{1-\xi_2} F(\xi_1, \xi_2)\, d\xi_1\, d\xi_2 = \frac{1}{2} \sum_{i=1}^{N_g} W_i\, F(\xi_{1i}, \xi_{2i})$$

(3.28)

where N_g = number of gauss points and W_i = Weights.

3.3 Global Assembly of Elemental Area Expression

Let $\underline{P}$, $\underline{V}$, $\underline{T}$, $\underline{W}_P$, $\underline{W}_V$ and $\underline{W}_T$ be the global matrices containing the nodal values of pressure, velocities, temperature and the corresponding weights. Define

$$\Delta = \begin{bmatrix} \underline{P} \\ \underline{V} \\ \underline{T} \end{bmatrix} \quad ; \quad \underline{W} = \begin{bmatrix} \underline{W}_P \\ \underline{W}_V \\ \underline{W}_T \end{bmatrix}$$

Then the global area expressions are:

$$\begin{array}{c} \oint_\Omega I_1\, d\bar{A} \\[3mm] \oint_\Omega I_2\, d\bar{A} \\[3mm] \oint_\Omega I_3\, d\bar{A} \end{array} = \underline{W}^T \underline{\underline{K}}\, \Delta$$

(3.29)

$$\underline{k} \;=\; \begin{bmatrix} \underline{k}_{11} & \underline{k}_{12} & \underline{k}_{13} \\[6pt] \underline{k}_{21} & \underline{k}_{22} & \underline{k}_{23} \\[6pt] \underline{k}_{31} & \underline{k}_{32} & \underline{k}_{33} \end{bmatrix}$$

The matrices $\underline{K}_{11}, \underline{K}_{12} \cdots \cdots \underline{K}_{33}$ can be obtained from corresponding elemental matrices $\underline{K}^{e}_{11}, \underline{K}^{e}_{12}, \cdots \cdots \underline{K}^{e}_{33}$ by the procedure of expansion and addition as given by the following relations:

$$\underline{K}_{11} \;=\; \sum_{e=1}^{n_e} \underline{K}^{e}_{11}$$

and

$$(K^{e}_{11})_{rs} \;=\; (k^{e}_{11})_{pq}$$

where

$$r \;=\; C'_{ep}$$
$$s \;=\; C'_{eq}$$

$$\underline{K}_{12} \;=\; \sum_{e=1}^{n_e} \underline{K}^{e}_{12}$$

and

$$(\underline{K}^{e}_{12})_{r,2s-1} \;=\; (\underline{k}^{e})_{p,2q-1}$$

$$(\underline{K}^{e}_{12})_{r,2s} \;=\; (\underline{k}^{e})_{p,2q}$$

where

$$r = C_{ep}$$

and

$$s = C_{eq}$$

$$\underline{\underline{K}}_{13} = \sum_{e=1}^{n_e} \underline{\underline{K}}_{13}^e$$

and

$$(\underline{\underline{K}}_{13}^e)_{r,s} = (\underline{\underline{k}}^e)_{p,q}$$

where

$$r = C_{ep}'$$

and

$$S = C_{eq}$$

$$\underline{\underline{K}}_{21} = \sum_{e=1}^{n_e} \underline{\underline{K}}_{21}^e$$

and

$$(\underline{\underline{K}}_{21}^e)_{2r-1,s} = (\underline{\underline{k}}_{21}^e)_{2p-1,s}$$

$$(\underline{\underline{K}}_{21}^e)_{2r,s} = (\underline{\underline{k}}_{21}^e)_{2p,s}$$

where

$$r = C_{ep}$$

$$S = C_{eq}'.$$

$$K_{22} = \sum_{e=1}^{n_e} k_{n}^{e}$$

and

$$(K_{22}^{e})_{2r-1,2s-1} = (k_{22}^{e})_{2p-1,2q-1}$$

$$(K_{22}^{e})_{2r,2s-1} = (k_{22}^{e})_{2p,2q-1}$$

$$(K_{22}^{e})_{2r-1,2s} = (k_{22}^{e})_{2p-1,2q}$$

$$(K_{22}^{e})_{2r,2s} = (k_{22}^{e})_{2p,2q}$$

where, $\quad r = C_{ep}$

$\qquad\qquad s = C_{eq}$.

$$K_{31} = \sum_{e=1}^{n_e} K_{31}^{e}$$

and $\quad (K_{31}^{e})_{r,s} = (k_{31}^{e})_{p,q}$

where, $\quad r = C_{ep}$

$\qquad\qquad s = C_{eq}'$

$$K_{32} = \sum_{e=1}^{n_e} K_{32}^{e}$$

and $\quad (K_{32}^{e})_{r,2s-1} = (k_{32}^{e})_{p,2q-1}$

$\qquad\qquad (K_{32}^{e})_{r,2s} = (k_{32}^{e})_{p,2q}$

where $\quad r = C_{ep}$

$\qquad\qquad s = C_{eq}$.

$$\underset{=33}{k} = \sum_{e=1}^{n_e} \underset{=33}{K^e}$$

$$\text{and} \quad (\underset{=33}{K^e})_{r,s} = (\underset{=33}{k^e})_{p,q}$$

$$\text{where} \quad r = C_{ep}$$

$$S = C_{eq}$$

where r, S are the global node numbers of the local nodes p,q of element e.

C is the connectivity for nodal velocity and temperature variables and C' is the connectivity for nodal pressure variable.

3.4 Element Boundary Expression

Consider a typical boundary element (fig. 3.2). The variation of $\bar{u}$, $\bar{v}$ and $\bar{T}$ along this is also quadratic. Thus

$$\bar{u} = [N_1^b \quad N_2^b \quad N_3^b] \begin{bmatrix} u_1^b \\ u_2^b \\ u_3^b \end{bmatrix}$$

i.e., $\quad \bar{u} = \underset{b}{N^T} \underset{}{u^b}$ \hfill (3.30)

Similarly,

$$\bar{v} = \underline{N}_b^T \, \underline{v}^b \tag{3.31}$$

and

$$\bar{T} = \underline{N}_b^T \, \underline{T}^b \tag{3.32}$$

For the weights:

$$W_u = \underline{N}_b^T \, \underline{W}_u^b$$

$$W_v = \underline{N}_b^T \, \underline{W}_b^b \tag{3.34}$$

and

$$W_T = \underline{N}_b^T \, \underline{W}_T^b \tag{3.35}$$

Here $\underline{u}^b$, $\underline{v}^b$, $\underline{T}^b$ and $\underline{W}_u^b$, $\underline{W}_v^b$, $\underline{W}_T^b$ are the nodal values at the boundary local nodes. The boundary shape functions are given by:

$$N_1^b = \xi(\xi - 1)/2$$

$$N_2^b = 1 - \xi^2$$

$$N_3^b = \xi(1 + \xi)/2$$

where ξ is natural coordinate of the boundary element

$$\xi = (2\tilde{\tau} - \bar{l}_b)/\bar{l}_b$$

and l_b = length of the element b.

Substituting the equations [3.30 - 3.35] into equations [2.34 - 2.36] from Chapter II, the following boundary element expressions result:

$$\int_{\tau_b} I_4 \, d\bar{\tau} + \int_{\tau_b} I_5 \, d\bar{\tau}$$

$$= \underline{W}^{bT} \, \underline{b}^b \tag{3.36}$$

$$\int_{\tau_b} I_6 \, d\bar{\tau}$$

where

$$\underline{W}^{bT} = \begin{bmatrix} \underline{W}_P^b \\ \underline{W}_u^b \\ \underline{W}_v^b \\ \underline{W}_T^b \end{bmatrix} \quad ; \quad \underline{b}^b = \begin{bmatrix} 0 \\ f_x^b \\ f_y^b \\ q^b \end{bmatrix} \tag{3.37}$$

Here

$$\underline{f}_x^b = \int_{\tau_b} \underline{N}_b \, \bar{t}_x \, d\bar{\tau} \tag{3.38}$$

$$\underline{f}_y^b = \int_{\tau_b} \underline{N}_b \, \bar{t}_y \, d\bar{\tau} \tag{3.39}$$

and

$$q^b = - \frac{K_0 \, T_\infty}{\mu_0 (\omega r)^2} \int_{\tau_b} \underline{N}^b \, \bar{q}_n \, d\bar{\tau} \tag{3.40}$$

where $\bar{t}_x$ and $\bar{t}_y$ are the tractions and $\bar{q}_n$ is the normal heat flux.

To evaluate these integrals, first we transform the coordinates from $\bar{\tau}$ to ξ

$$\int_{\tau_b} (\ldots) \, d\bar{\tau} = \int_{-1}^{1} (\ldots\ldots) \frac{l_b}{2} \, d\xi$$

and then use the three point 1-D Gauss integration Scheme.

$$\int_{-1}^{1} F(\xi) d\xi = \sum_{i=1}^{n_{gb}} W_i F(\xi_i)$$

where W_i are the weights, n_{gb} is the number of gauss points and ξ_i are the gauss points.

3.5 Evaluation of $\underline{q}^b$, $\underline{f}_x^b$ and $\underline{f}_y^b$ on the Boundaries

Referring to figure (2.3), it is observed that convective and conductive boundary conditions occur on sides 2,3 and 4. On other sides, it is either unspecified or zero as on side 6.

As on sides 2 and 4, the expression for non-dimensionalised convection is given as:

$$\bar{q}_n = \frac{h_o h}{K_o} (\bar{T}_b - 1) \tag{3.41}$$

From equation (3.32) $\bar{T}_b$ can be expressed as:

$$\bar{T}_b = \underline{N}_b^T \, \bar{\underline{T}}^b$$

Substitution of the above equation in equation (3.41) results in:

$$\underline{q}^b = - \frac{h_o h}{K_o} \int_{\tau_b} [\underline{N}_b \, \underline{N}_b^T \, d\bar{\tau}] \bar{\underline{T}}^b + \frac{h_o h}{K_o} \int_{\tau_b} \underline{N}_b \, d\bar{\tau} \tag{3.42}$$

on side 3, the non-dimensionalised heat flux equation is given by:

$$\bar{q}_n = -c_1 \, \bar{\xi}_s \, \bar{V}_s + c_2 \, (\bar{T} - 1)$$

where,

$$C_1 = \frac{\mu_o (\omega r)^2}{h_o} \quad \text{and} \quad C_2 = \frac{h_o \, K_r}{2r \, K_o}$$

The evaluation of the term $\bar{t}_s \, \bar{v}_s$ is dependent on whether the region considered is AB or BC (see fig. (3.3)) i.e., in backward slip region or forward slip region

For backward slip region, the expression for $\bar{t}_s$ is

$$\bar{t}_s - \bar{t}_x \, \sin\Theta - \bar{t}_y \, \cos\Theta$$

$$\bar{v}_s = \bar{u} \, \sin\Theta - \bar{v} \, \cos\Theta$$

and

$$\bar{q}_n = - C_1 \, \sin\Theta \, (\bar{u} \, \sin\Theta - \bar{v} \, \cos\Theta) \, \bar{t}_x + C_1 \, \cos\Theta \, (\bar{u} \, \sin\Theta - \bar{v} \, \cos\Theta)$$
$$+ C_2 \, (\bar{T} - 1)$$

$$(3.43a)$$

and similarly in forward slip region

$$q_n = C_1 \, \sin\Theta \, (\bar{u} \, \sin\Theta - \bar{v} \, \cos\Theta) \, \bar{t}_x - C_1 \, \cos\Theta \, (\bar{u} \, \sin\Theta - \bar{v} \, \cos\Theta) \, \bar{t}_y$$
$$+ C_2 (\bar{T} - 1) \qquad (3.43b)$$

Substituting equations (3.43) and (3.30-3.32) into equation (3.40) we get for backward slip region:

$$\underline{q}^b = \int_{\tau_b} [\underline{N}_b \, \sin\Theta \, \underline{N}_b^T \, \bar{t}_x] \, \underline{u}^b \, d \quad -\tau_b \int [(N_b \, \cos\Theta \, \underline{N}_b^T \, \bar{t}_y] \, \underline{v}^b \quad d\bar{\tau}$$

$$- \frac{h_o \, T_{oo} \, K_r}{2r\mu_o (\omega r)^2} \, \tau_b \int [\underline{N}_b \, \underline{N}_b^T \, \underline{T}^b] d\tilde{\tau} + \frac{h_o \, T_{oo} \, K_r}{2r \, \mu_o \, (\omega r)2} \, \tau_b \int \underline{N}_b \, d$$

$$(3.44a)$$

$$\underline{q}^b = \tau_b^\prime [-\underline{N}_b \, Sin\Theta \, \underline{N}_b \, \overline{t}_x] \, \underline{u}^b \, d\overline{\tau} - \tau_b^\prime [\underline{N}_b \, Cos\Theta \, \underline{N}_b^T \, \overline{t}_y] \, \underline{v}^b \, d\overline{\tau}$$

$$- \frac{h_o \, T_\infty \, K_r}{2\mu_o(\omega r)^2} \, \tau_b^\prime [\underline{N}_b \, \underline{N}_b^T] \, \underline{T}^b \, d\overline{\tau} \; + \; \frac{h_o \, T_\infty \, K_r}{2r\mu_o(\omega r)^2} \, \tau_b^\prime \, \underline{N}_b \, d$$

$$(3.4b)$$

The expressions for $\underline{q}^b$ contain the unknown nodal values of $\underline{u}^b$, $\underline{v}^b$, $\underline{T}^b$ and $\overline{t}_x$, $\overline{t}_y$. These terms are taken to the left-hand side after evaluating $\overline{t}_x$ and $\overline{t}_y$ from previous iteration.

Evaluation of $\underline{f}_x^b$ and $\underline{f}_y^b$ is confined now only to side 3. As on other sides it is either unspecified or zero. On side 3, we have a relation between $\overline{t}_x$ and $\overline{t}_y$. This relation is dependent on whether the region considered is backward slip or forward slip region.

For region AB, the relation between $\overline{t}_x$ and $\overline{t}_y$ is as shown below:

$$\overline{t}_s = \mu \, \overline{t}_n \quad if \quad \overline{t}_s < \frac{\sigma_y \, h_o}{\sqrt{3} \, \mu_o \omega r}$$

$$= \frac{\sigma_y \, h_o}{\sqrt{3} \mu_o \, \omega r} \quad otherwise .$$

where $\overline{t}_n$ = normal force. $= - (\overline{t}_n \, Cos\Theta + \overline{t}_y \, Sin\Theta)$

$$\therefore \quad \frac{\overline{t}_x}{\overline{t}_y} = \frac{\cos\theta - \eta\sin\theta}{\sin\theta + \eta\cos\theta} \quad \text{if} \quad \overline{t}_s < \frac{\sigma_y h_o}{\sqrt{3}\,\mu_o\,\omega r} \tag{3.15a}$$

$$\text{or} \quad \overline{t}_x - \overline{t}_y \cot\theta = \frac{\sigma_y h_o}{\sqrt{3}\,\mu_o\,\omega r} \quad \text{otherwise} \tag{3.15b}$$

Similarly for region BC, we have

$$\frac{\overline{t}_x}{\overline{t}_y} = \frac{\cos\theta + \eta\sin\theta}{\sin\theta - \eta\cos\theta} \quad \text{if} \quad \overline{t}_s < \frac{\sigma_y h_o}{\sqrt{3}\,\mu_o\,\omega r} \tag{3.16a}$$

$$\text{or} \quad \overline{t}_x - \overline{t}_y \cot\theta = -\frac{\sigma_y h_o}{\sqrt{3}\,\mu_o\,\omega r} \quad \text{otherwise} \tag{3.16b}$$

3.6 Global Assembly of Elemental Boundary Expressions

Let,

$$\begin{bmatrix} \int_{\tau_x} T_4 \, d\overline{\tau} + \int_{\tau_y} I_5 \, d\overline{\tau} \\[2ex] \int_q I_6 \, d\overline{\tau} \end{bmatrix} = \underline{W}^T (\underline{A}_1 \, \underline{\Delta} + \underline{B}_1) \tag{3.47}$$

where the matrices $\underline{W}$ and $\underline{\Delta}$ have been derived earlier. The matrix $\underline{B}$, is the assembly of the known terms in the expression for $\underline{q}^b$, on the sides 2,3 and 4 while the coefficients of $\overline{u},\underline{v}^b$ and $\underline{T}^b$ constitute to the matrix $\underline{A}_1$. These matrices are obtained by expanding the appropriate terms of $\underline{q}^b$ and adding over the relevant boundary elements.

3.7 Global Equation

Combining the equations [3.29] and [3.47] we get

$$\underline{W}^T \ \underline{K} \ \underline{\Delta} \ = \ \underline{W}^T \ [\ \underline{A}_1 \ \underline{\Delta} \ + \ \underline{B} \ ]$$

Since $\underline{W}^T \neq 0$, we have

$$\underline{K} \ \underline{\Delta} \ = \ \underline{A}_1 \ \underline{\Delta} \ + \ \underline{B}$$

or $\underline{A} \ \underline{\Delta} \ = \ \underline{B}$

where $\underline{A} \ = \ \underline{K} - \underline{A}_1$ (3.48)

3.8   Boundary Conditions

3.8.1   Special Boundary Conditions

In this section the application of the mechanical
boundary conditions on side 3 is discussed. These conditions
being the equations [3.45a, 3.45b] and [3.46a, 3.46b] and
$v_n = 0,$

i.e., $u + v \tan \theta = 0$ (3.49)

These boundary conditions are applied by making some
row operations on the middle set of equations (equations
corresponding to $\underline{V}$). Initially in the equation corresponding
to a node on side 3, both the right hand sides are unknown.
Then using equations [3.45], [3.46] and [3.49] we make the
right hand side corresponding to u-equation known. Then
u-equation is replaced by the expression [3.49].

3.8.2 Essential Boundary Conditions

The essential boundary conditions are applied by finding out the row corresponding to that variable in the global matrix and making it all zeros except for the diagonal, which is made into unity. The corresponding value of the variable is inserted in the right hand side.

For applying u-velocity condition at node R

We make $A(NOC+2*R-1,J) = 0$ for $J = 1, N$ and $J \neq NOC+2*R-1$

$$= 1 \text{ for } J = NOC+2*R-1$$

Similarly for applying V-velocity condition at node R we make $A(NOC+2*R,J) = 0$ for $J = 1, N$ and $J \neq NOC+2*R$

$$= 1 \text{ for } J = NOC+2*R$$

For applying temperature boundary condition at node R we make $A(NOC+2*NOT+R,J) = 0$ for $J=1, N$ and $J \neq NOC+2*NOT$

$$= 1 \text{ for } J = NOC + 2 * NOT + R.$$

3.9 Programme Implementation

Two programmes were developed in the process of solving the problem.

In the first program a non-frontal technique was adopted. The assembled global matrix was fully stored because of the lack of symmetry and bandedness. After applying all the boundary conditions, NAG routine FO4ARF was used for solving the equation. This routines calculates approximate solution by using Crout's Factorisation method.

The drawbacks with the program was the huge demand it places on memory and CPU time. The typical CPU time it took for 10 iterations was around 2 hours.

The second program was developed because of the drawbacks in the earlier program and the inability to increase the elements further. This program incorporated Frontal technique [11] for solving the equations. This program was much faster than the earlier program and occupied lesser core memory. The only limitation being the disk space. The main and crucial drawback with this program was that it does not do complete pivoting. This lead to erroneous calculations of nodal pressure values because the diagonal term in the continuity equations were very small owing to the penalty formulation.

Finally it was decided to stick on to the earlier program using NAG routine. All the results presented here were calculated using this program.
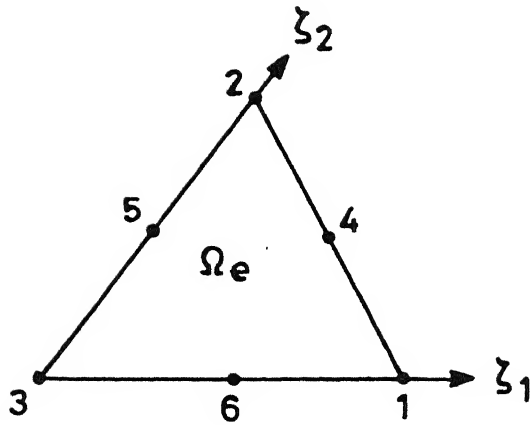
4, 5, 6 are the mid points of the corresponding sides

Fig. 3.1 Typical element e and the local node numbers.
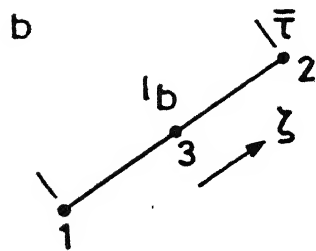
Fig. 3.2 Typical boundary element b and the boundary local node numbers.
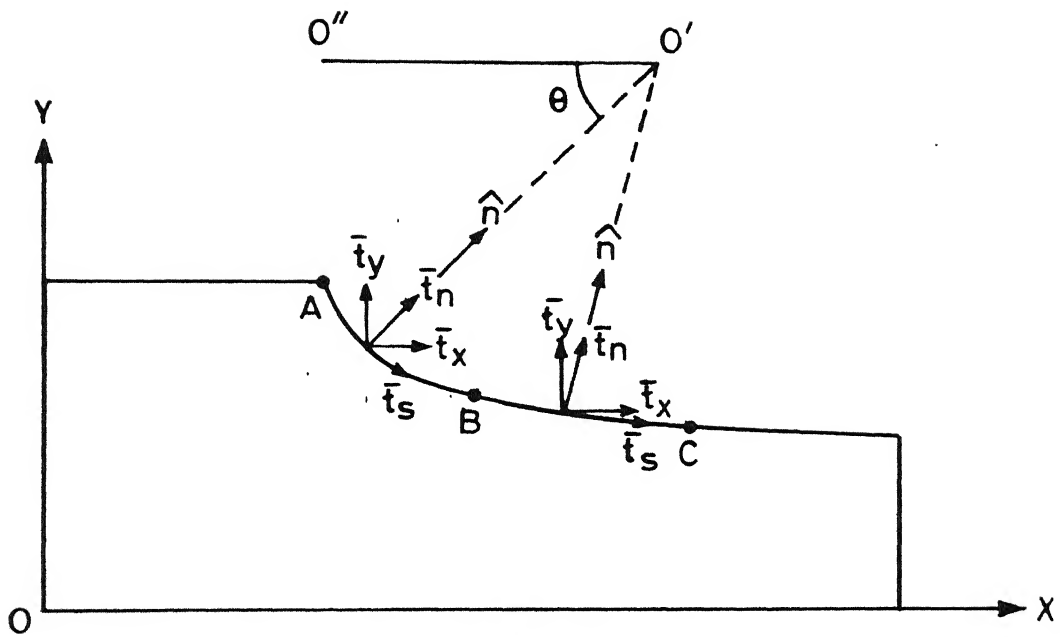
AB – forward slip region
BC – backward slip region
O'O" – horizontal datum

Fig. 3.3 Backward and forward slip regions on the roll-work interface.

CHAPTER IV

TEMPERATURE MEASUREMENT IN ROLLING

In this chapter the experimental setup along with the method adopted in measuring the temperature is discussed.

The rolling equipment used was a two-high rolling machine with hardened and lapped steel rolls. The machine has a gear arrangement to vary the reduction ratio.

The method of embedded thermocouple was used in the measurement. A Chromel-Alumel combination of thermocouple was embedded on the work material as shown in Fig. 4.1. Before the thermocouple was embedded, it was coated with a enamel paint. This formed as a insulation cover on the wire and prevented the thermocouple wire from coming in direct contact with the work material. The leads were then taken out and connected to the recorder. When the sheet was rolled, the thermocouple embedded in the work showed a temperature rise on the recorder. A sketch of the setup is shown in Fig. 4.2.

The above experiments were conducted on three pieces of aluminium strip for three different reduction ratios. The speed of the roll was kept a near constant in all the experiments. The experimentally measured values and theoretically calculated values of temperature are presented in next chapter.
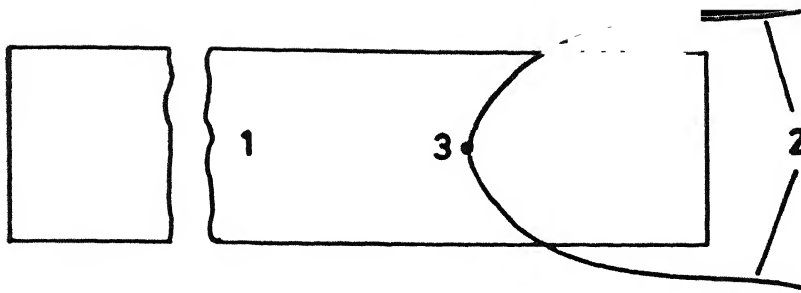
1 - Strip metal
2 - Thermocouple wires
3 - Thermocouple bead

Fig. 4.1 Arrangement of thermocouples on the work-
piece.
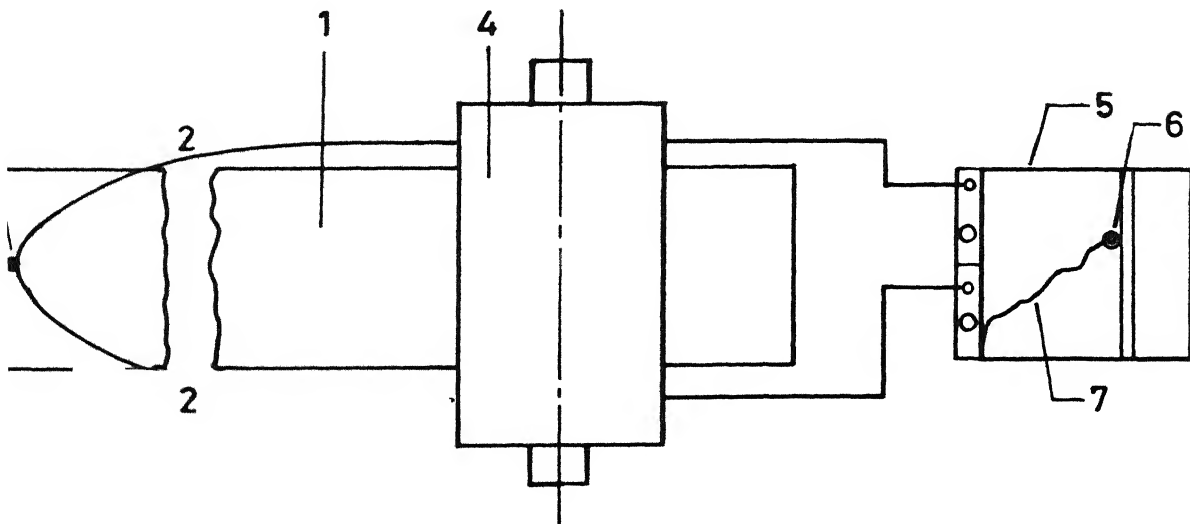
1 - Strip metal   5 - Recorder
2 - Thermocouples   6 - Pen
3 - Thermocouple bead   7 - Graph
4 - Roll

Fig. 4.2 Schematic diagram of experimental setup.

CHAPTER IV

RESULTS AND DISCUSSION

This chapter presents results for the variation of velocity and temperature along the interface. The temperature obtained by experiments are also shown. The two materials used for theoretical analysis were Aluminium and steel. Experiments were conducted only for Aluminium sheet owing to the limitations of the rolling machine.

Material Properties

Following are the thermal and mechanical properties which have been used in the analysis.

Aluminium

Yield strength : σ_y = 88.0 (MPa) (assumed to be constant)

Density at room temperature = ρ_o = 2707 (kg/m^3)

Coefficient of linear expansion = α = $(-91.0+0.38T) \times 10^{-6}$ (per^{o}C)

Specific heat = c = $674+0.6T$ (J kg^{-1} per^{o}C)

Thermal Conductivity = K_m = 239 (W/m-^{o}C) (assumed to be constant)

Steel

Yield strength = σ_y = 217-0.15T (MPa)

at room temperature = ρ_o = 7870 kg/m^3

Coefficient of linear expansion = α = $(-48+0.2T)$ per^{o}C

Specific heat = c = $296.6 + 0.48T$ J/kg-^{o}C

Thermal conductivity = K_m = $76.8 - 0.01T$.

The roll material used was medium carbon steel. Its thermal conductivity K_r was taken as 30 Joules/m/^{o}C/sec. These values were taken from TPRC Journals.

The program was executed using a 56-element mesh shown in Fig. 4.1. The results obtained experimentally for aluminium for reduction ratios 15.38%, 25% reduction compare reasonably well with the values obtained from the theoretical model.

The theoretical analysis was carried out for five different reductions of Aluminium and two different reductions of steel at various angular velocities of the roll. The graphs for temperature and velocity distribution along the interface are presented. The details

Aluminium

Case 1:
Initial thickness = 3.25 mm
Final thickness = 2.75 mm
Reduction ratio = 15.38%
Width = 50 mm
Angular velocity of the roll = 2.0944 rad/sec.
Roll radius = 65 mm.

The graphs for this case are shown in Fig. 4.2a, 4.2b and the experimentally record value is depicted in Fig.4.2c.

Case 2:
Initial thickness = 3.25 mm
Final thickness = 2.45 mm
Reduction ratio = 25%
Width of the sheet = 38 mm

Angular velocity of the roll = 2.4 rad/sec.

Roll radius   =   65 mm

The corresponding graphs for this case and Figs.4.3a,
4.3b and the experimentally recorded value in Fig. 4.3c.

Case 3: Initial thickness   =   6.274 mm

Final thickness   -   4.900 mm

Reduction ratio   =   21.86%

Width of the sheet =   38 mm

Angular velocities of the roll being 1.92308, 2.40384 and
3.8461 Rad/sec.

Roll radius   =   79.375 mm.

The corresponding graphs for this case are Figs.4.4 - 4.6.

Case 4: Initial thickness   =   6.274 mm

Final thickness   =   4.445 mm.

Reduction ratio   -   29.40%

Width of the sheet =   38 mm

Angular velocities of the roll being 1.92308, 4.40384
and 3.8461 Rad/sec.

Roll radius   =   79.375 mm.

The corresponding graphs being Figs. 4.7 - 4.9.

Case 5:   Initial thickness   =   2.032 mm

Final thickness   =   1.346 mm

Reduction ratio   =   33.75%

Width of the sheet =   38 mm

Angular velocities of the roll being 1.92308, 4.40384
and 3.8461 Rad/sec.

Roll radius   =   79.375 mm.

The figures for this being 4.10 - 4.12. In all
the above cases of the aluminium specimens, the frictional
constant was assumed to be 0.2.

Steel

Case 1:   Initial thickness   = 1.0 mm

Final thickness   = 0.84 mm

Reduction ratio   = 16%

Width of the sheet = 50 mm

Angular velocities of the roll being 2.015748, 4.031476,
5.03937 Rad/sec.

Roll radius   = 65 mm.

The figures for this case are shown in Figs. 4.13 - 4.15.

Case 2:   Initial thickness = 1.0 mm

Final thickness   = 0.76 mm

Reduction ratio   = 24%

Width of the sheet = 50 mm

Angular velocities of the roll being 2.015748, 4.031496,
5.03937 Rad/sec.

Roll radius   = 65 mm.

The figures for this case are 4. 16 - 4.18.

The frictional constant for the above three cases
being 0.08.

Discussion

An examination of the temperatures measured by experiment and predicted by theory clearly show that there is reasonable agreement. The theoretically predicted temperature profile as shown in all the cases shows an initial peak and a gradual decrease along the interface towards the exit. The experimentally measured temperature profile also shows a propensity for decreasing (along the interface) towards the exit. It is also observed that the decrease in the experimental temperature values along the interface is more gradual than the theoretical temperature values.

The velocity profiles as observed from the graphs on the interface show that there is a initial decrease and a gradual rise later towards the exit. This might be attributed to the coarse mesh adopted in the analysis. The location of neutral point where the value of the non-dimensional tangential velocity V_s is equal to unity is in good agreement with the neutral point location calculated from Avitzur's and Sim's formula.

Some of the special features noticed in the results are the decrease in the interface temperature towards exit contrary to what most of the researchers had predicted. Altan predicted almost a constant temperature distribution along the interface. Jesweith and Rice measured the

temperature rise experimentally and found the temperature
to rise slightly initially and then even out along the
interface towards exit. This might be due to the sticking
friction constraint put by Altan in his analysis. The
comparison with Jesweith and Rice's method leads to
conclusion that the thermocouple used in the present
work required longer time to respond. The other major factor
being the method of measurement. In the present work thermo-
couples were embedded in the work. In Jesweith and Rice
work the thermocouple was embedded on the roll. Thus in
our case the thermocouple bead always was lagging in velocity
with roll and came in continuous contact with the cooler
parts of the roll unlike in Jesweith and Rice's work.

The possible explanation for the drop in temperature
rise along the interface towards exit as seen in the graphs,
may be obtained from observing the velocity profiles V_s
along the interface. It is seen that the velocity gradient,
i.e., strain rate $(\frac{dV_s}{dx})$ is decreasing towards the exit. This
results in reduced plastic work and hence a drop in temperature
rise.

It is also observed from the graphs that the temper-
ature rise increases with increase in reduction ratio and
angular velocity of the roll. The temperature profiles are
smoother for lower velocities of the roll. The change in
the velocity profiles along the interface with increase in
angular velocities is hardly perceptible.

Scope for Future Work

In the present work attempts were made to predict the roll-interface pressure distribution, roll-interface frictional force distribution and roll torque but were unsuccessful. This was owing to the erroneous calculation of pressures. So a further extension to this work would be to calculate these parameters with both back and front pulls and arrive at some optimisation. Another useful extension would be to take into account the effects of strain rate and total strain in calculation of mechanical properties of the material. Further scope also lies in not assuming the 2-D constraints and using 3-D FEM technique predict the spread of the sheet metal and the sheet profile after rolling.
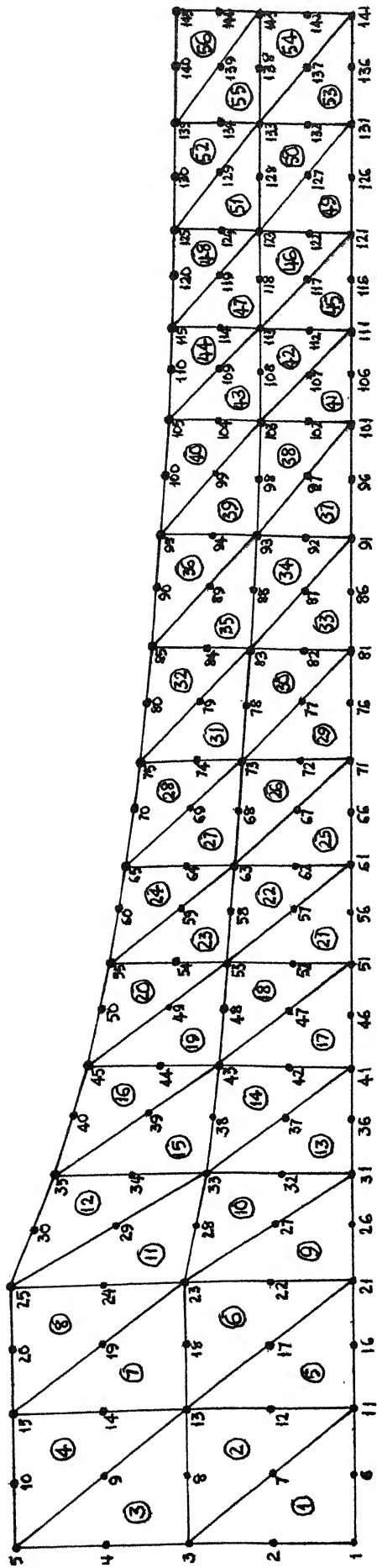
Fig 4.1   The 56-Element finite element mesh
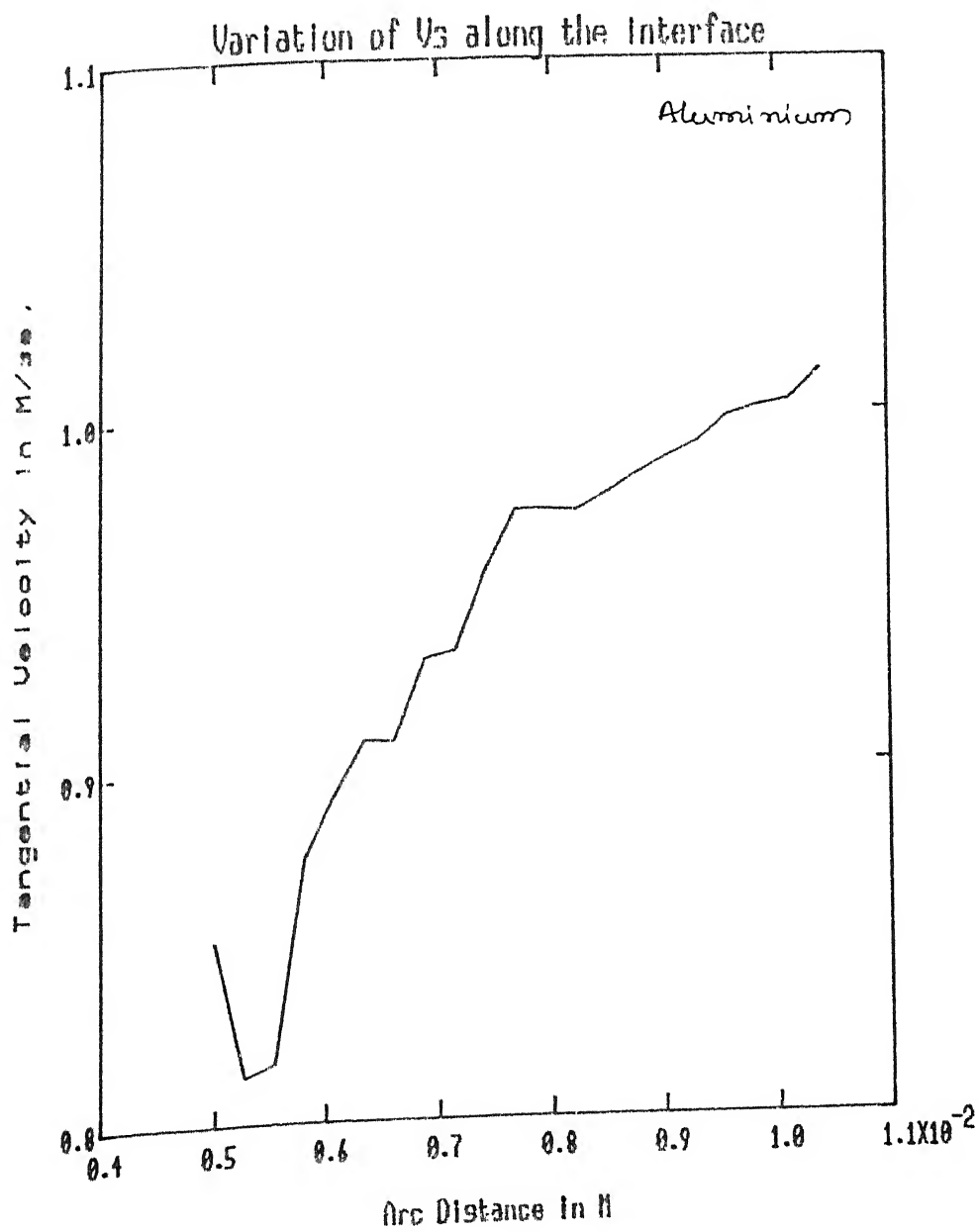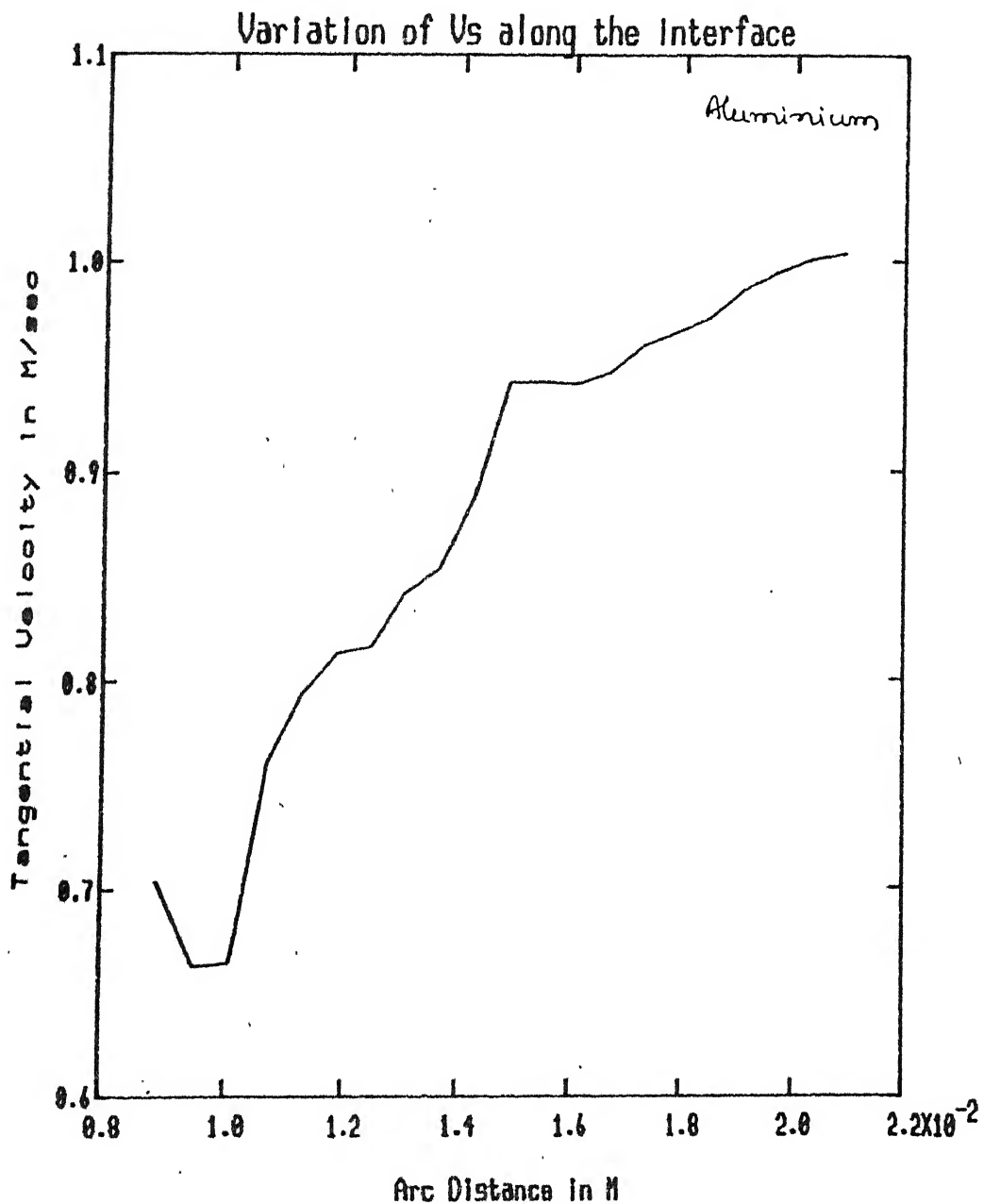
Fig. 4.2a. Variation of V_s along the Interface
Reduction ratio = 15.38%
Angular velocity of the roll = 2.0944 Rad/sec.

Variation of Temperature along the Interface
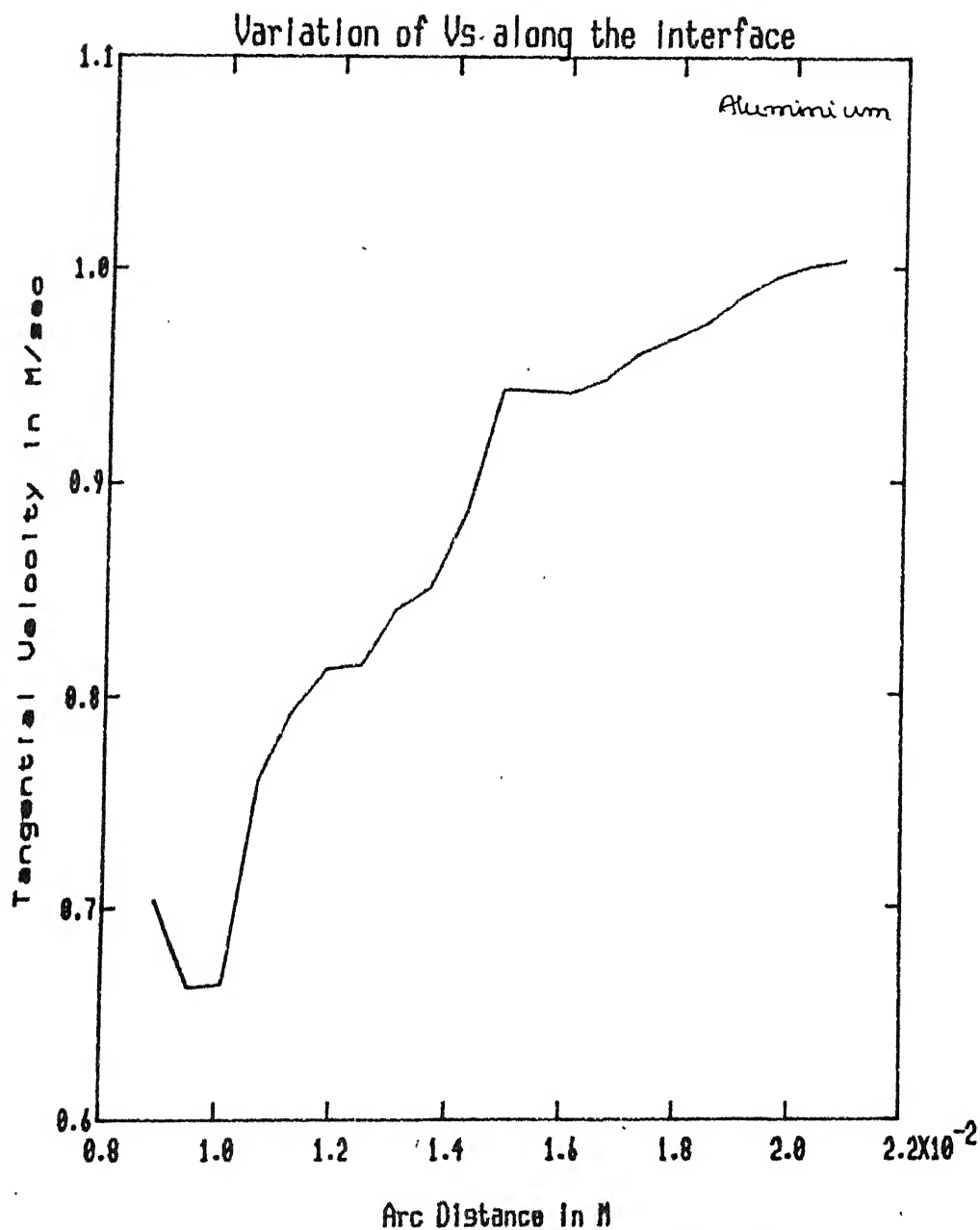
Aluminium

Temperature In Kelvi:

Arc Distance In M

4.2 b Variation of Temperature along the Interface
       Reduction Ratio = 15.38%

       Angular Velocity of the Roll = 2.0944 Rad/sec.

Sensitivity = 1mv (full scale)
Measured voltage = 0.48mv
Temperature rise = 9°c
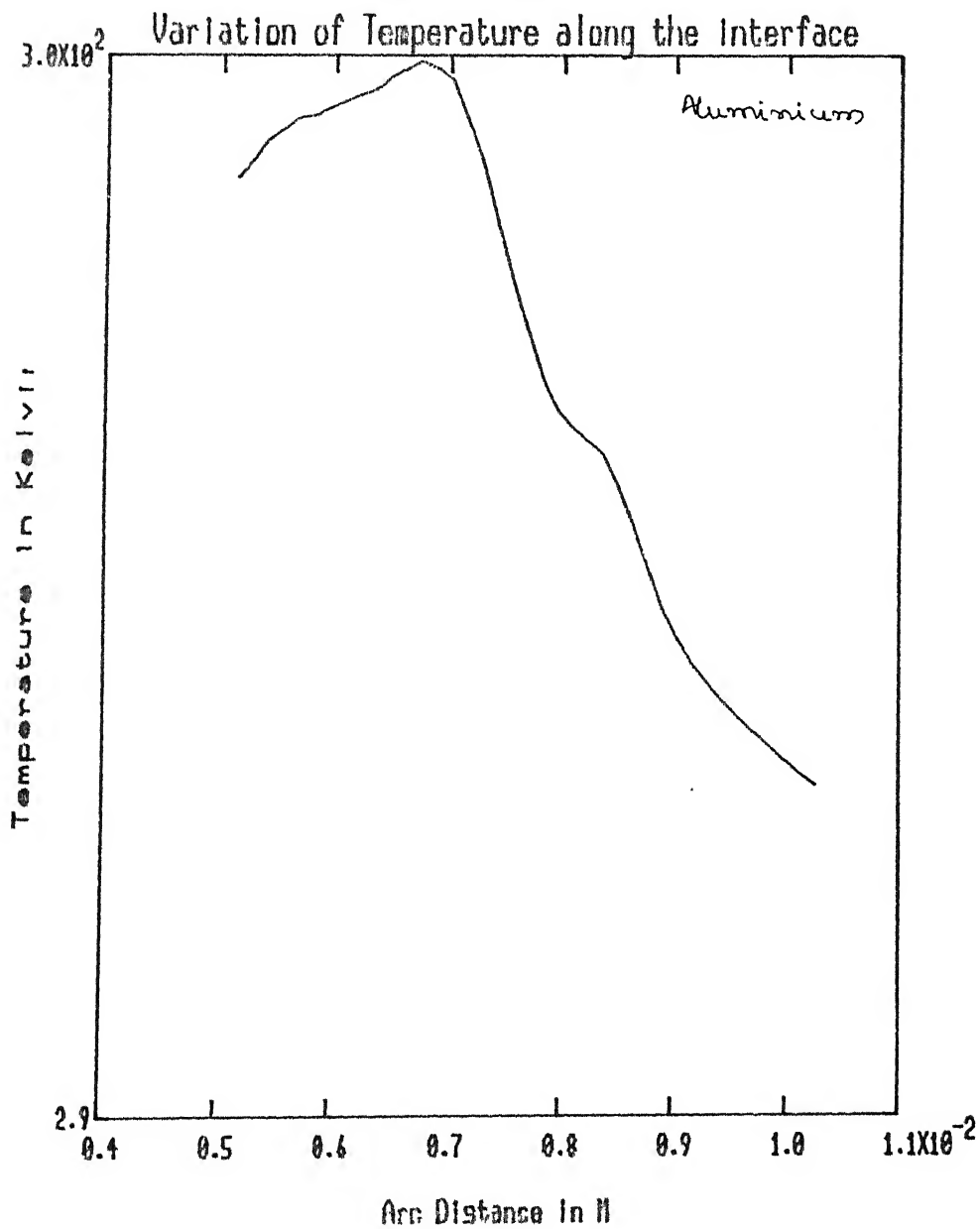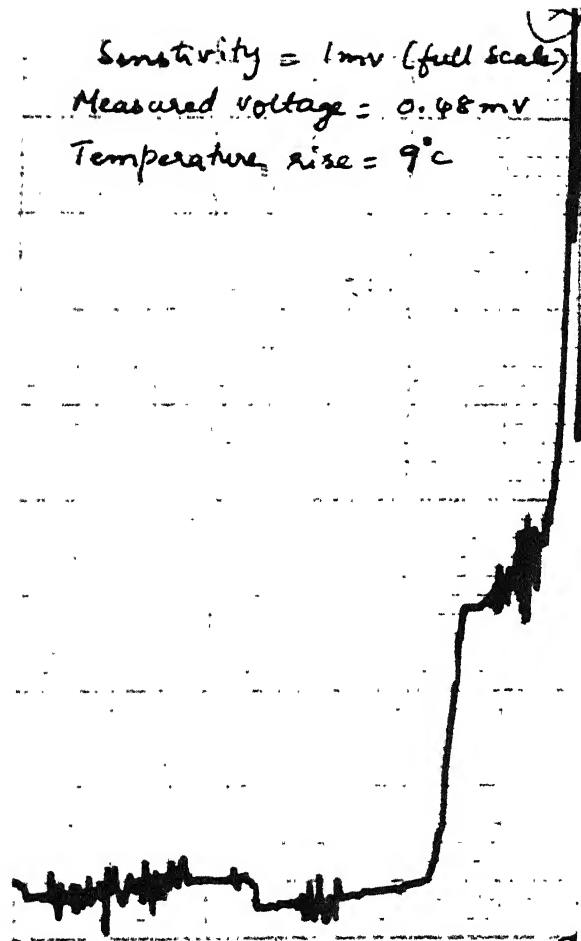
fig 4.2c EXPERIMENTALLY RECORDED GRAPH

REDUCTION = 15.38%
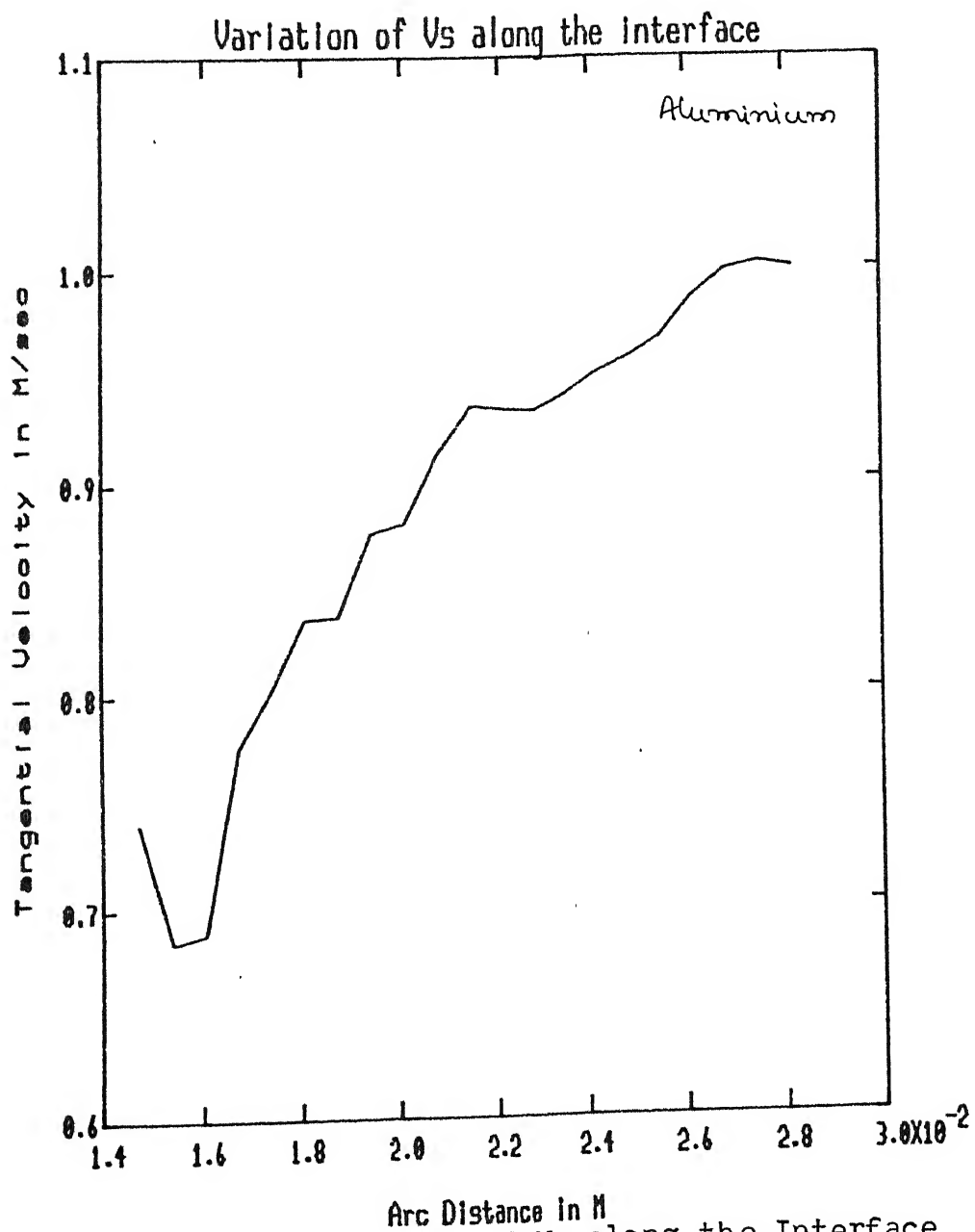
Fig.4.3a. Variation of V$_s$ along the Interface
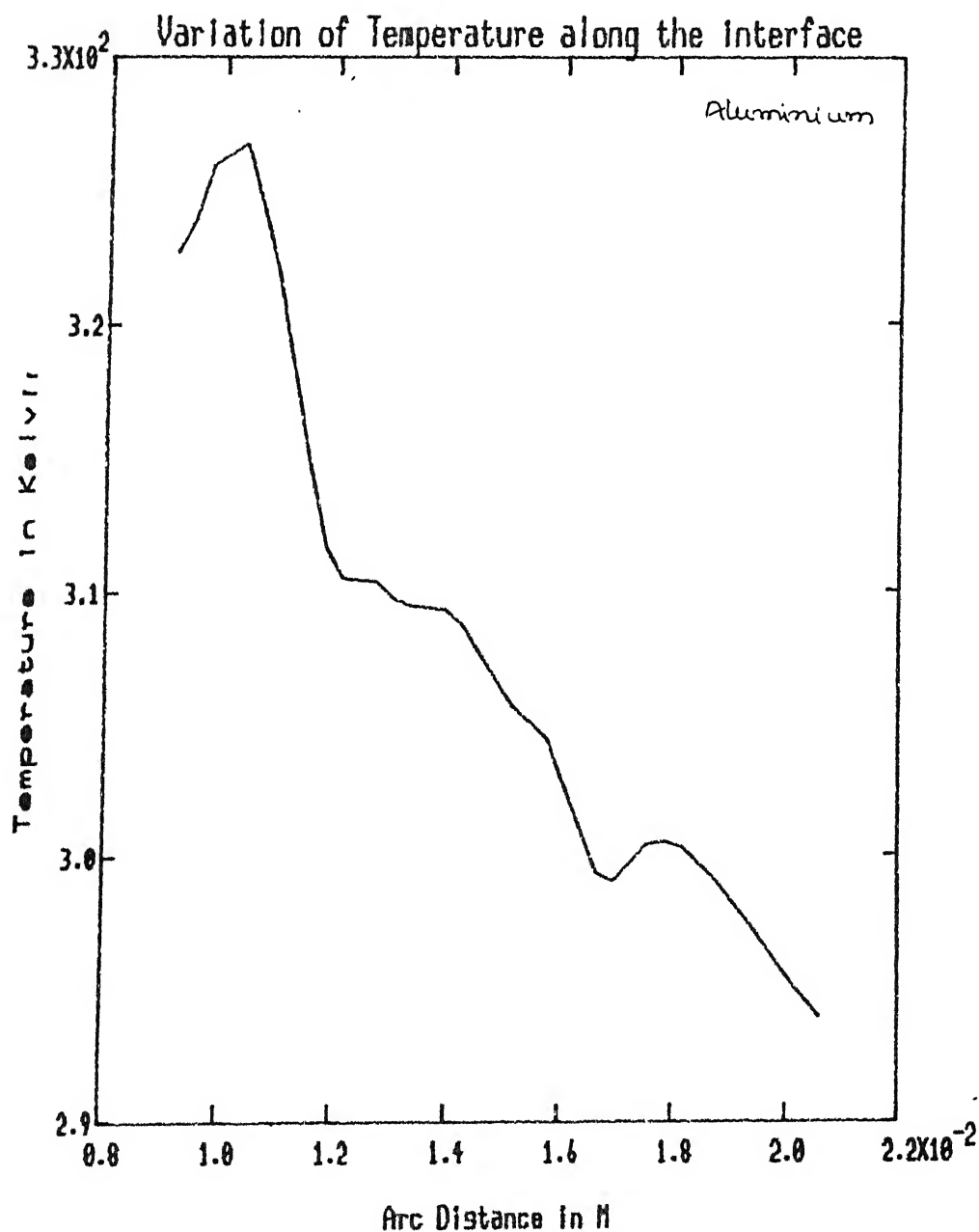Reduction ratio = 25%
Angular velocity of the roll = 2.4 Rad/sec.
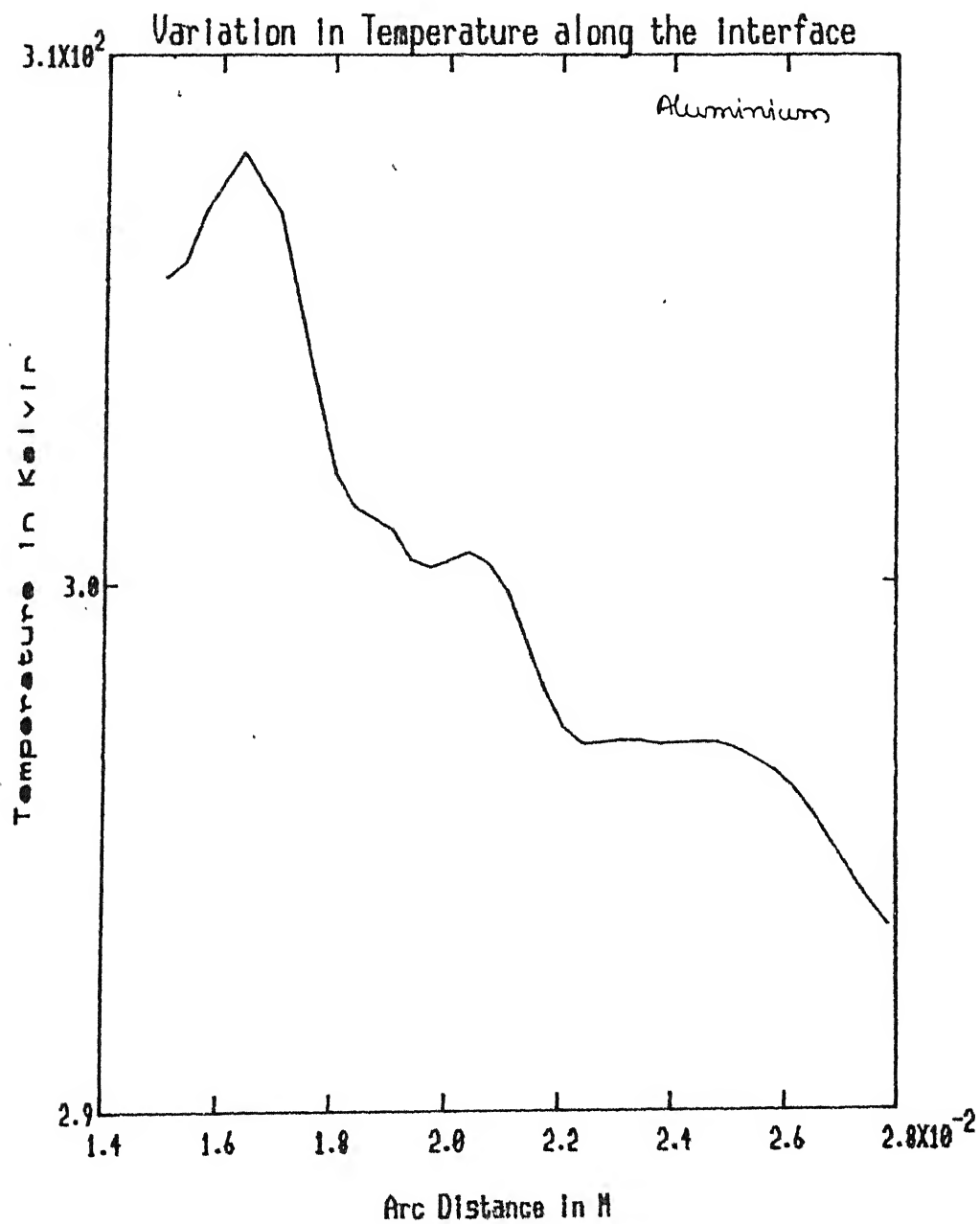
Fig.4.3b. Variation in Temperature along the Interface
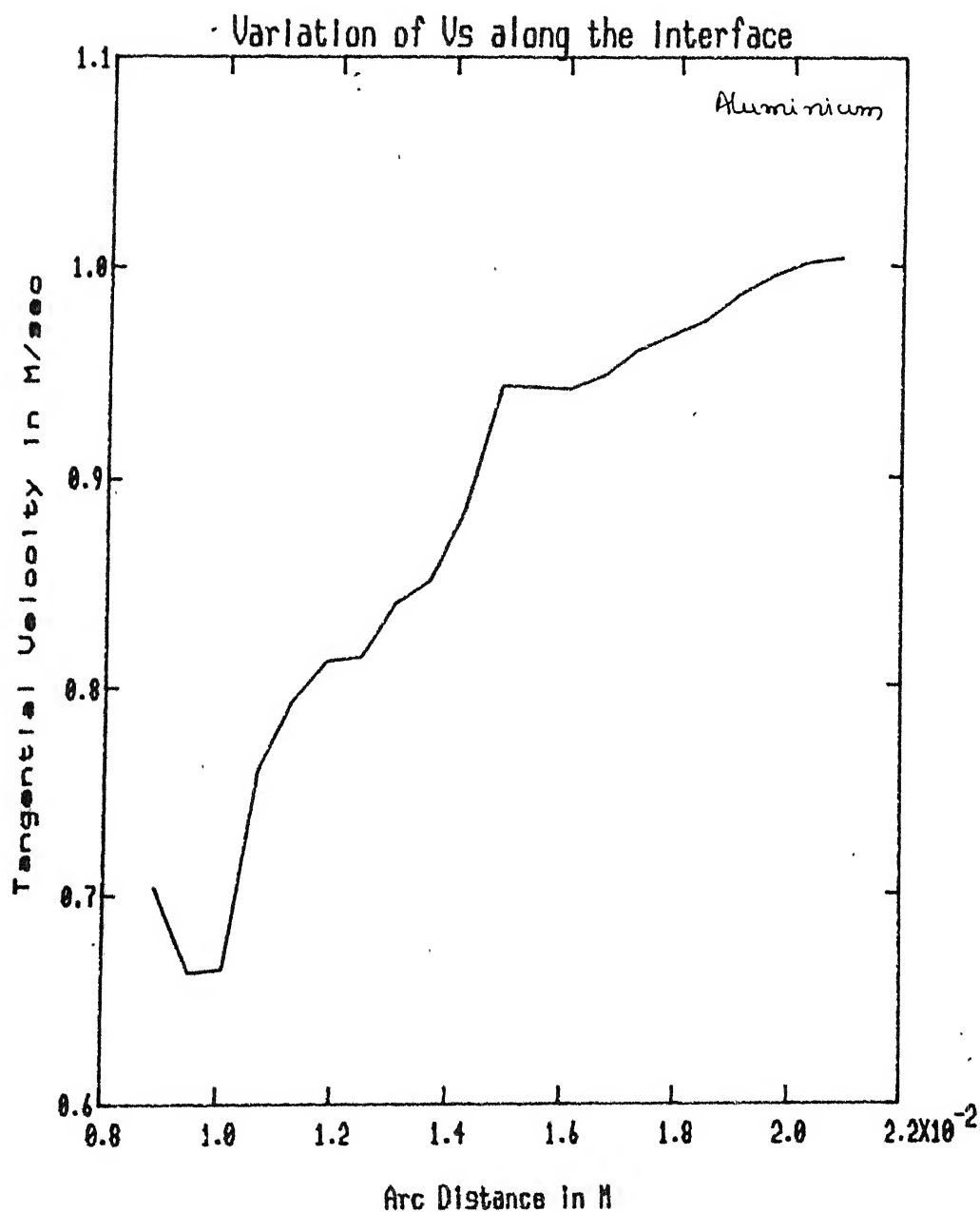Reduction ratio = 25%
Angular velocity of the roll = 2.4 Rad/sec.

Reduction Ratio =
Sensitivity = 1 mV (full scale)
Reading = 0.46 mV
Temperature rise = 12°C

Exit
Entry point
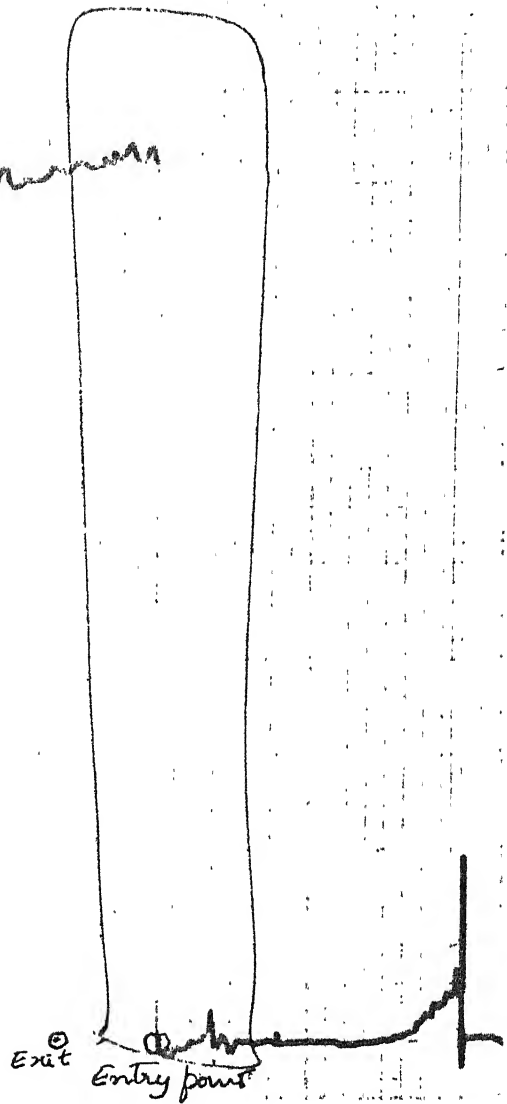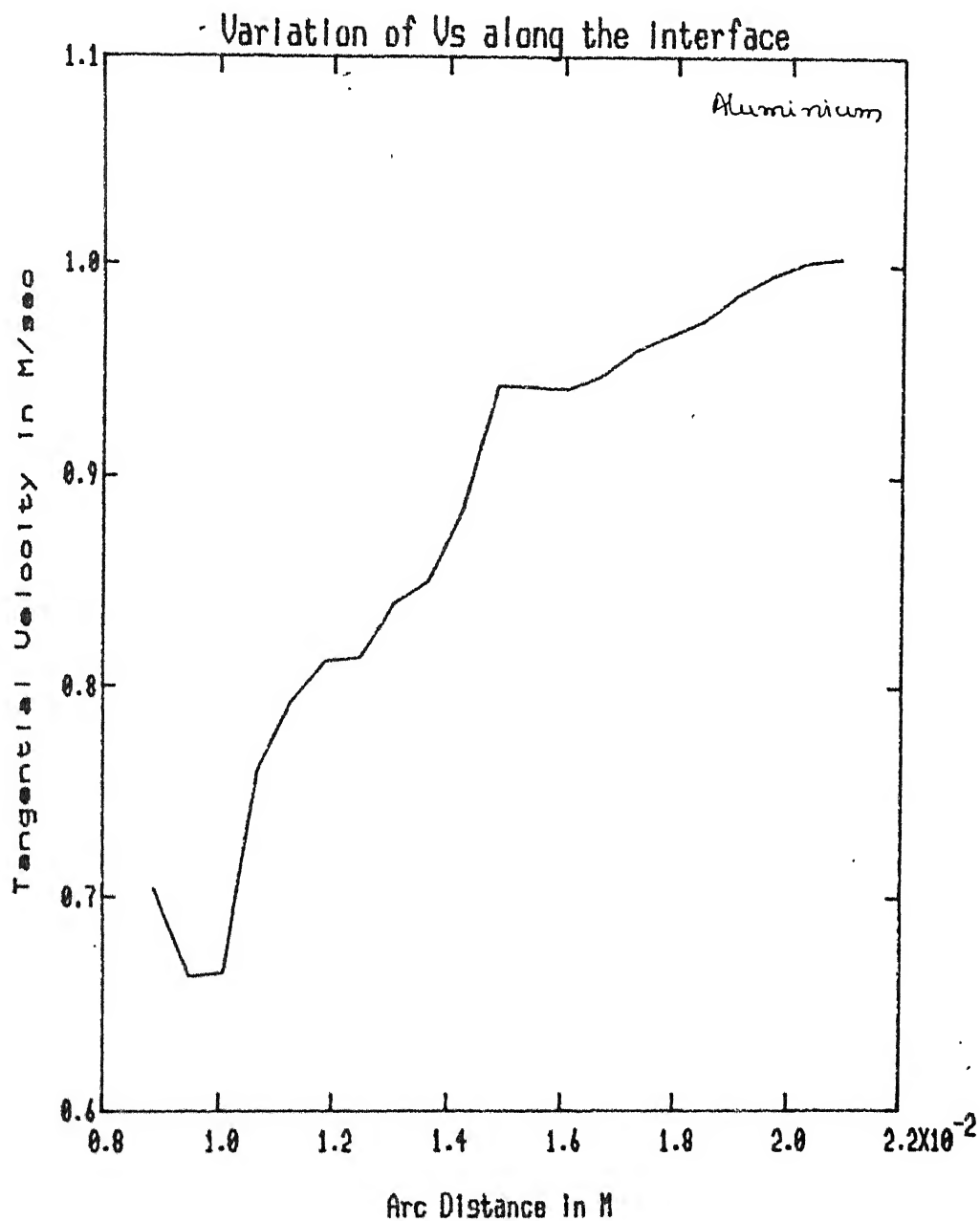
Fig 4.3c   EXPERIMENTALLY RECORDED GRAPH

REDUCTION - 75.00%
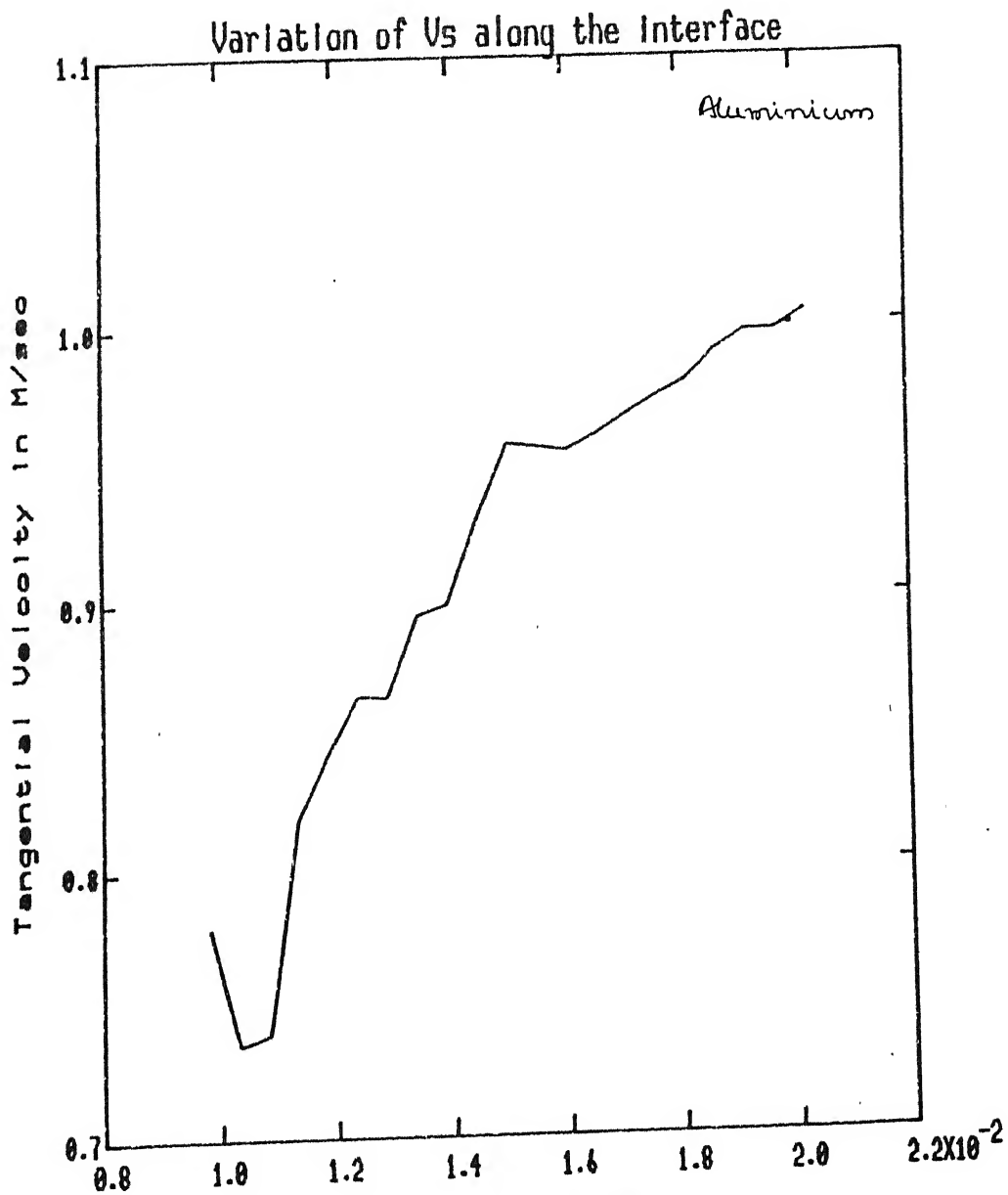
Fig. 4.7a. Variation of V_s along the Interface
Reduction ratio = 21.46%
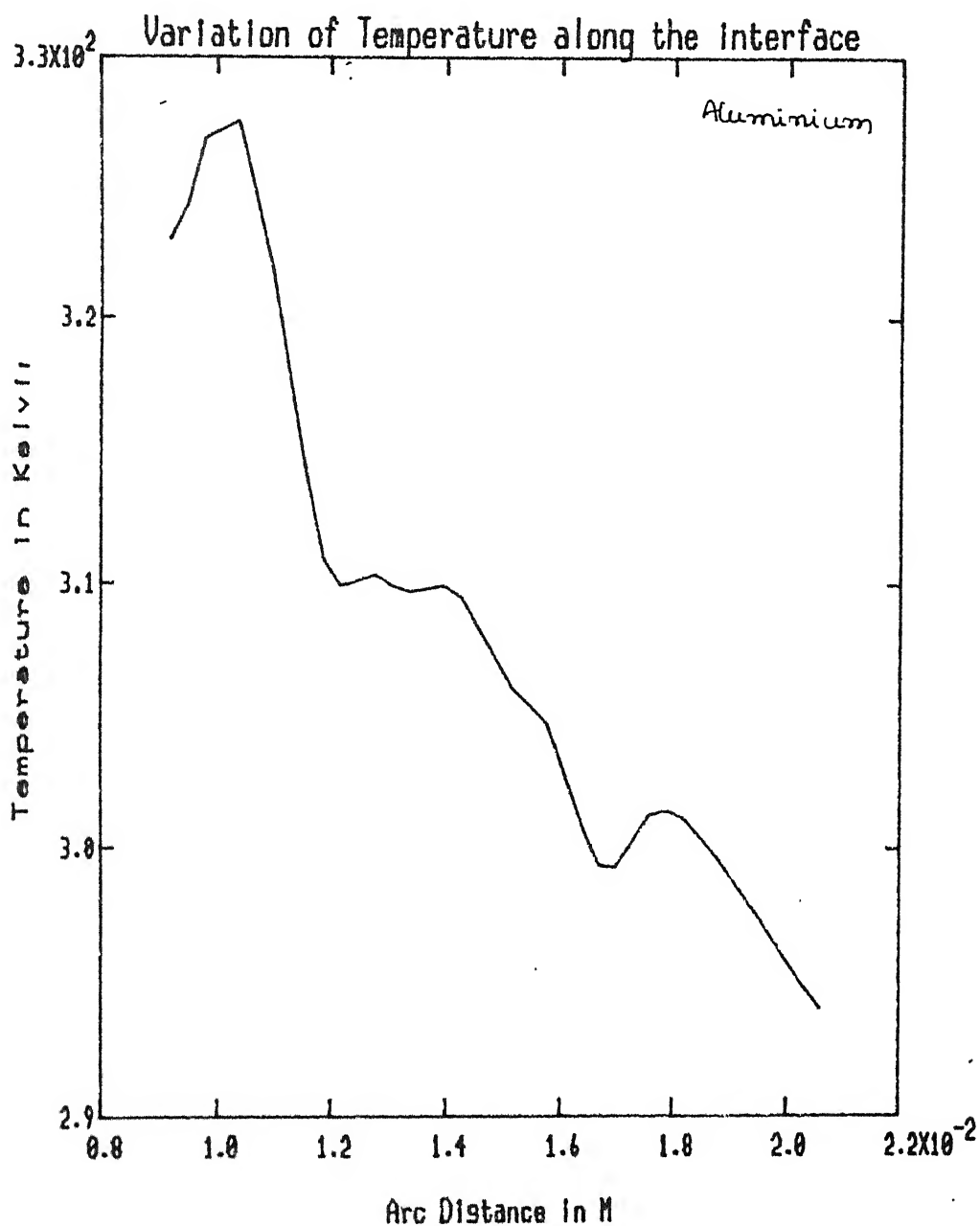Angular velocity of the roll = 1.92308 Rad/sec
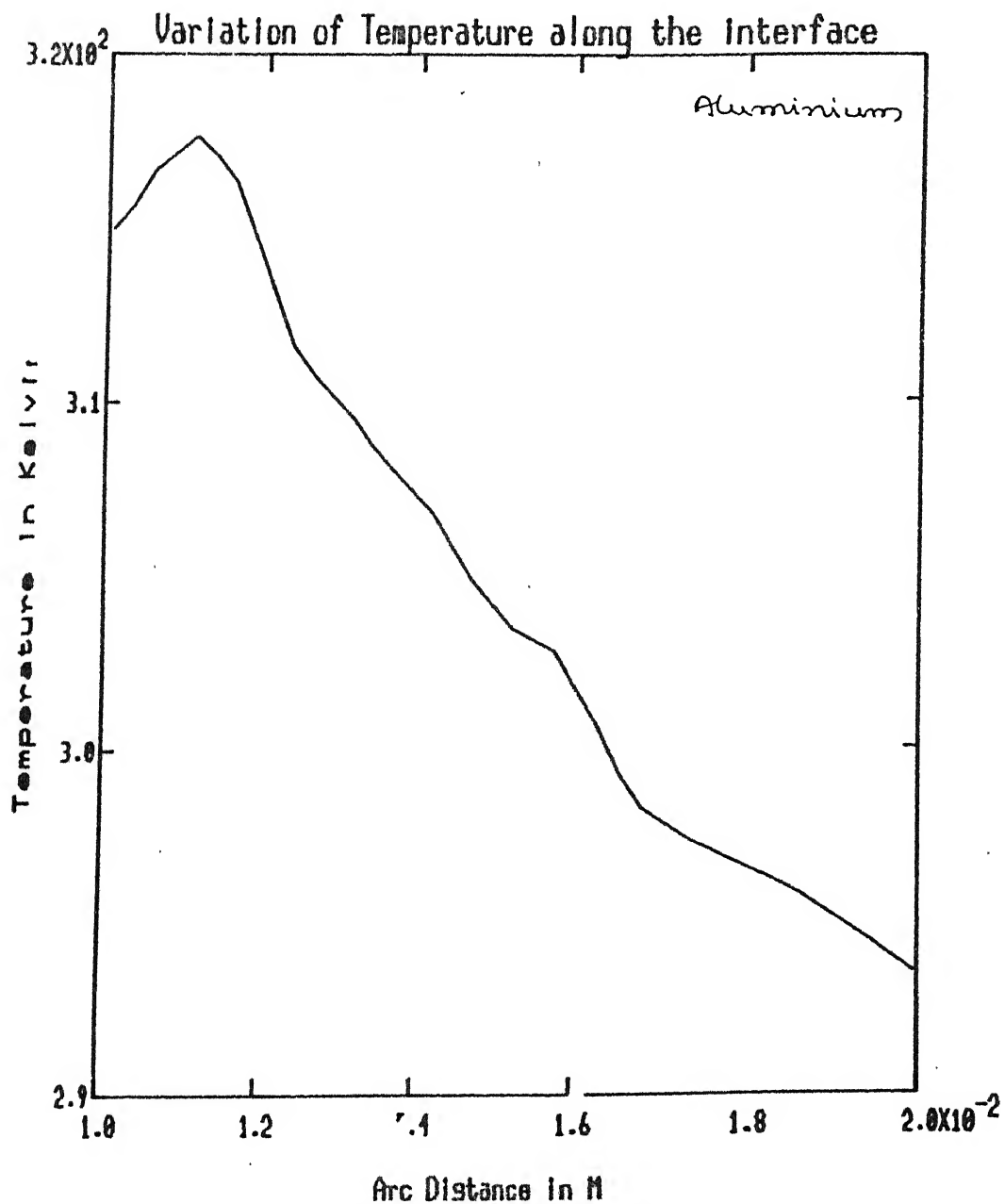
Fig. 4.7b. Variation of Temperature along the Interface
Reduction ratio = 22.86%
Angular velocity of the roll = 1.92308 Rad/s
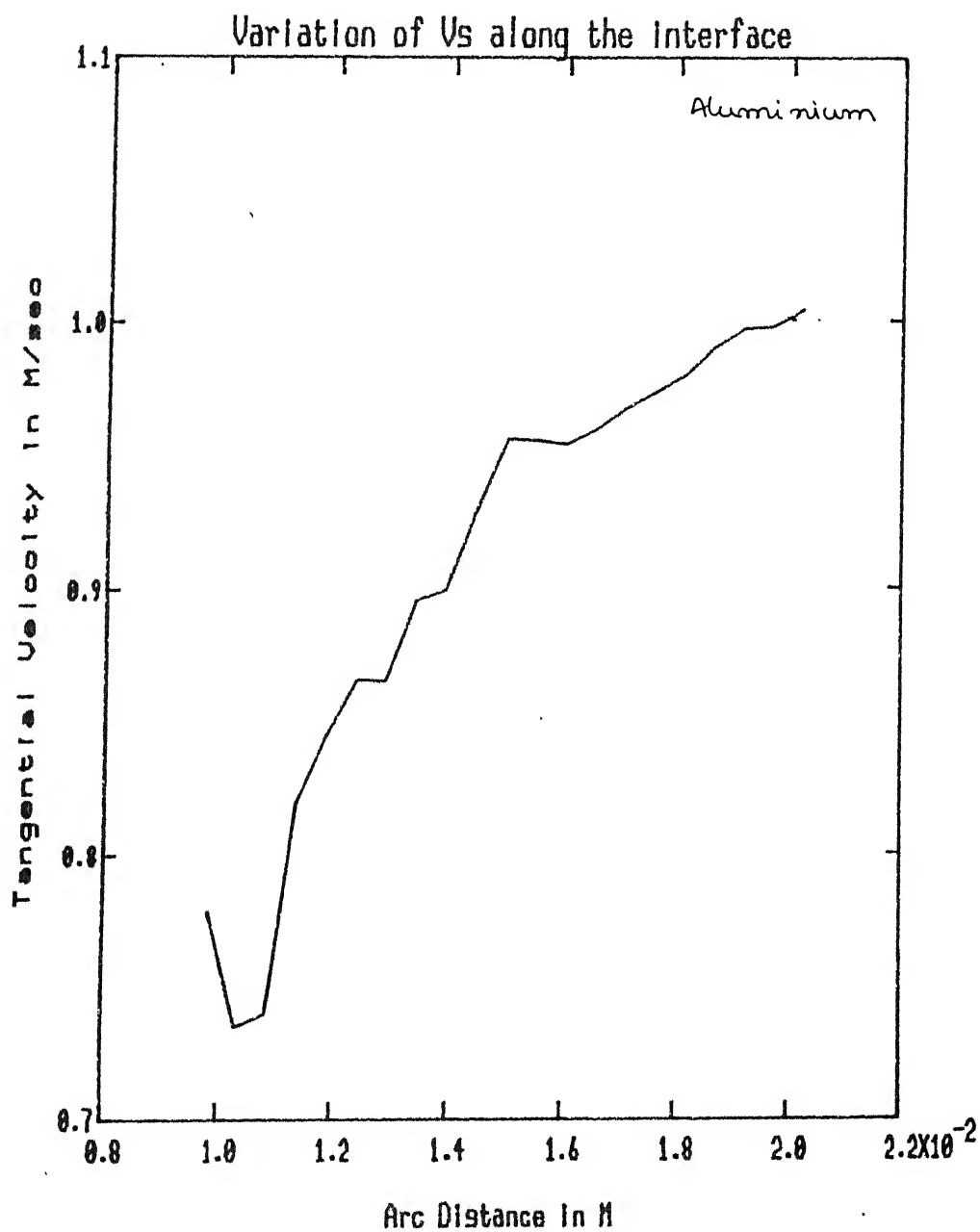
Fig. 4.5a.   Variation of V$_s$ along the Interface
Reduction ratio   =   21.86%
Angular velocity of the roll   = 2.40384 Rad/sec.
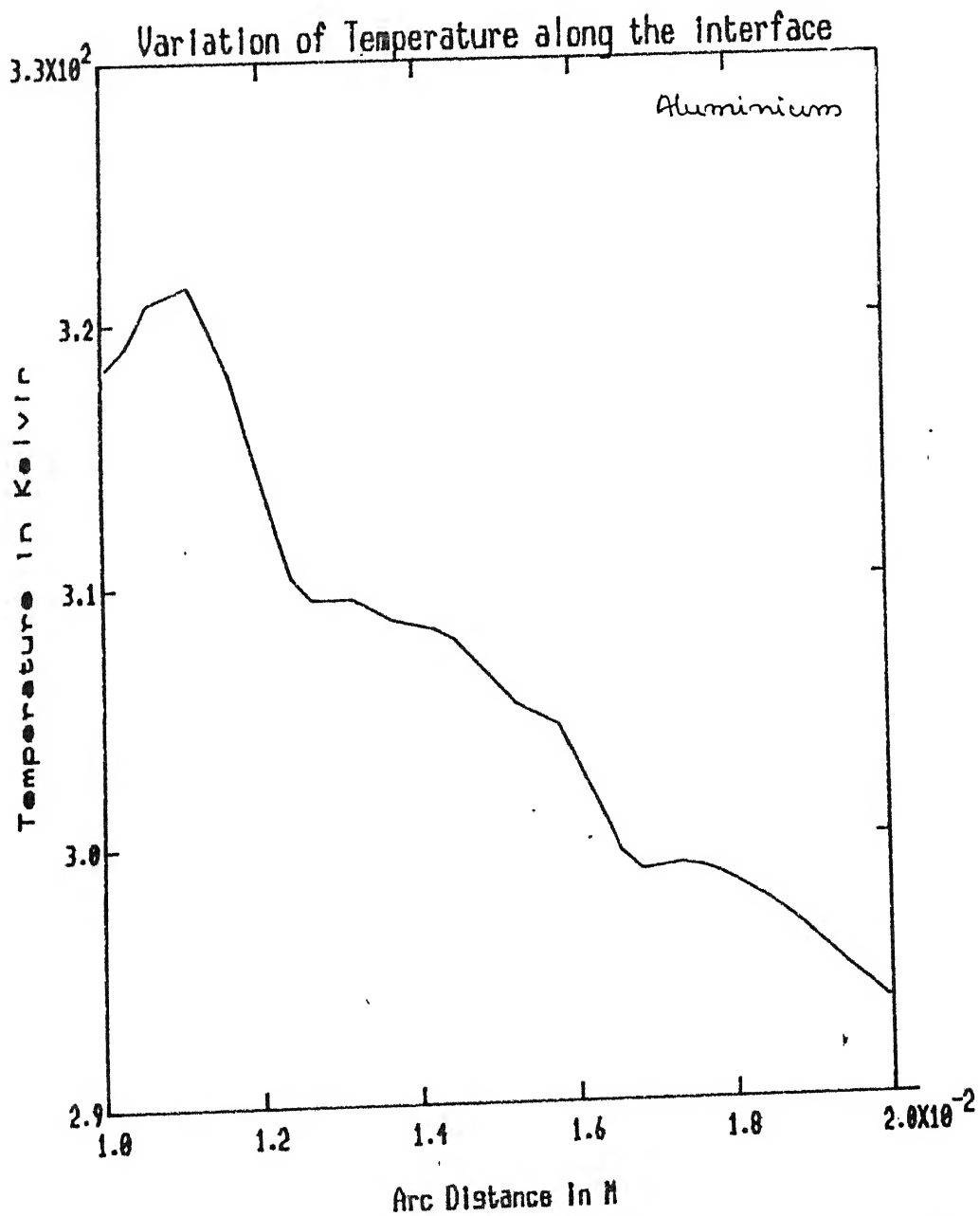
Fig. 4.5b. Variation of temperature along the interface
Reduction ratio = 21.46%
Angular velocity of the roll = 2.40384 rad/sec.
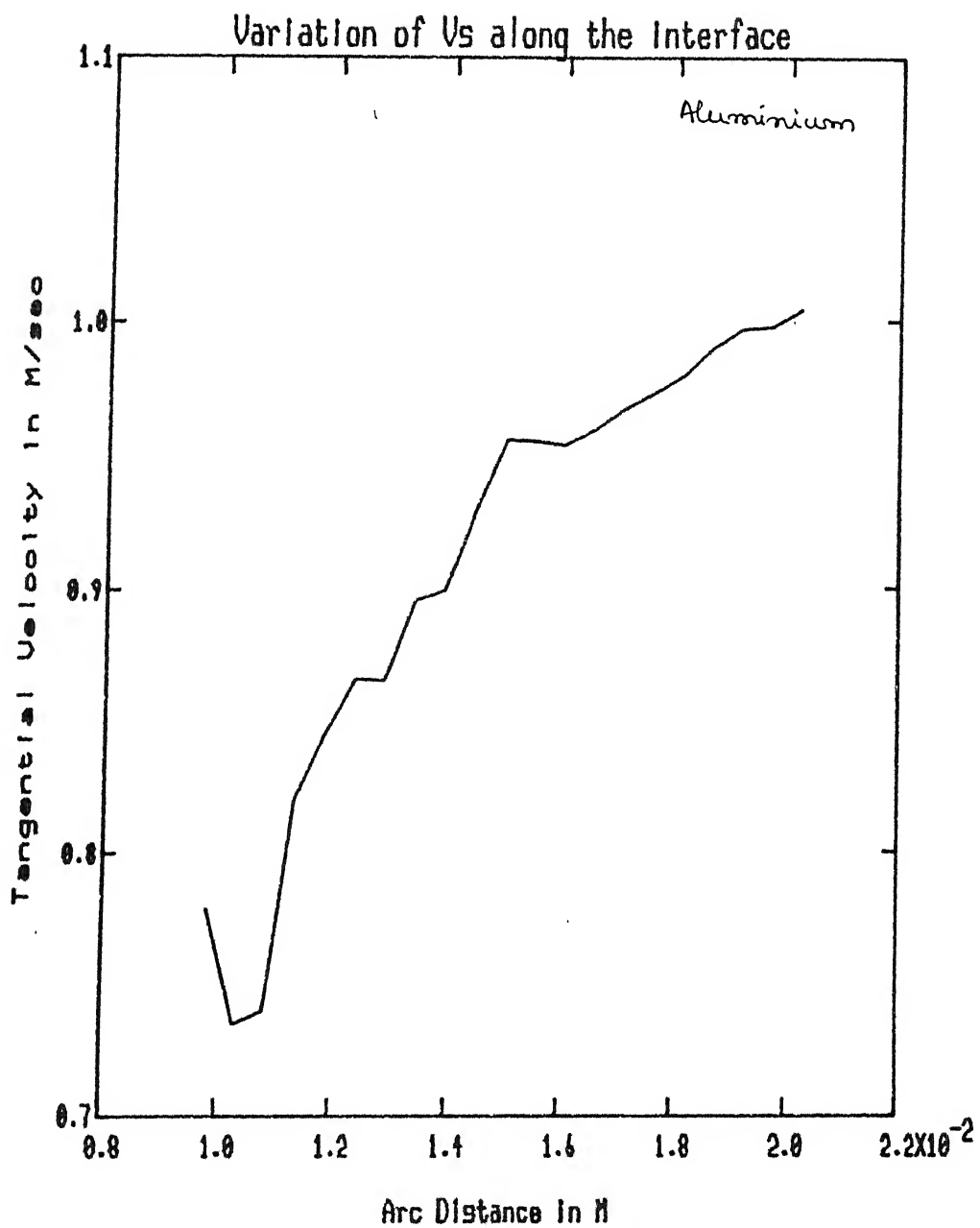
Fig. 4.6a. Variation of V_s along the interface
Reduction ratio = 29.40%
Angular velocity of the roll = 3.8461 Rad/sec.
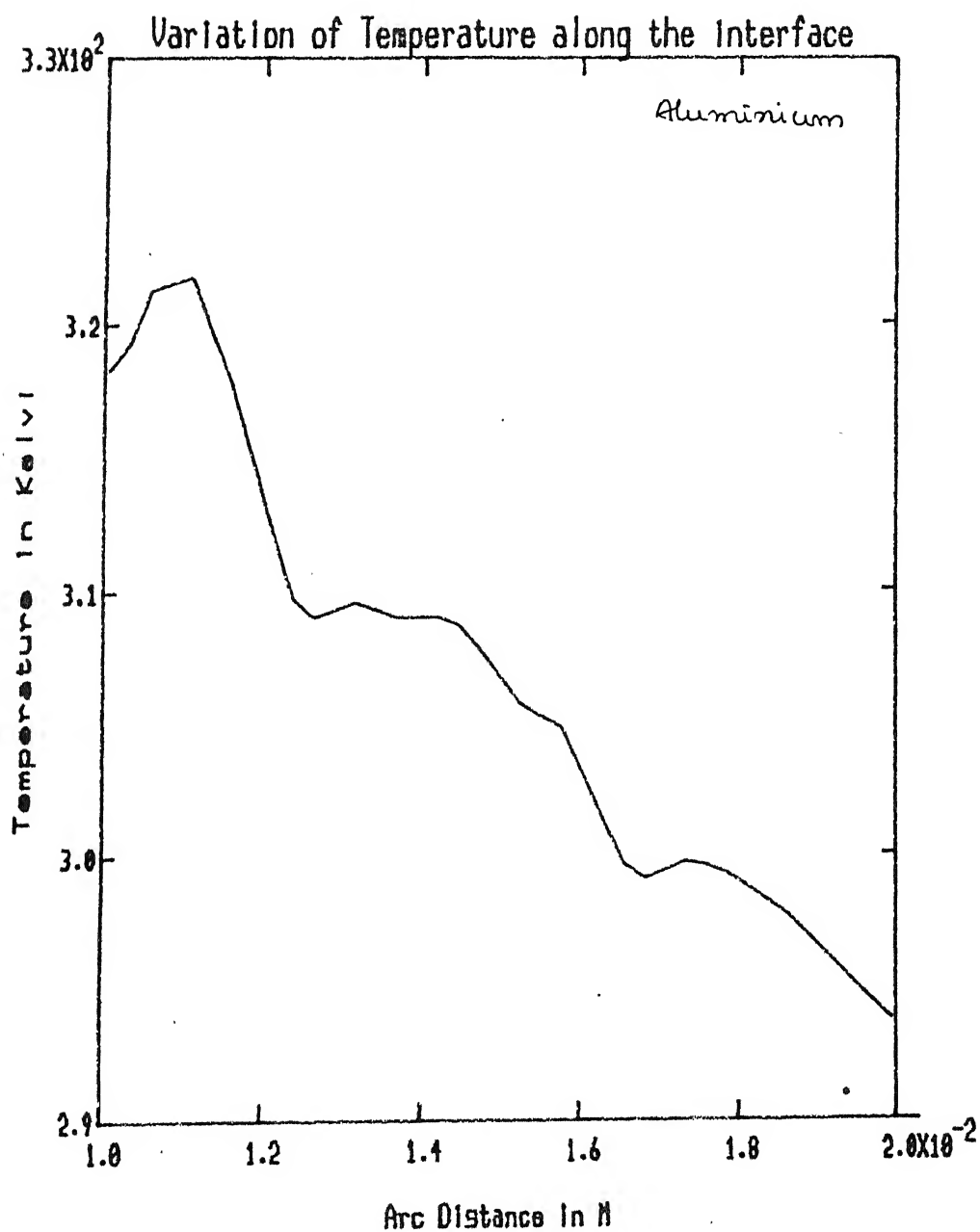
Fig. 4.6b. Variation of temperature along the
interface.
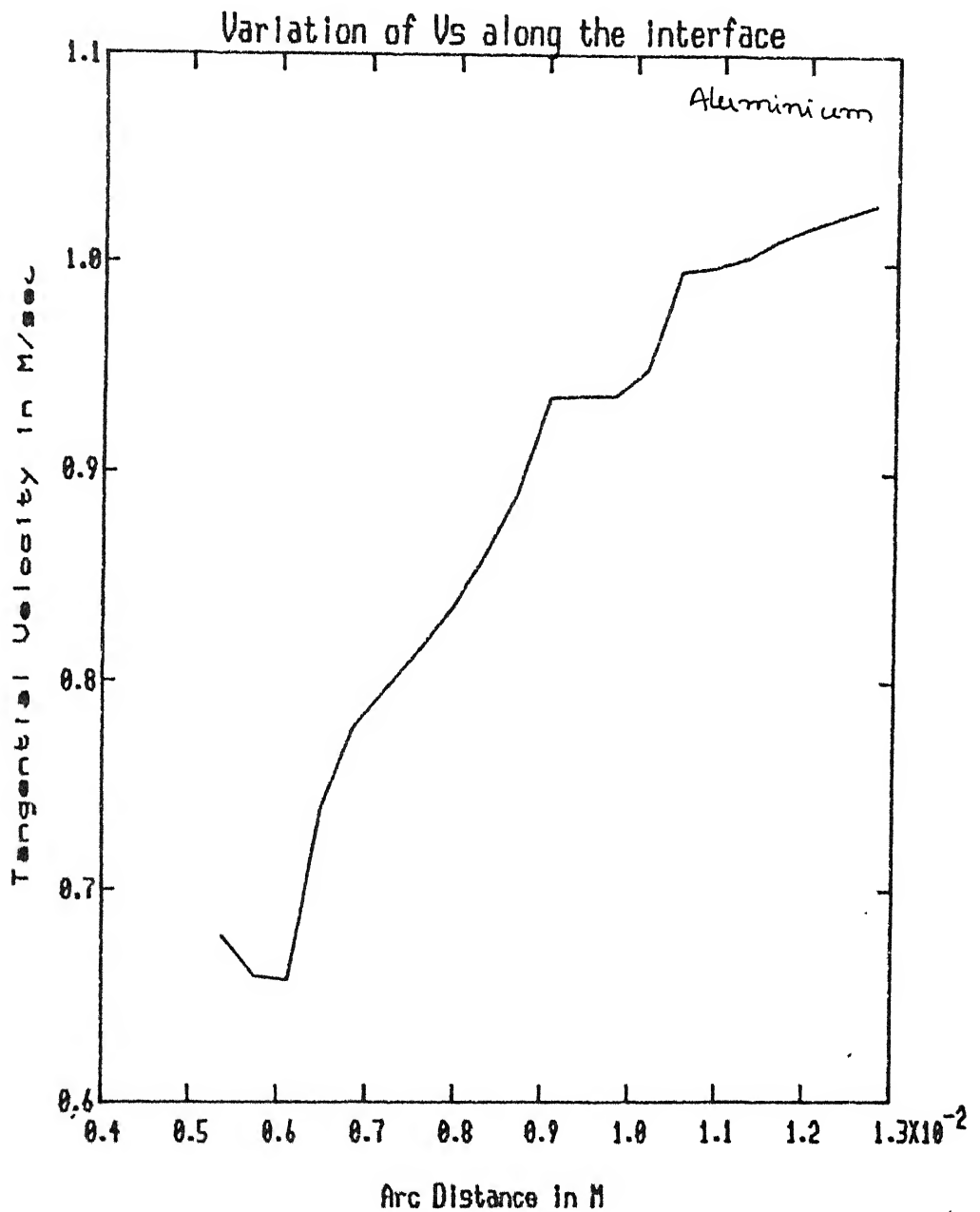Reduction ratio = 29.86%
Angular velocity of the roll = 3.8461 Rad/se

Fig. 4‑7a.   Variation of V_s along the Interface

Reduction ratio   =   29.46%
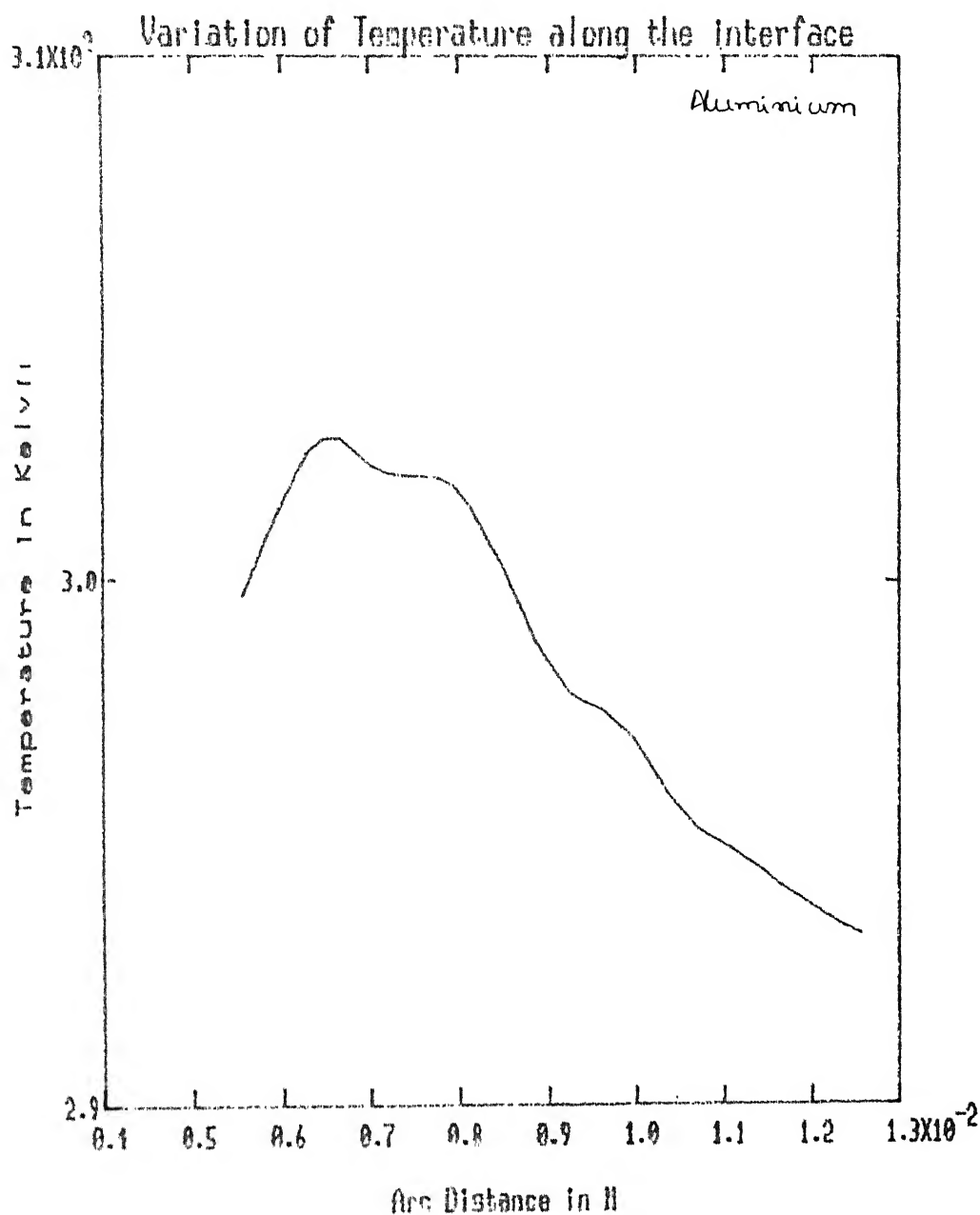Angular velocity of the roll   = 1.92308 rad/sec
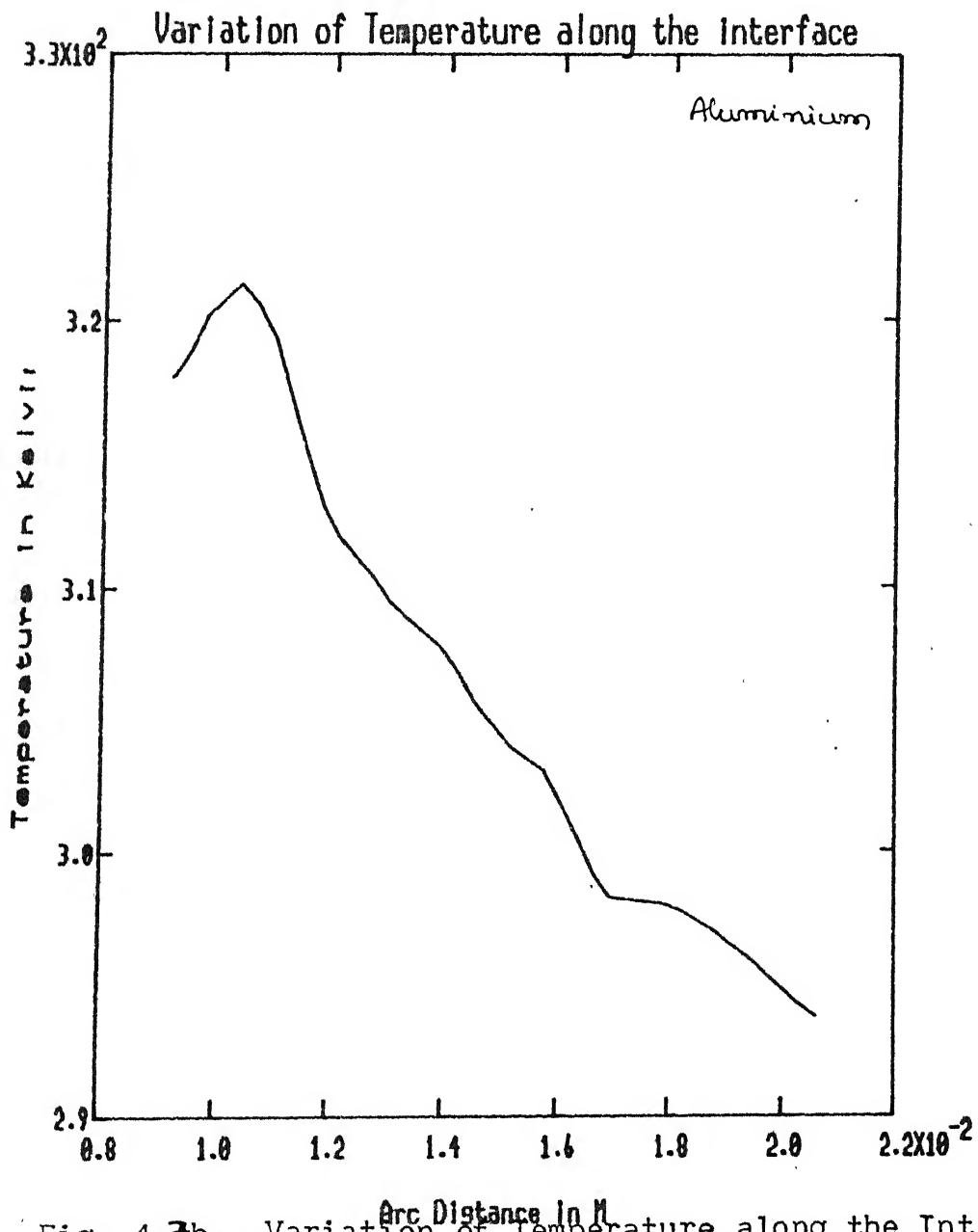
Fig. 4.7b. Variation of Temperature along the Interface
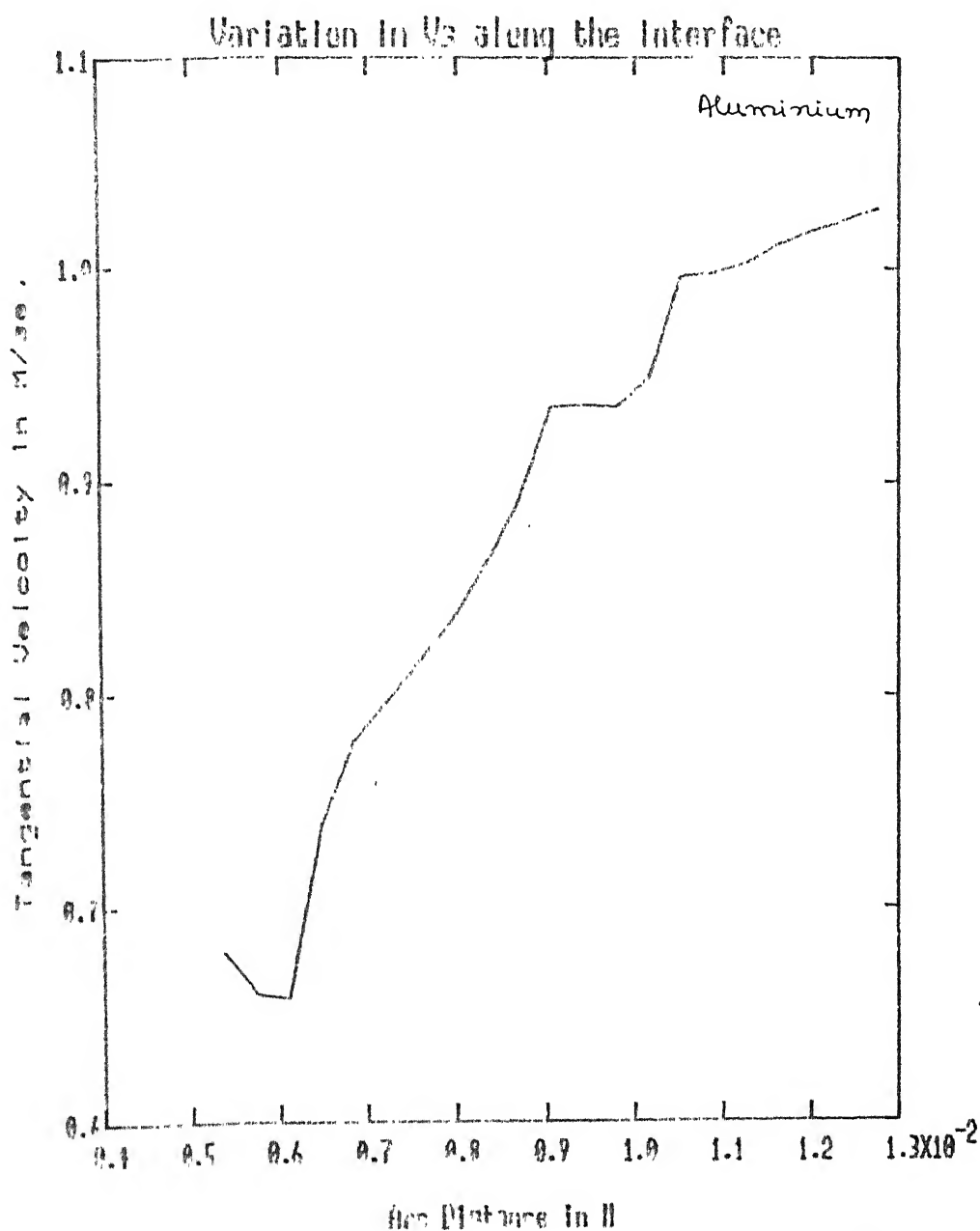Reduction ratio = 29.40%
Angular velocity of the roll = 1.92308 Rad/se

Fig. 4.8a. Variation of V_s along the Interface
Reduction ratio = 29.86%
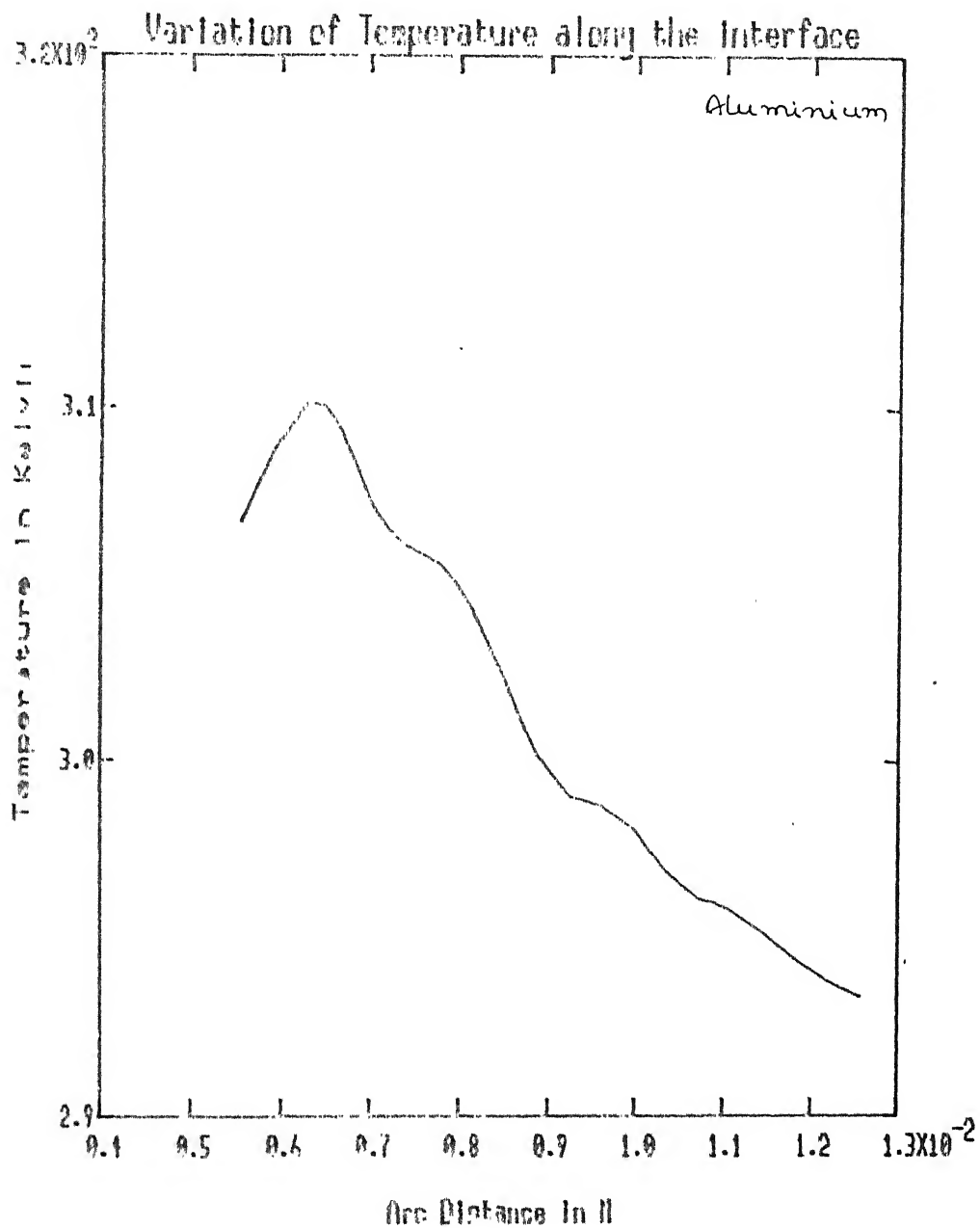Angular velocity of the roll = 2.40384 Rad/sec.

Fig. 4.8b.   Variation of Temperature   along the Interface
             Reduction ratio   = 29.46%
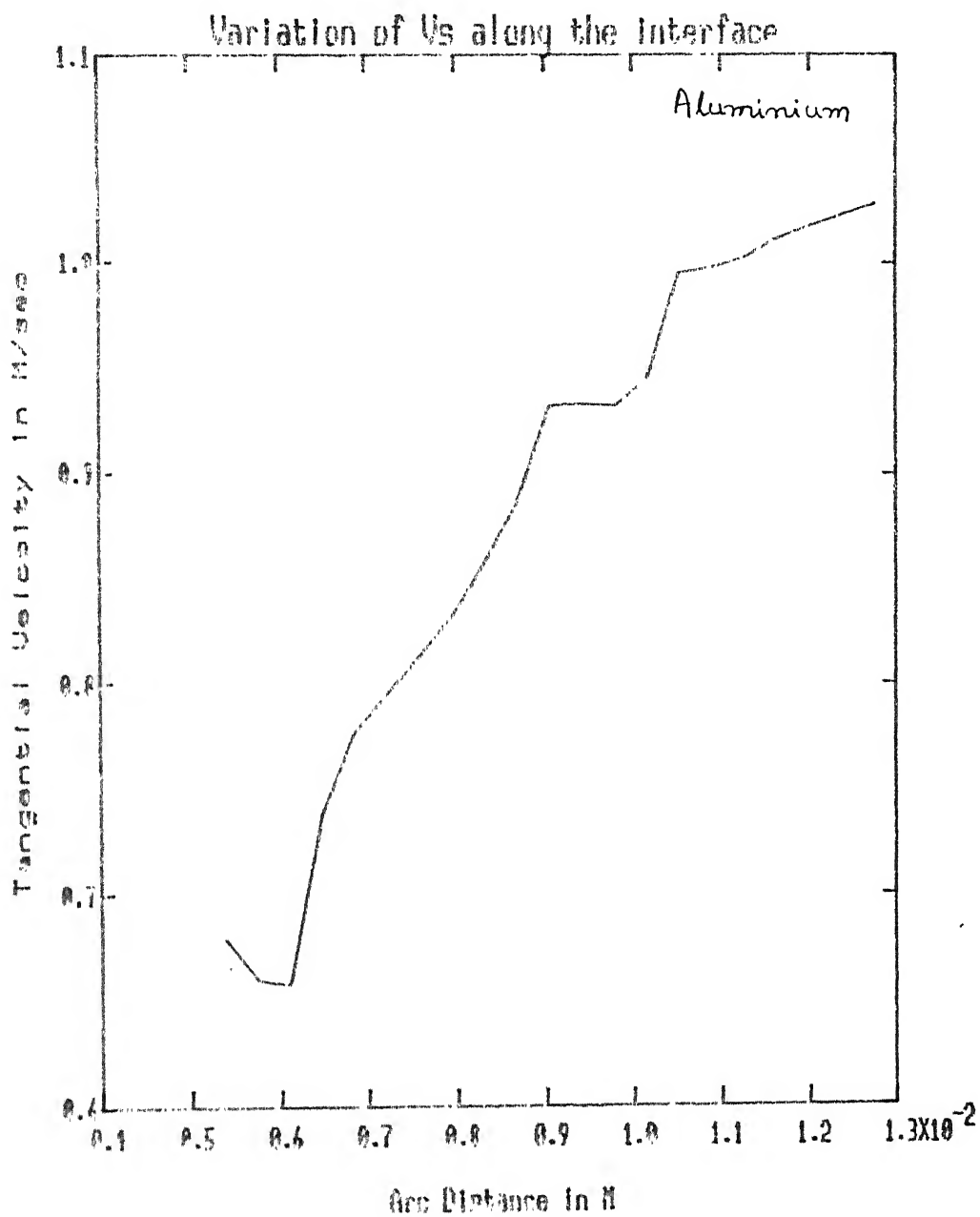   Angular velocity of the roll = 2.40384 Rad/se

Fig. 4.9a.   Variation of V_s along the Interface:
Rediction ratio   = 29.40%
Angular velocity of the roll = 3.8461 Rad/sec

4.6a

Fig. 4.9a.   Variation of V_s along the Interface.
             Rediction ratio   =   29.46%
             Angular velocity of the roll = 3.8461 Rad/sec.
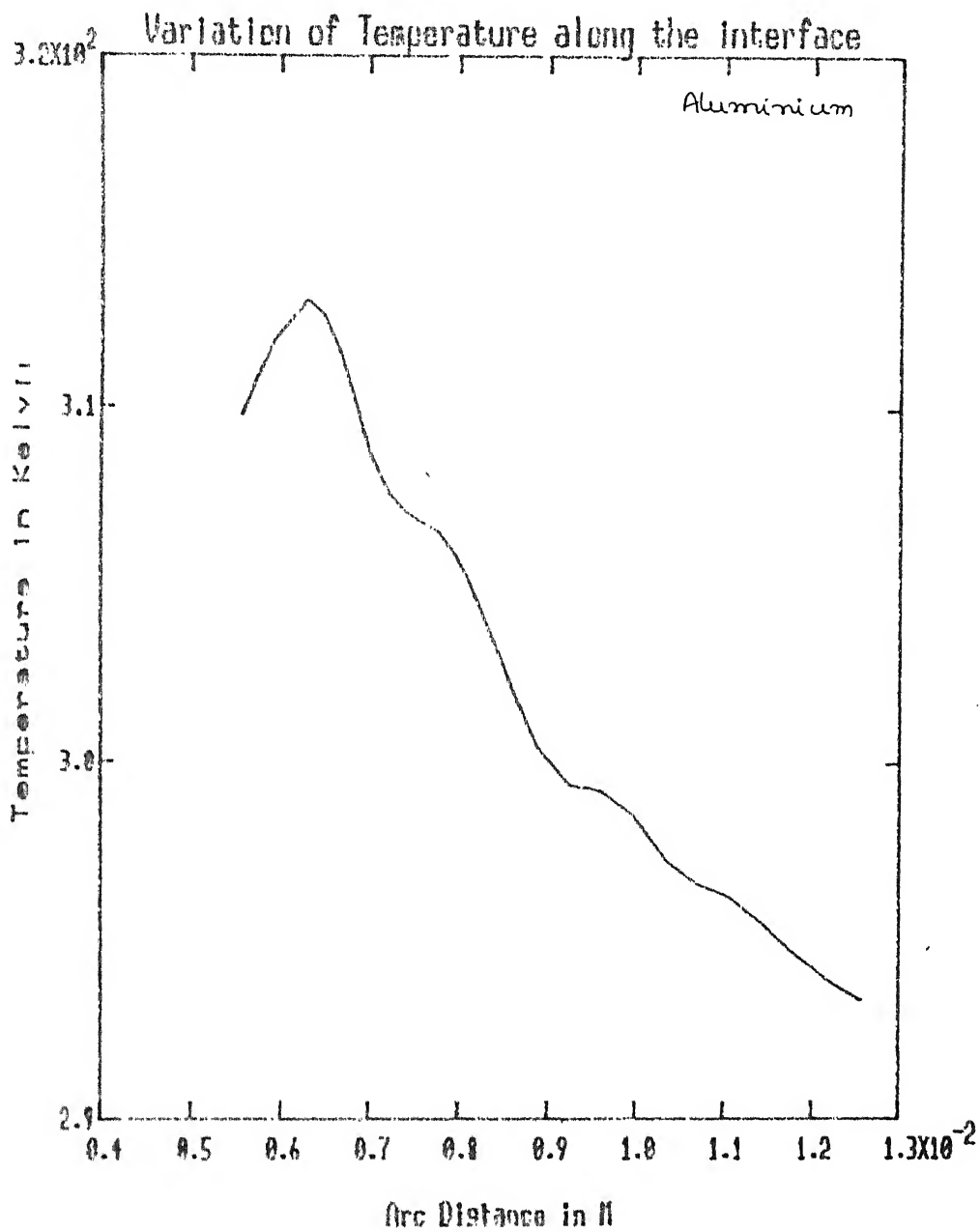
Fig. 4.9b.   Variation of Temperature along the Interface
              Reduction ratio   = 29.46%
              Angular velocity of the roll = 3.8461 Rad/sec.

Fig.4.10a. Variation of V_s along the Interface
            Reduction ratio   =   33.75%
            Angular velocity of the roll = 1.92308 Rad/sec

Fig. 4.10b. Variation of temperature along the interface
Reduction ratio = 33.75%
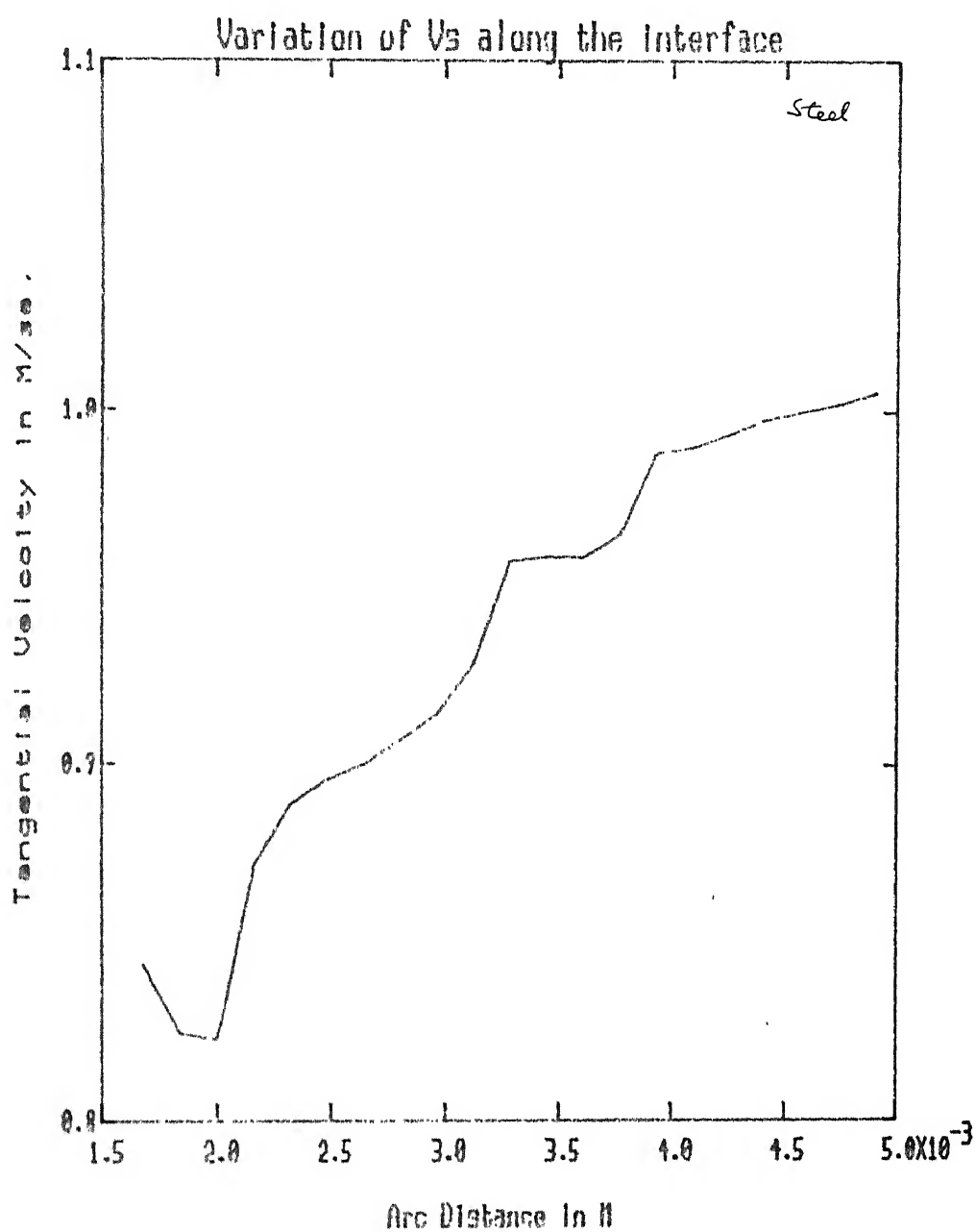Angular velocity of the roll = 1.92308 Rad/sec.

Fig.4.11a. Variation of V_s along the interface
   Reduction ratio = 33.75%
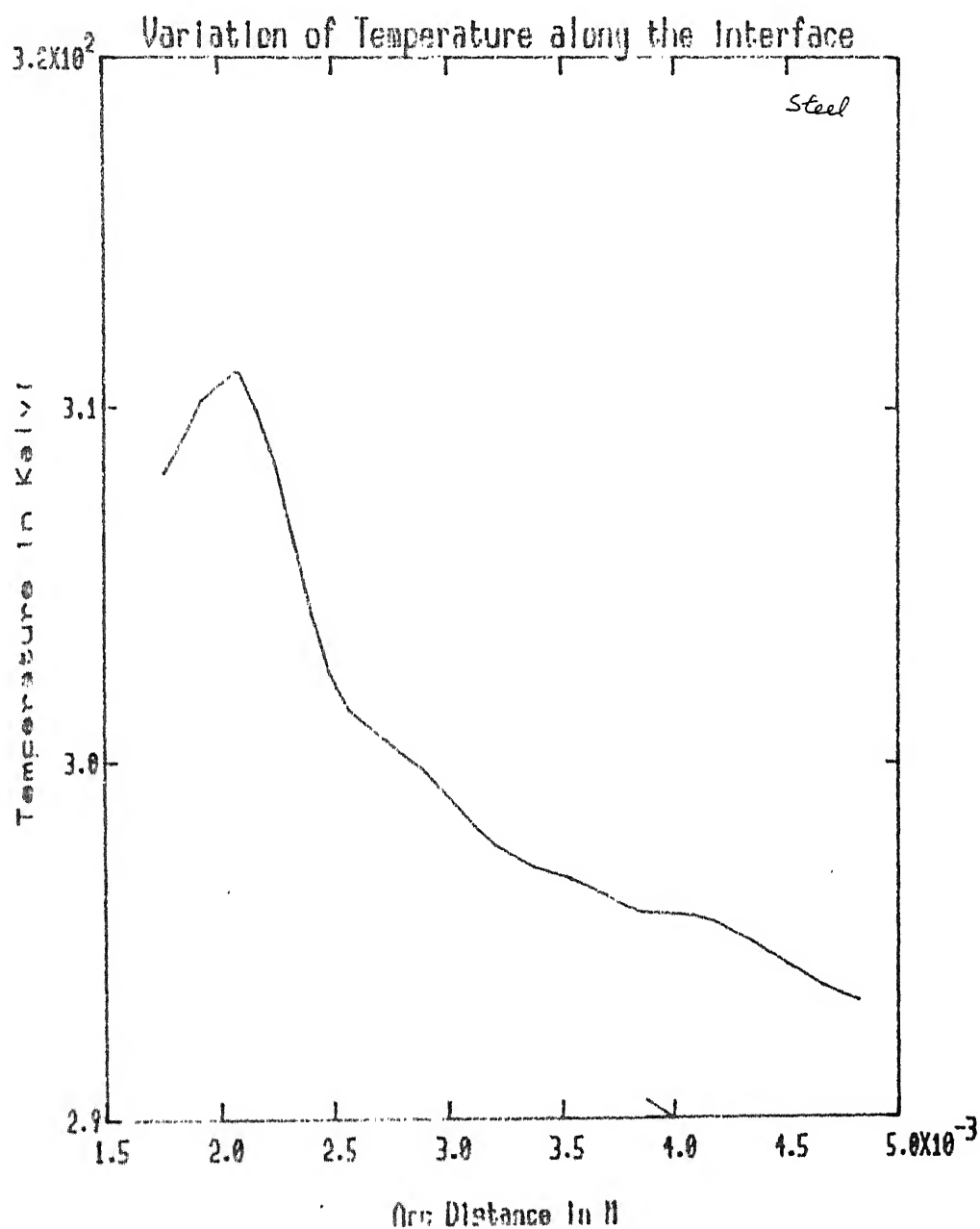   Angular velocity of the roll = 2.40384 Rad/sec.

Fig. 4.11b. Variation of temperature along the interface
Reduction ratio = 33.75%
Angular velocity of the roll = 2.40384 Rad/sec.

Fig. 4.12a. Variation of V_s along the Interface
Reduction ratio = 33.75%
Angular velocity of the roll = 3.8461 Rad/sec.

Fig. 4.12b.   Variation of temperature along the
               interface
               Reduction ratio = 33.75%
               Angular velocity of the roll = 3.8461 Rad/sec.

Fig. 4.13a. Variation of V_s along the interface
Reduction ratio = 16%
Angular velocity of the roll = 2.015748 Rad/sec.

Fig. 4.13b. Variation of temperature along the interface
Reduction ratio = 16%
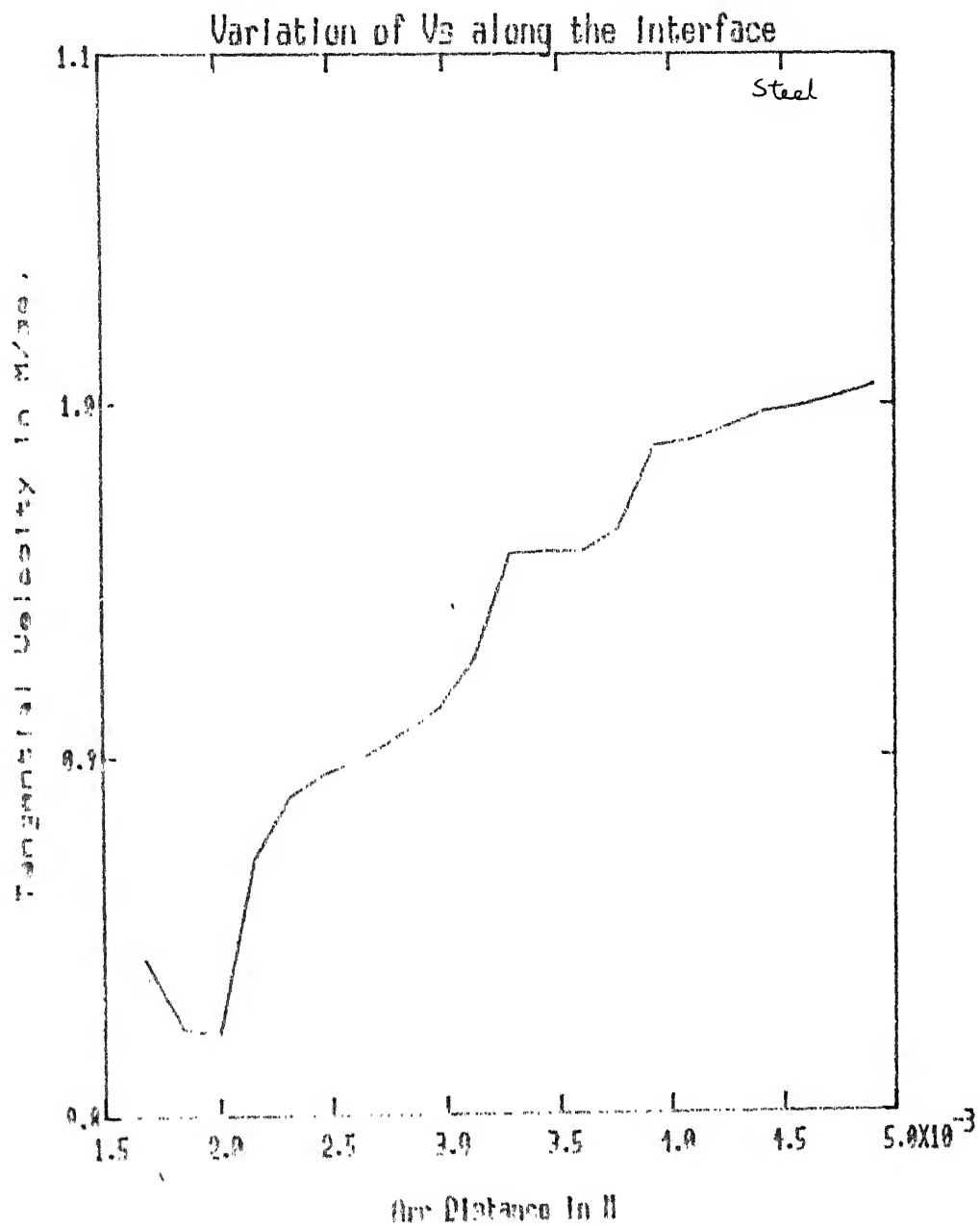Angular velocity of the roll = 2.015748 Rad/sec.

Fig. 4.14a. Variation of V_s along the interface
Reduction ratio = 16%
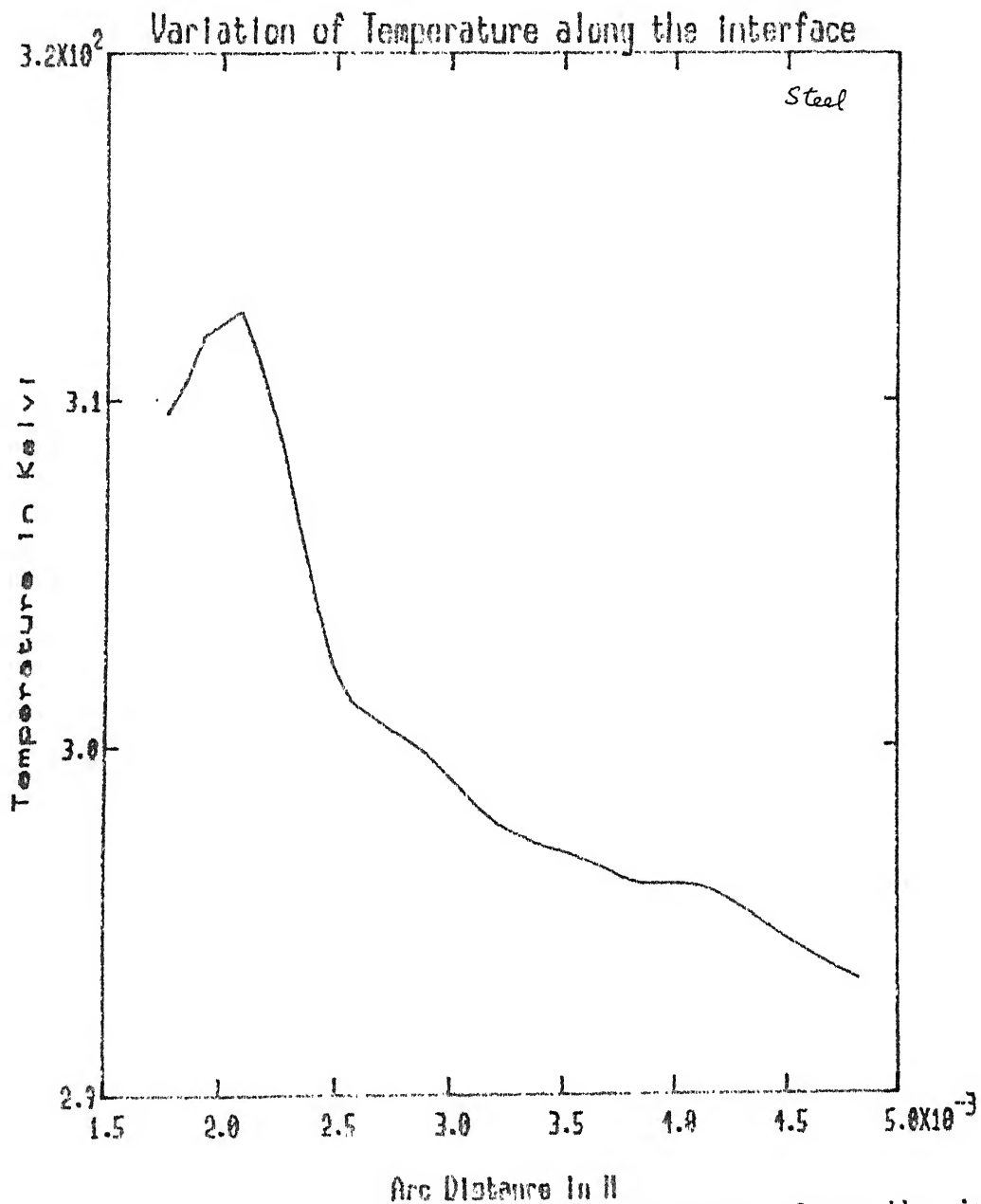Angular velocity of the roll = 4.013496 Rad/sec.

Fig. 4.14b. Variation of temperature along the interface
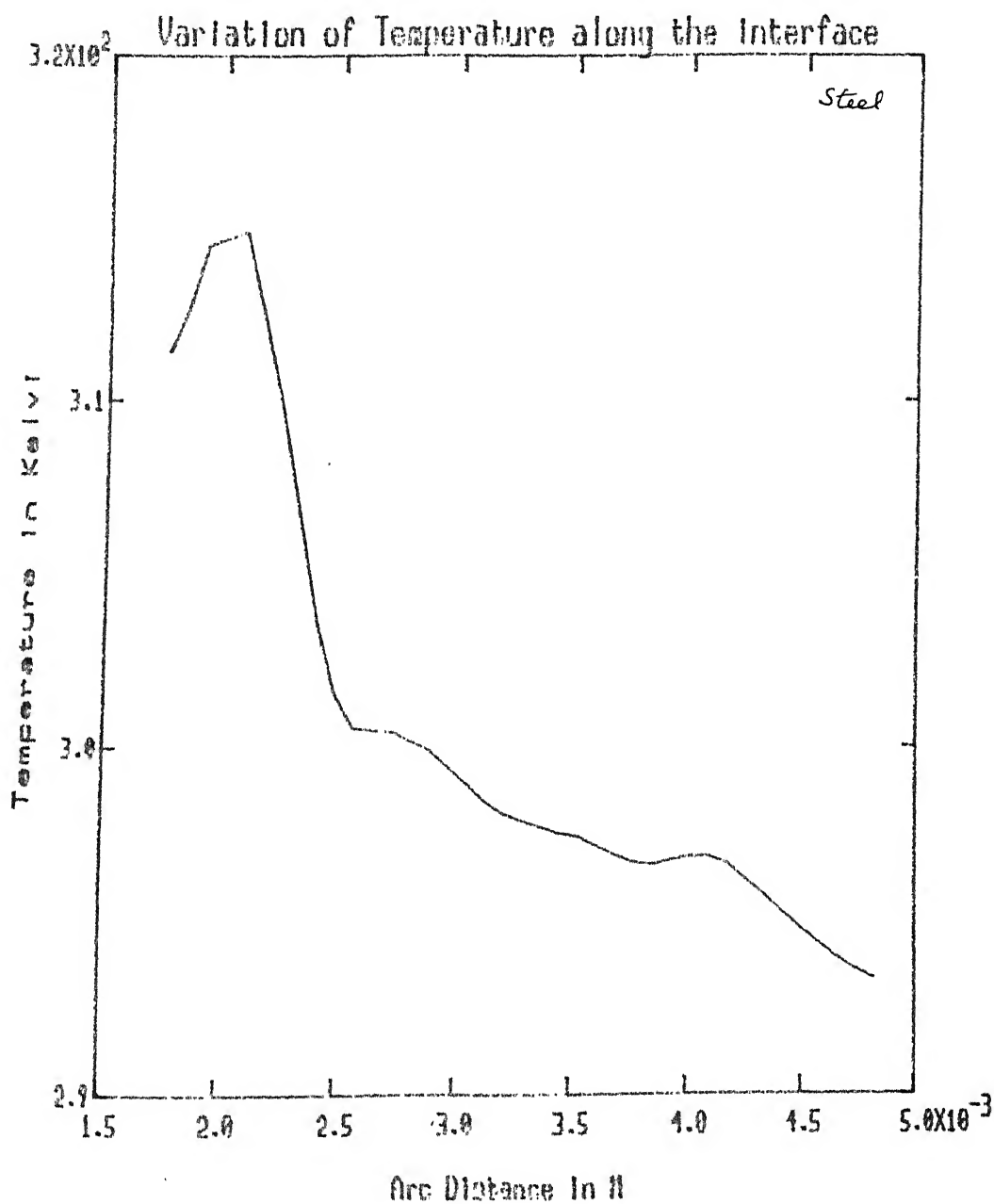Reduction ratio = 16%
Angular velocity of the roll = 4.013496 Rad/

Fig. 4.15b.   Variation of temperature along the interface
             Reduction ratio   =   16%
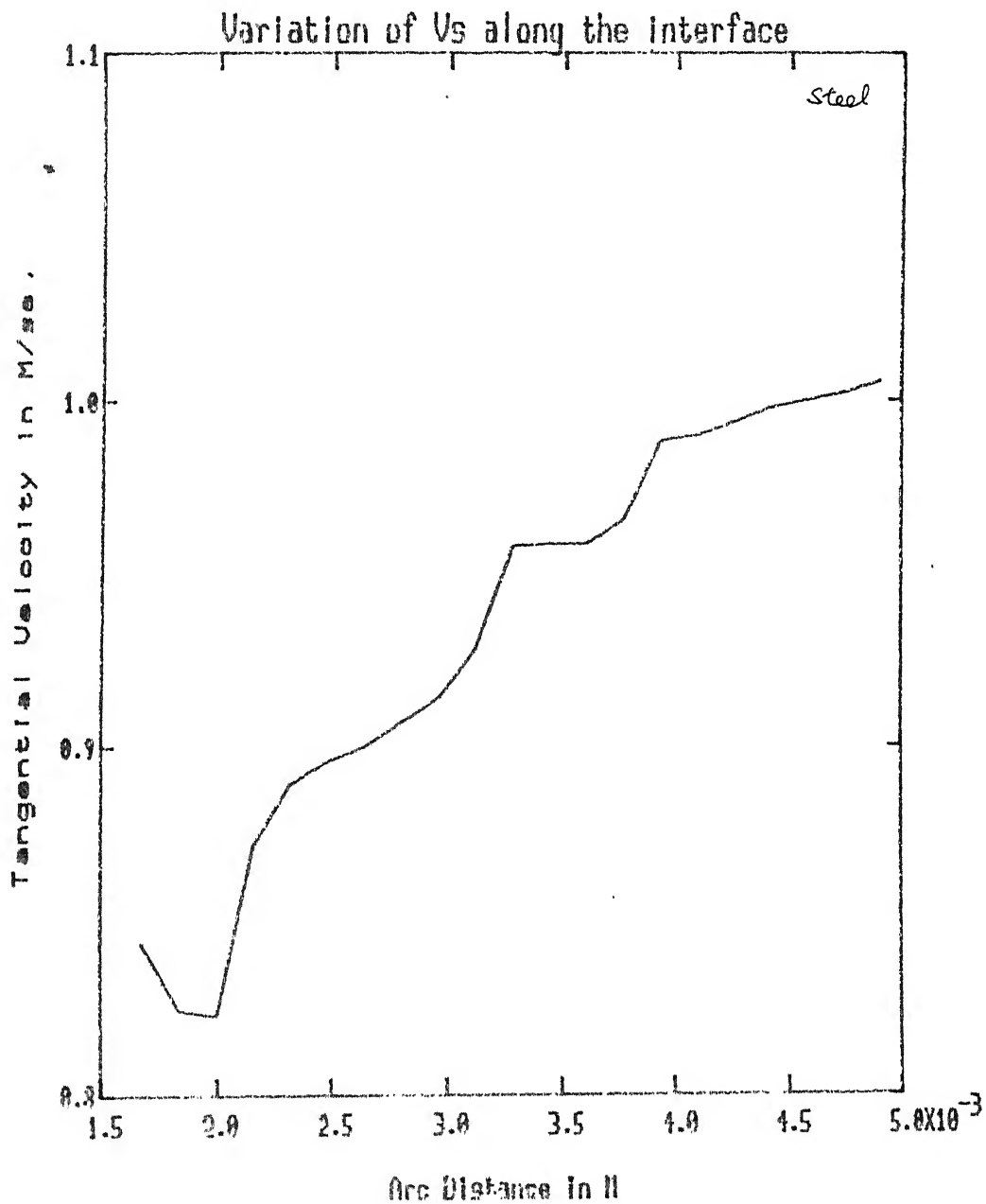   Angular velocity of the roll = 5.03937 Rad/sec.

Variation of Vs along the interface

Steel

Fig. 4.15a. Variation of V$_s$ along the interface
Reduction ratio = 16%
Angular velocity of the roll = 5.03937 Rad/sec.

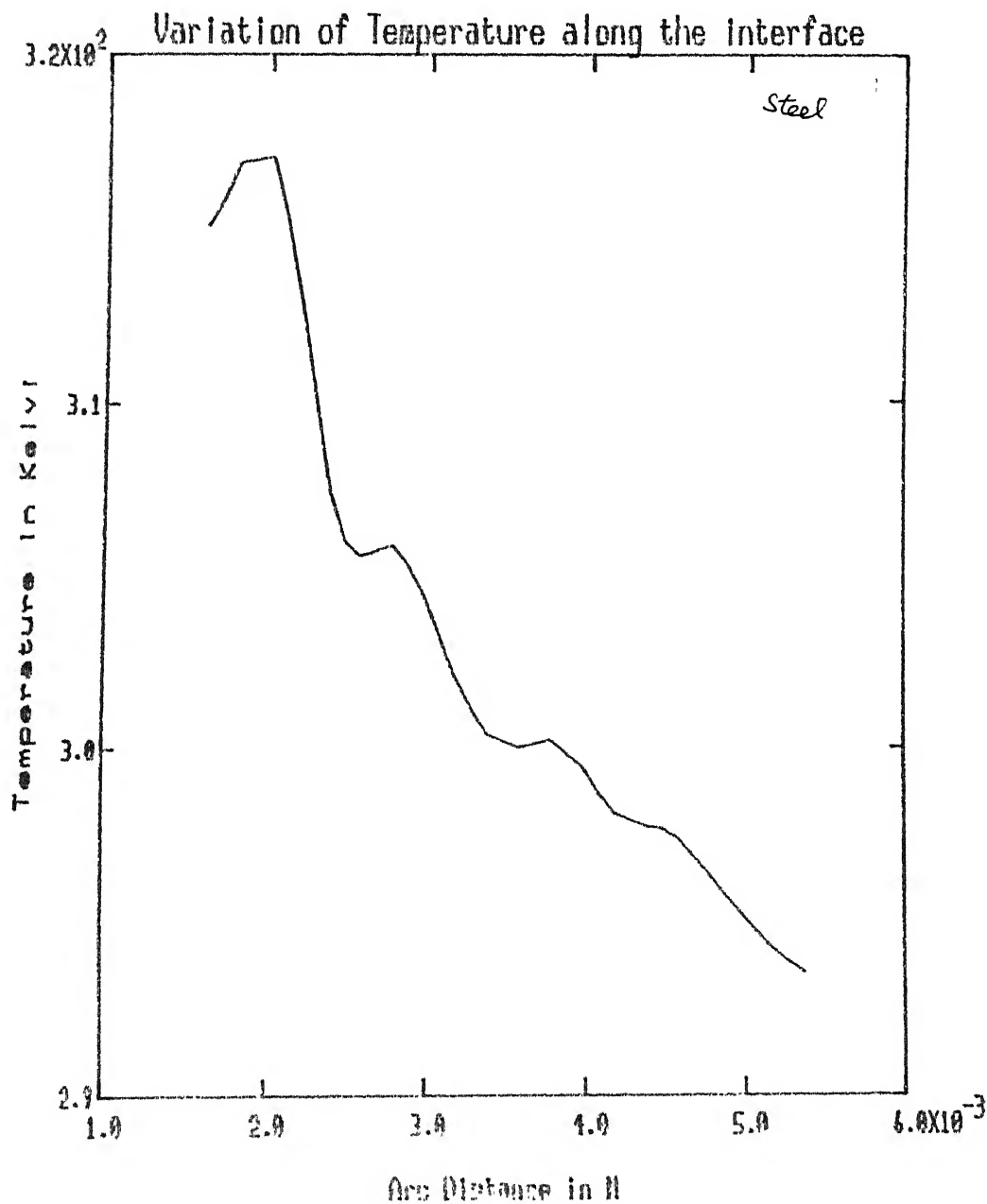Fig. 4.16b.   Variation of Temperature along the interface
              Reduction ratio =   24%
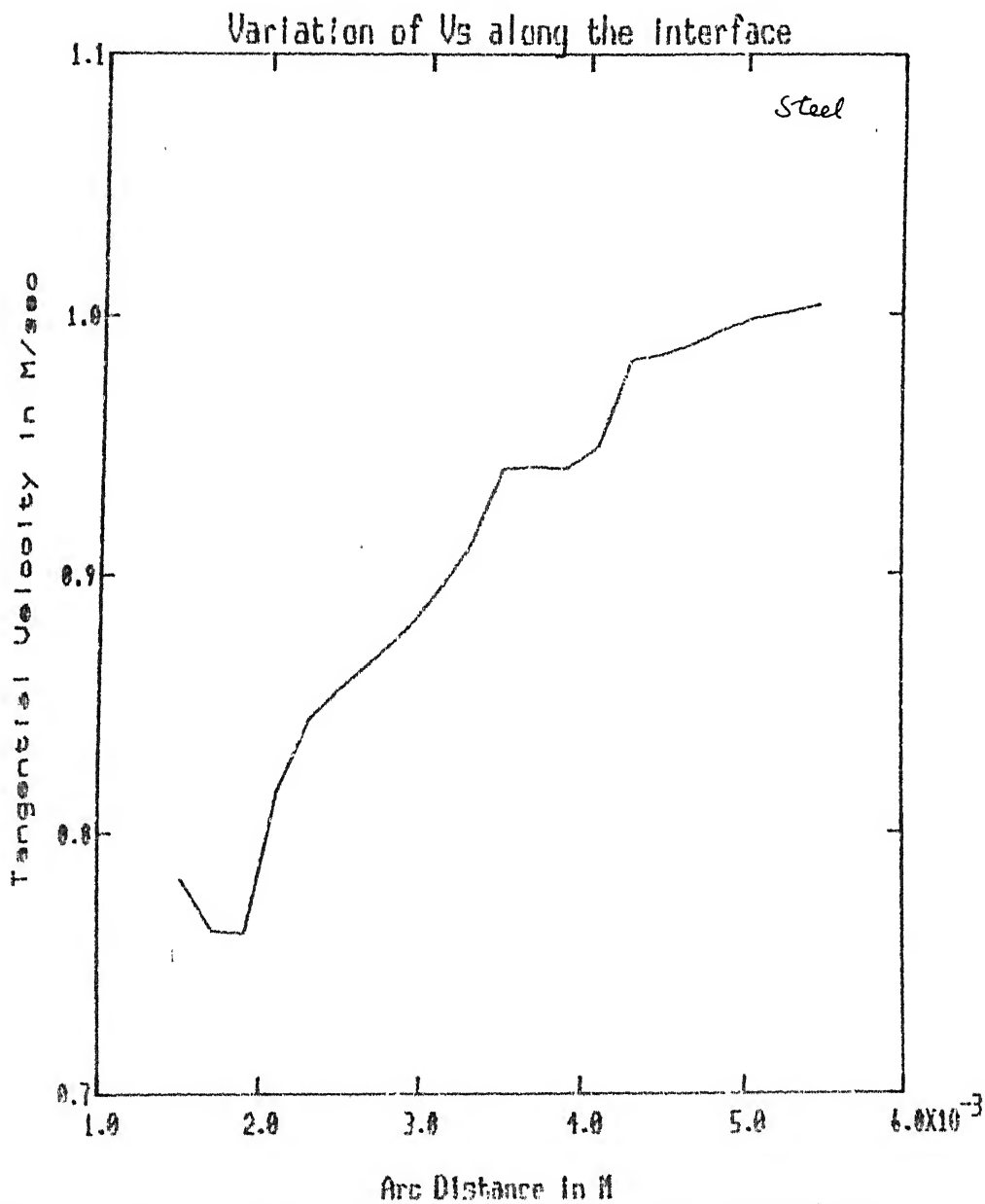   Angular velocity of the roll = 2.015748 Rad/sec.

Fig. 4.16a. Variation of V_s along the interface
Reduction ratio = 24%
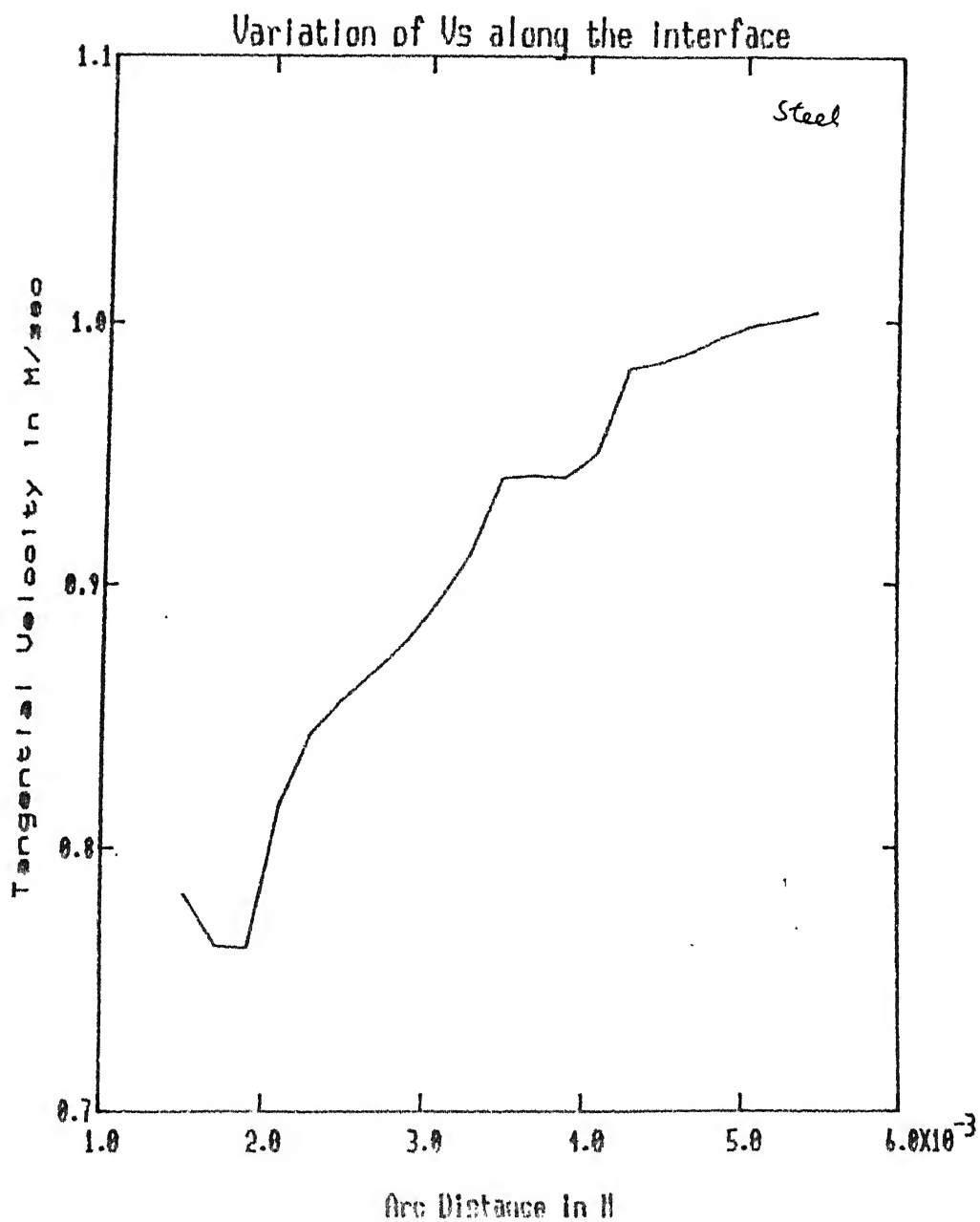Angular velocity of the roll = 2.015748 Rad/sec.

Fig. 4.17a. Variation of V_s along the interface
Reduction ratio = 24%
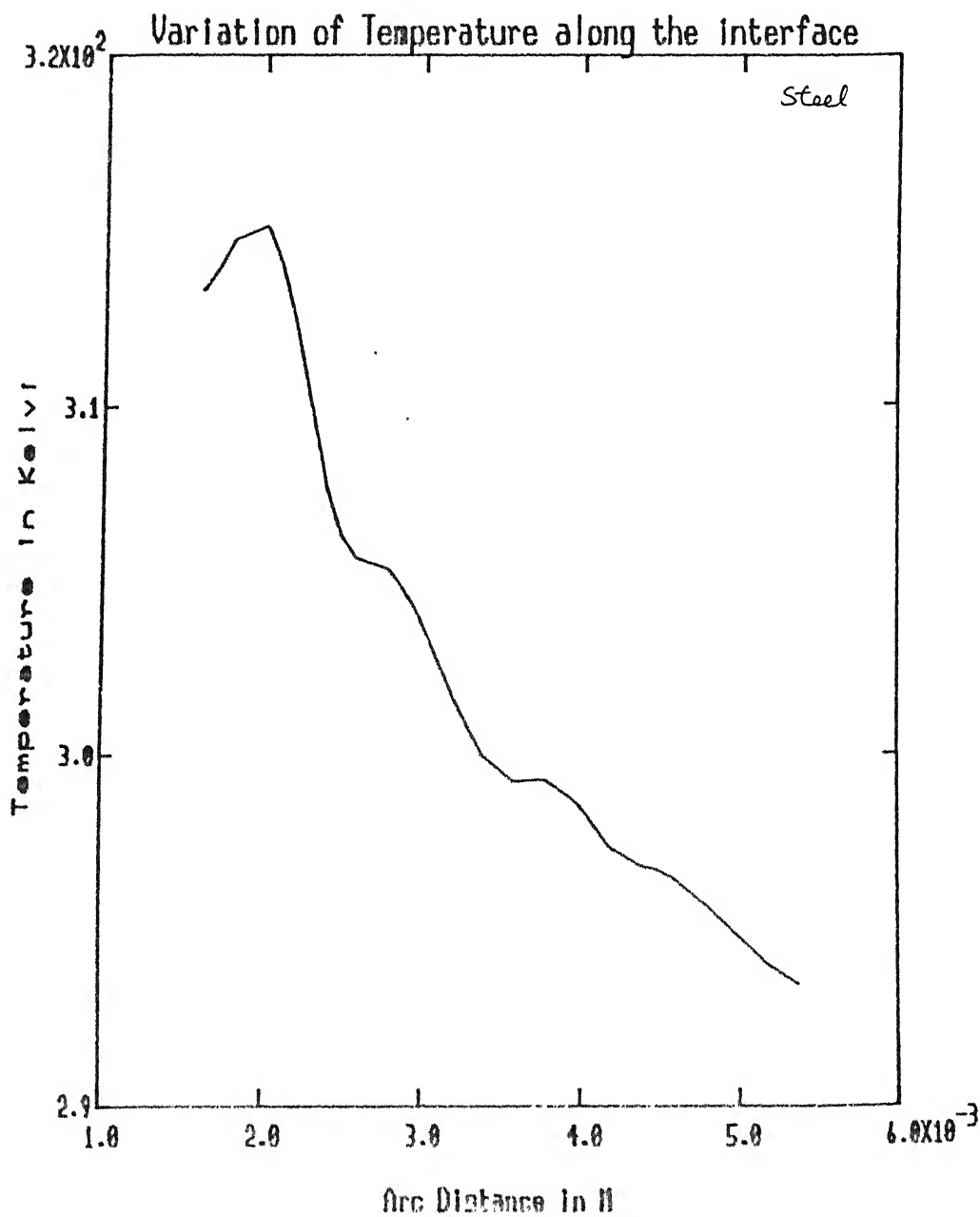Angular velocity of the roll = 4.031496 Rad/sec.

Fig. 4.17b. Variation of temperature along the interface
Reduction ratio = 24%
Angular velocity of the roll = 4.031496 Rad/sec.

REFERENCES

1. Joop C. Nagtegaal and Frans E. Veldpaus
   "On the implementation of finite strain plasticity
   equations in a numerical model", Numerical Analysis
   of Forming Processes, 1984, p. 351.

2. G.D. Lahoti, S.N. Shah and T. Altan
   "Computer aided analysis of the deformations and
   temperatures in strip rolling", Journal of Engineering
   for Industry, Trans. of ASME, Vol. 100, May 1978,
   p. 159.

3. Zienkiewivz, Onate and Heinrich
   "A general formulation for coupled thermal flow of
   metals using finite elements", Int. J. Num. Meth.
   Eng., Vol. 17, 1981, p. 1497.

4. G.C. Cornfield and R.H. Johnson
   "Theoretical prediction of plastic flow in hot rolling
   including the effects of various temperature distri-
   butions", J. Iron & Steel Inst., Vol. 211, 1973, p. 567

5. W. Johnson and H. Kudo
   "The use of upper-bound solutions for the determination
   of temperature distributions in fast hot rolling and
   axisymmetric extrusion process", Jl. of Mech. Sci.,
   Vol. 1, 1960, p. 175.

6. J. Jeswiet and W.B. Rice
   "Measurement of strip temperature in roll gap during
   cold rolling", Annals. of the CIRP, Vol. 24, 1975,
   p. 153.

7. A.N. Karagiozis and J.G. Lenard
   "Temperature distribution in a slab during hot rolling",
   J. of Eng. Materials and Tech., Vol. 110, Jan. 1988,
   p. 17.

8. Avitzur
   "Metal Forming Process".

9. Chaturvedi
   "Rolling of Sheet Metals".

10. J.P. Holman
    "Heat Transfer", McGraw Hill Edition, 1981.

11. C. Taylor and P. Huges
    "A numerical solution of the Navier-Stokes
    equations using the finite element technique",
    Computers and Fluids, Vol. 1, 1973, p. 73.

12. B.M. Irons
    "A frontal solution program for finite element analysis
    Int. J. Num. Meth. in Engg., Vol. 2, 1970.

13. J.N. Reddy
    "An introduction to the finite element method",
    McGraw Hill Book Company, 1984.

14. O.C. Zienkiewicz
    "The finite element method", Tata McGraw Hill edition,
    1981.

15. G. Li and S. Kobayashi, "Rigid plastic finite element
    analysis of plane stran rolling", J. of Engg. for
    Industry, Vol. 18, 1982, p. 55.